

ADSORPTION OF HALOACETONITRILES BY  
CARBONIZED METAL-ORGANIC FRAMEWORKS

Miss Phattarawarin Rodbutr



A Thesis Submitted in Partial Fulfillment of the Requirements  
for the Degree of Master of Science in Hazardous Substance and  
Environmental Management  
Inter-Department of Environmental Management  
Graduate School  
Chulalongkorn University  
Academic Year 2019  
Copyright of Chulalongkorn University

การดูดซับสารฮาโลอะซีโตไนไตรล์ด้วยวัสดุโครงข่ายโลหะอินทรีย์ที่ถูกคาร์บอนไนซ์



วิทยานิพนธ์นี้เป็นส่วนหนึ่งของการศึกษาตามหลักสูตรปริญญาวิทยาศาสตรมหาบัณฑิต  
สาขาวิชาการจัดการสารอันตรายและสิ่งแวดล้อม สหสาขาวิชาการจัดการสิ่งแวดล้อม

บัณฑิตวิทยาลัย จุฬาลงกรณ์มหาวิทยาลัย

ปีการศึกษา 2562

ลิขสิทธิ์ของจุฬาลงกรณ์มหาวิทยาลัย

Thesis Title                    ADSORPTION OF HALOACETONITRILES BY  
                                         CARBONIZED METAL-ORGANIC  
                                         FRAMEWORKS  
By                                    Miss Phattarawarin Rodbutr  
Field of Study                 Hazardous Substance and Environmental  
                                         Management  
Thesis Advisor                Associate Professor Patiparn Punyapalakul, Ph.D.

---

Accepted by the Graduate School, Chulalongkorn University in Partial  
Fulfillment of the Requirement for the Master of Science

..... Dean of the Graduate School  
(Associate Professor THUMNOON NHUJAK,  
Ph.D.)

THESIS COMMITTEE

..... Chairman  
(Associate Professor SRILERT CHOTPANTARAT,  
Ph.D.)

..... Thesis Advisor  
(Associate Professor Patiparn Punyapalakul, Ph.D.)

..... Examiner  
(Jenyuk Lohwacharin, Ph.D.)

..... Examiner  
(Assistant Professor Vorapot Kanokkantapong,  
Ph.D.)

..... External Examiner  
(Chalita Ratanatawanate, Ph.D.)

CHULALONGKORN UNIVERSITY

ภัทรวรินทร์ รอดบุตร : การดูดซับสารฮาโลอะซิโตไนไตรล์ด้วยวัสดุโครงข่ายโลหะอินทรีย์ที่ถูกคาร์บอนไนซ์. ( ADSORPTION OF HALOACETONITRILES BY CARBONIZED METAL-ORGANIC FRAMEWORKS ) อ.ที่ปรึกษาหลัก : รศ. ดร.ปฎิภาณ ปัญญาพลกุล

งานวิจัยนี้มีวัตถุประสงค์เพื่อศึกษาประสิทธิภาพการดูดซับสารกลุ่มฮาโลอะซิโตไนไตรล์ (HANS) ได้แก่ Chloroacetonitrile (MCAN), Dichloroacetonitrile (DCAN), Bromoacetonitrile (MBAN) และ Dibromoacetonitrile (DBAN) โดยวัสดุโครงข่ายโลหะอินทรีย์ (MOFs) ที่ผ่านกระบวนการคาร์บอนไนเซชันและสังเคราะห์ด้วยกรดจำนวน 5 ชนิด ได้แก่ WC-ZIF-8, WC-MIL-53, WC-MIL-88B, WC-Uio-66 และ WC-HKUST-1 และเปรียบเทียบประสิทธิภาพการดูดซับกับถ่านกัมมันต์ชนิดผง (PAC S10) วัสดุดูดซับที่ใช้ได้รับการตรวจสอบคุณสมบัติโดยเทคนิค XRD, SEM-EDS, ไอโซเทอร์มการดูดซับไนโตรเจน, FTIR and XPS จากผลการดูดซับเบื้องต้นแสดงให้เห็นว่า WC-MIL-88B, WC-ZIF-8 และ PAC มีประสิทธิภาพสูงที่สุดในการดูดซับสารกลุ่ม HANS ตามลำดับ และพบว่าขนาดของโมเลกุลและความไม่ชอบน้ำของสารกลุ่ม HANS ส่งผลต่ออัตราการเร็วดูดซับของสารกลุ่ม HANS ตามลำดับดังนี้ DBAN>DCAN>MBAN>MCAN ไอโซเทอร์มของการดูดซับพบว่า สารกลุ่ม HANS ชนิดไดฮาโลเจน (DBAN และ DCAN) สามารถถูกดูดซับโดย WC-MOFs ได้ดีกว่า HANS ชนิดโมโนฮาโลเจน (MBAN และ MCAN) จากการวิเคราะห์โดยเทคนิค XPS พบว่าหมู่ฟังก์ชัน O-C=O และ Fe-O ของ WC-MIL-88B มีบทบาทสำคัญสำหรับการดูดซับ HANS จากผลการดูดซับแบบผสม WC-MIL-88B สามารถดูดซับสารกลุ่มฮาโลอะซิโตไนไตรล์ที่มีความเข้มข้นต่ำ (0-100ppb) โดยลำดับและความสามารถในการดูดซับไม่เปลี่ยนจากกรณีการดูดซับแบบเดี่ยว

จุฬาลงกรณ์มหาวิทยาลัย  
CHULALONGKORN UNIVERSITY

สาขาวิชา	การจัดการสารอันตรายและ สิ่งแวดล้อม	ลายมือชื่อนิสิต .....
ปีการศึกษา	2562	ลายมือชื่อ อ.ที่ปรึกษาหลัก .....

# # 6087537820 : MAJOR HAZARDOUS SUBSTANCE AND ENVIRONMENTAL MANAGEMENT

KEYWORD Metal organic frameworks (MOFs), Adsorption, Carbonization,  
D: Haloacetonitriles

Phattarawarin Rodbutr : ADSORPTION OF HALOACETONITRILES BY CARBONIZED METAL-ORGANIC FRAMEWORKS . Advisor: Assoc. Prof. Patiparn Punyapalakul, Ph.D.

This research investigated adsorption efficiency of four including; Chloroacetonitrile (MCAN), Dichloroacetonitrile (DCAN), Bromoacetonitrile (MBAN) and Dibromoacetonitrile (DBAN) on five acid-washed carbonized metal-organic frameworks (MOFs) (WC-ZIF-8, WC-MIL-53, WC-MIL-88B, WC-UiO-66 and WC-HKUST-1) compared with powder activated carbon (PAC S10). The synthesized materials were characterized by XRD, SEM-EDS, nitrogen adsorption isotherms, FTIR and XPS. The screening experiment revealed that WC-MIL-88B, WC-ZIF-8, and PAC had highest adsorption capacities for four HANs, respectively. The HANs molecular size and their hydrophobicity influenced the adsorption rates of HANs in the order of DBAN>DCAN>MBAN>MCAN. The adsorption isotherms showed that Di-halogenic HANs (DBAN and DCAN) can be adsorbed by WC-MOFs much better than mono-halogenic HANs (MBAN and MCAN). From XRD analysis, O-C=O and Fe-O functional groups of WC-MIL-88B might play the important role for adsorption of four HANs., adsorption sites of WC-MIL-88B are expected to be enough for mixed-solute HANs adsorption in low concentration range (0-100ppb), and the order of adsorption capacities does not change from the single-solute adsorption.



Field of Study:	Hazardous Substance and Environmental Management	Student's Signature .....
Academic Year:	2019	Advisor's Signature .....

## ACKNOWLEDGEMENTS

I would first like to thank my thesis advisor Assoc. Prof. Patiparn Punyapalakul, Ph.D. of faculty of Environment Engineering at Chulalongkorn University. My advisor always welcome whenever I ran into a trouble spot or had a question about my research or writing. He teaches me to be an adult who has my own responsibility and self-reliance but steered me in the right the direction whenever he thought I needed it.

I would also like to thank the seniors who were involved in this research project: Phacharapol, Alongorn and Dujdeaun. Including my friend who always helps when I asked: Thanaporn, Jaruwat, Paphinwit, Supannapa and Suchunya. Without their participation, this thesis could not have been successfully conducted.

The most important encouragement was from my parents who trust me anyway. My grandparent, Mrs. Sakran & Mr. Suna Rodbutr, spent lots of money and time for my master study, in addition for, Mr. Sumeth Junsuthonpoj always cheer me up and stay beside me in a bad day. I love them so much.

I would also like to acknowledge of the Hazardous Substance and Environmental Management (IP-HSM), Chulalongkorn for support fund to my thesis.

# TABLE OF CONTENTS

	<b>Page</b>
ABSTRACT (THAI) .....	iii
ABSTRACT (ENGLISH).....	iv
ACKNOWLEDGEMENTS.....	v
TABLE OF CONTENTS.....	vi
LIST OF FIGURES .....	ix
LIST OF TABLES.....	xiii
ABBREVIATIONS .....	xiv
CHAPTER I INTRODUCTION.....	1
1.1 STATE OF PROBLEM.....	1
1.2 OBJECTIVE.....	3
1.3 HYPOTHESIS .....	3
1.4 SCOPE OF STUDY .....	3
CHAPTER II THEORETICAL BACKGROUND AND LITERATURE REVIEWS..	8
2.1 DISINFECTION BY-PRODUCT (DBPs) .....	8
2.2 HALOACETONITRILES (HANs) .....	10
2.3 METAL ORGANIC FRAMEWORKS (MOFs) .....	14
2.4 ADSORBENT IN THIS STUDY .....	15
2.4.1 ZIF-8.....	15
2.4.2 MIL-53 (Al).....	15
2.4.3 MIL-88B (Fe).....	16
2.4.4. UiO-66.....	16
2.4.5. HKUST-1 .....	16
2.5 ADSORPTION THEORY.....	17
2.5.1 ADSORPTION APPLICATION .....	17
2.5.2 ADSORPTION MECHANISM .....	18

2.5.3 MODEL FOR ADSORPTION MECHANISM .....	18
2.6. CARBONIZATION .....	23
2.6.1 CARBONIZATION ATMOSPHERE .....	23
2.6.2. CARBONIZATION TEMPERATURE .....	24
CHAPTER III RESEARCH METHODOLOGY .....	27
3.1. EQUIPMENTS AND MATERIALS .....	27
3.1.1. EQUIPMENTS AND GLASSWARES .....	27
3.1.2. CHEMICAL .....	28
3.2. MATERIALS SYNTHESIS .....	29
3.2.1. ZIF-8, C-ZIF-8 and WC-ZIF-8 .....	29
3.2.2. MIL-53(Al), C-MIL-53(Al) and WC-MIL-53(Al) .....	29
3.2.3. MIL-88B (Fe), C-MIL-88B (Fe), WC-MIL-88B (Fe) .....	30
3.2.4. UiO-66 (Zr), C-UiO-66 (Zr) and WC-UiO-66 (Zr) .....	30
3.2.5. HKUST-1, C-HKUST-1, and WC-HKUST-1 .....	31
3.2.6. Powder activated carbon (PAC) .....	32
3.3. ADSORBENT CHARACTERIZATION .....	32
3.4. REAGENT PREPARATION .....	32
3.4.1. Phosphate buffer .....	32
3.4.2. Distilled water reagent .....	33
3.4.3. Tap water reagent .....	33
3.5. ADSORBATE PREPARATION .....	33
3.6. ADSORBENTS PREPARATION .....	34
3.7. POINT OF ZERO CHARGE STUDY .....	34
3.8. ADSORBENT SCREENING .....	34
3.9. ADSORPTION KINETIC STUDY .....	35
3.10. ADSORPTION ISOTHERM STUDY (SINGLE SOLUTE) .....	35
3.11. ADSORPTION ISOTHERM STUDY (MIXED SOLUTE) .....	35
3.12. EXTRACTION AND ANALYTICAL METHODS .....	36
3.12.1. HANs extraction .....	36



3.12.2. GC/ECD setting.....	36
CHAPTER IV MATERIALS CHARACTERIZATION RESULTS .....	37
4.1 INTRODUCTION .....	37
4.2 SURFACE FUNCTIONAL GROUP ANALYSIS BY FTIR .....	38
4.3 POWDER X-RAY DIFFRACTION– POWDER-XRD.....	43
4.3 SCANNING ELECTRON MICROSCOPE AND ENERGY DISPERSIVE X- RAY SPECTROMETER (SEM-EDS).....	47
4.4. PORE AND SURFACE AREA ANALYSIS.....	53
4.5 POINT OF ZERO CHARGE (PZC).....	63
CHAPTER V ADSORPTION EXPERIMENT RESULTS .....	65
5.1 INTRODUCTION .....	65
5.2. ADSORBENT SCREENING.....	65
5.3. ADSORPTION KINETIC .....	68
5.4. ADSORPTION ISOTHERM (SINGLE SOLUTE) .....	92
5.5. ADSORPTION SELECTIVITY (IN MIXED SOLUTE) .....	99
5.6 SURFACE ELEMENT ANALYSIS BY X-RAY PHOTOELEC-TRON SPECTROSCOPY (XPS).....	102
5.7 DEGRADATION OF HANs .....	107
CHAPTER VII CONCLUSIONS.....	109
REFERECES .....	112
REFERENCES .....	116
VITA.....	118

## LIST OF FIGURES

<b>FIGURE 1.1</b> FLOW CHART FOR THE SCOPE OF STUDY.....	6
<b>FIGURE 1.2</b> INDEPENDENT, DEPENDENT AND CONTROLLED VARIABLES OF THE EXPERIMENTS.....	7
<b>Figure 2.1</b> Distribution diagram for dissolved chlorine species. (at pH 7.5, [HOCl] = [OCl <sup>-</sup> ]) (Weiner, 2012).....	9
<b>FIGURE 2.2</b> THE STRUCTURE OF HANS.....	11
<b>FIGURE 2.3</b> MOFs STRUCTURE; (A) ZIF-8(ZN), (B) MIL-53(AL), (C) MIL- 88B (FE), (D) UiO-66(ZR) AND (E) HKUST-1(CU).....	17
<b>FIGURE 2.4</b> ZIF-8 THROUGH DIRECT CARBONIZATION .....	25
<b>Figure 4.1</b> Apperance of the synthesized adsorbents (a) ZIF-8(Zn), (b) MIL-53 (Al), (c) MIL-88B (Fe), (d) UiO-66(Zr) and (e) HKUST- 1(Cu).....	38
<b>FIGURE 4.2</b> FTIR SPECTRA OF MOFs (UP) AND WC-MOFs (DOWN); (A) ZIF-8(ZN) AND WC-ZIF-8; (B) MIL-53(AL) AND WC-MIL-53 .....	41
<b>FIGURE 4.2</b> FTIR SPECTRA OF MOFs (UP) AND WC-MOFs (DOWN); (C) MIL-88B (FE) AND WC-MIL-88B; (D) UiO-66(ZR) AND WC-UiO-66 .....	42
<b>FIGURE 4.2</b> FTIR SPECTRA OF MOFs (UP) AND WC-MOFs (DOWN); (E) HKUST-1(CU) AND WC-HKUST-1. ....	43
<b>FIGURE 4.3</b> XRD PATTERN OF MOFs AND C-MOFs; (A) ZIF-8(ZN) AND C- ZIF-8; (B) MIL-53(AL) AND C-MIL-53; (C) MIL-88B(FE) AND C- MIL-88B; (D) UiO-66(ZR) AND C-UiO-66; AND (E) HKUST-1(CU) AND C-HKUST-1. ....	47
<b>FIGURE 4.4</b> SEM IMAGES OF (A1) ZIF-8(ZN), (A2) C-ZIF-8 AND (A3) WC- ZIF-8; (B1) MIL-53 (AL), (B2) C-MIL-53 AND (B3) WC-MIL-53; (C1-C3) MIL-88B(FE), (C4) C-MIL-88B AND (C5-C6)WC-MIL-88B; (D1) UiO-66(ZR), (D2) C-UiO-66 AND (D3) WC-UiO-66; AND (E1) HKUST-1(CU), (E2) C-HKUST-1 AND (E3) C-HKUST-1 .....	52
<b>FIGURE 4.5</b> NITROGEN SORPTION ISOTHERM OF MOFs C-MOFs AND WC- MOFs; (A) ZIF-8(ZN), C-ZIF-8 AND WC-ZIF-8; (B) MIL-53(AL) C-	

MIL53 AND WC-MIL-53 ; (c) MIL-88B (Fe), C-MIL-88B AND WC-MIL-88B; (D) UiO-66 (Zr), C-UiO-66 AND WC-UiO-66; AND (E) HKUST-1(Cu), C-HKUST-1 AND WC-HKUST-1 AT 77 °K. OPENED AND CLOSED SYMBOLS ARE REPRESENTED THE NITROGEN ADSORPTION AND DESORPTION. ....57

**FIGURE 4.6** BJH PORE SIZE DISTRIBUTIONS DERIVED FROM SORPTION ISOTHERM OF (A) ADSORPTION ZIF-8(ZN), (B) DESORPTION ZIF-8(ZN), (C) ADSORPTION C-ZIF-8, (D) DESORPTION C-ZIF-8, (E) ADSORPTION WC-ZIF-8 AND (F) DESORPTION WC-ZIF-8 .....58

**FIGURE 4.7** BJH PORE SIZE DISTRIBUTIONS DERIVED FROM SORPTION ISOTHERM OF (A) ADSORPTION MIL-53(AL), (B) DESORPTION MIL-53(AL), (C) ADSORPTION C- MIL-53, (D) DESORPTION C- MIL-53, (E) ADSORPTION WC- MIL-53 AND (F) DESORPTION WC- MIL-53.....59

**FIGURE 4.8** BJH PORE SIZE DISTRIBUTIONS DERIVED FROM SORPTION ISOTHERM OF (A) ADSORPTION MIL-88B(Fe), (B) DESORPTION MIL-88B(Fe), (C) ADSORPTION C- MIL-88B, (D) DESORPTION C- MIL-88B, (E) ADSORPTION WC- MIL-88B, AND (F) DESORPTION WC- MIL-88B. ....60

**FIGURE 4.9** BJH PORE SIZE DISTRIBUTIONS DERIVED FROM SORPTION ISOTHERM OF (A) ADSORPTION UiO-66(Zr), (B) DESORPTION UiO-66(Zr), (C) ADSORPTION C- UiO-66, (D) DESORPTION C- UiO-66, (E) ADSORPTION WC- UiO-66 AND (F) DESORPTION WC- UiO-66.....61

**FIGURE 4.10** BJH PORE SIZE DISTRIBUTIONS DERIVED FROM SORPTION ISOTHERM OF (A) ADSORPTION HKUST-1(Cu), (B) DESORPTION HKUST-1(Cu), (C) ADSORPTION C- HKUST-1, (D) DESORPTION C- HKUST-1, (E) ADSORPTION WC- HKUST-1 AND (F) DESORPTION WC- HKUST-1. ....62

**FIGURE 4.11** POINT OF ZERO CHARGES (PHZPC) OF WC-MIL-88B (Fe), WC-ZIF-8 AND PAC S10. ....64

**Figure 5.1** ADSORBENT SCREENING OF (A) MCAN; (B) DCAN; (C) MBAN AND (D) DBAN AT 1000 PPB WITH 0.2 G/L OF ADSORBENT AT 25 °C IN TAP WATER.....68

**FIGURE 5.2** ADSORPTION KINETIC PLOTTED BETWEEN  $Q_E$  ( $\mu\text{G/G}$ ) VERSUS TIME OF (▲) WC-MIL-88B (Fe), (◆) WC-ZIF-8 AND (●) PAC S10 WITH (A) MCAN; (B) DCAN; (C) MBAN AND (D) DBAN AT 25 °C IN TAP WATER. ....72

<b>FIGURE 5.3</b> ADSORPTION KINETIC PLOT BETWEEN $Q_e$ ( $\mu\text{g/g}$ ) VERSUS TIME OF WC-MIL-88B (Fe), WC-ZIF-8 AND PAC S10 WITH FOUR HANS AT 25 °C IN TAP WATER.....	73
<b>FIGURE 5.4</b> COMPARISON OF THE PREDICTED AND EXPERIMENT DATA FOR EQUILIBRIUM ADSORPTION OF FOUR HANS ON WC-MIL-88B.....	75
<b>FIGURE 5.5</b> COMPARISON OF THE PREDICTED AND EXPERIMENT DATA FOR EQUILIBRIUM ADSORPTION OF FOUR HANS ON WC-ZIF-8.....	76
<b>FIGURE 5.6</b> COMPARISON OF THE PREDICTED AND EXPERIMENT DATA FOR EQUILIBRIUM ADSORPTION OF FOUR HANS ON PAC S10. ....	77
<b>FIGURE 5.7</b> IUPAC CLASSIFICATION OF ADSORPTION (REFERENCE: IUPAC,1985).....	95
<b>FIGURE 5.8</b> ADSORPTION ISOTHERMS OF FOUR HANS (IN SINGLE SOLUTE) ON WC-MIL-88B, WC-ZIF-8 AND PAC S10 AT 25 °C IN TAP WATER. ....	99
<b>FIGURE 5.9</b> ADSORPTION ISOTHERMS OF WC-MIL-88B, WC-ZIF-8 AND PAC S10 FOR FOUR HANS IN SINGLE-SOLUTE AND MIXED -SOLUTE IN TAP WATER AT 25 °C.....	101
<b>FIGURE 5.10</b> C 1s XPS SPECTRA OF PRE- AND POST-WC-ZIF-8 AND WC-MIL-88B.....	103
<b>FIGURE 5.11</b> O 1s XPS SPECTRA OF PRE AND POST WC-ZIF-8 AND WC-MIL-88B.....	104
<b>FIGURE 5.12</b> ZN 2P XPS SPECTRA OF PRE AND POST WC-ZIF-8 .....	105
<b>FIGURE 5.13</b> Fe 2P XPS SPECTRA OF PRE AND POST WC-MIL-88B.....	105
<b>FIGURE 5.14</b> N 1s XPS SPECTRA OF PRE AND POST WC-ZIF-8 AND WC-MIL-88B (Fe) .....	106
<b>FIGURE 5.15</b> Cl 2P XPS SPECTRA OF PRE AND POST WC-ZIF-8 AND WC-MIL-88B.....	107

**FIGURE 5.16** THE DECREASE OF HANs CONCENTRATION BY THE TIME...108



## LIST OF TABLES

<b>TABLE 2.1</b> DBPs AND ITS HEALTH EFFECT .....	10
<b>TABLE 2.2</b> PROPERTIES OF SELECTED HANs SUBSTANCES .....	12
<b>TABLE 2.3</b> HANs GUIDELINE VALUES FOR DRINKING-WATER QUALITY (WHO, 2011) .....	13
<b>TABLE 2.4</b> SURFACE AREAS, PORE VOLUMES, MICROPORE VOLUMES, AND PERCENTAGES OF MICROPORES FOR NANOPOROUS CARBONS PREPARED AT VARIOUS TEMPERATURES .....	25
<b>Table 4.1</b> EDS ELEMENT DATA ANALYSIS.....	53
<b>TABLE 4.2</b> SURFACE AREA AND PORE CHARACTERISTIC OF SYNTHESIZED ADSORBENTS.....	55
<b>Table 5.1</b> KINETIC ADSORPTION PARAMETERS.....	74
<b>TABLE 5.2</b> HANs MOLECULAR DIPOLE MOMENT ANALYSIS .....	95
<b>TABLE 5.3</b> HANs MOLECULAR SIZE .....	96
<b>TABLE 5.4</b> ADSORPTION ISOTHERM PARAMETERS .....	96

## ABBREVIATIONS

BET	=	Brunauer-Emmett-Teller
C <sub>9</sub> H <sub>6</sub> O <sub>6</sub> , BTC	=	Benzene,1,3,5-tricarboxylic acid, Trimesic acid
C-MOFs	=	Carbonized-Metal organic frameworks
Cu(NO <sub>3</sub> ) <sub>2</sub> ·3H <sub>2</sub> O	=	Copper (II) nitrate trihydrate
DBAN	=	Dibromoacetonitrile
DCAN	=	Dichloroacetonitrile
DBPs	=	Disinfection by-products
DCAN	=	Dichloroacetonitrile
DI	=	Deionized water
DMF	=	Dimethylformamide
FeCl <sub>3</sub>	=	Ferric chloride
FT-IR	=	Fourier transform infrared spectrometer
GC-ECD	=	Gas chromatography electron-capture detection
H <sub>2</sub> SO <sub>4</sub>	=	Sulfuric acid
HAAs	=	Haloacetic acids
HAcAms	=	Haloacetamides
HANs	=	Haloactonitriles
HKUST-1	=	Hong Kong University of Science and Technology-1
K <sub>2</sub> HPO <sub>4</sub>	=	Dipotassium phosphate
KH <sub>2</sub> PO <sub>4</sub>	=	Potassium phosphate
MBAN	=	Bromoacetonitrile
MCAN	=	Chloroacetinitrile
MIL-53	=	Materials of Institut Lavoisier-53
MOFs	=	Metal Organic Frameworks
MTBE	=	Methyl tert-butyl ether
N-DBPs	=	Nitrogenous disinfection by-products

PAC	=	Powder activated carbon
ppb	=	Part per billion, microgram per liter
ppm	=	Part per million, milligram per liter
PZC	=	Point of zero charge
SEM	=	Scanning electron microscopy
TEM	=	Transmission electron microscopy
THMs	=	Trihalomethanes
ZIF-8	=	Zeolitic Imidazolate Framework-8
ZrCl <sub>4</sub>	=	Zirconium chloride
WC-MOFs	=	Washed carbonized Metal Organic Framework
XRD	=	X-ray Diffraction
XPS	=	X-ray Photoelectron Spectroscopy



## CHAPTER I

### INTRODUCTION

#### 1.1 STATE OF PROBLEM

Since the last decade, the world's population is growing by roughly 80 million people each year. Consequently, the demand for fresh and clean water supply is increasing by 64 billion cubic meters a year (Water, 2018). Thailand also has the same trend. At the same time, water pollution is a major environmental concern worldwide. For example, it has been estimated that one-third of world population can be affected by the lack of safe drinking water (Schwarzenbach, Egli, Hofstetter, Von Gunten, & Wehrli, 2010). In general, most of raw water comes from natural freshwater source and it is below the quality for consumption, but high-quality water supply is needed to respond high demand for water consumption

Therefore, the water purification plant has been designed to remove all contaminants which can cause the effect on consumers and produce high-quality water, i.e. coagulation and flocculation, sedimentation, filtration, and disinfection. For disinfection process, chlorine is considered as the most widely used disinfectant due to its efficiency, cost, and convenient for operation. On the other hand, when aqueous free chlorine reacts with natural organic matter (NOM), disinfection by-products (DBPs) are presented in water. Epidemiological studies of DBPs show that potential health risks from DBPs include cancer and reproductive developmental effects, with bladder cancer, showing the most consistency in human epidemiologic studies from several countries (Hrudey, 2009; Jeong et al., 2012)

Haloacetonitriles (HANs) were grouped as Nitrogenous DBPs or N-DBPs that are generally detected at much lower concentrations than carbonaceous DBPs or C-DBPs) (Shah and Mitch,2011), however, N-DBPs are still of high importance as they are often more effect to human health than C-DBPs (Liew et al., 2012a; Plewa et al., 2008a). However, the existing research about toxicity, formation, and control of N-DBPs has resulted in increased interest by their adverse impacts on the environment and effect on public health from several studies (Carter et al., 2019). Therefore, this research has chosen HANs to study of adsorption by novel adsorbents.

From many reviews, Metal–organic frameworks (MOFs), also known as coordination polymers, represent an interesting type of solid crystalline materials that can be straightforwardly self-assembled through the coordination of metal ions/clusters with organic linkers, which mimic the porous nature of zeolite materials. MOFs can be used as gas storage and separation, optical materials, chemical sensing, catalysis, and biomedicine.

Considering the ability of MOFs for gas storage by their extremely high porosities, pore volume and surface areas. Thus, MOFs are challenging to use for liquid storage in HANs adsorption process. However, application as adsorbent for removal of contaminants in aqueous phase of MOFs still has many problems due to their stability against hydrolysis reaction in water condition. Hence, improving stability of porous structure of MOFs and reducing the release of metal from MOFs framework should be concerned. Carbonization under nitrogen flow is one of the most popular modified method that can enhance adsorption efficiency for MOFs, due to increasing of surface area and strengthen porous structure as well as increase of active

functional groups on carbonized materials. Thus, this research has selected carbonization method to modify selected MOFs and investigated the effect of carbonization on adsorption kinetics and isotherms of HANs in aqueous phase.

## 1.2 OBJECTIVE

1. Investigate adsorption rates and capacities of Haloacetonitriles (HANs) by washed carbonized metal-organic frameworks (MOFs) (WCZIF-8, WCMIL-53, WCUIO-66, WCMIL-88b, WCHKUST-1) in tap water.
2. Investigate the effects of molecular structures of HANs on adsorption capacities of washed carbonized MOFs.
3. Investigate adsorption selectivity of adsorbent on HANs adsorption with competitive HANs under mixed solute.

## 1.3 HYPOTHESIS

1. Carbonized Metal-Organic Frameworks (C-MOFs) have higher surface area and surface complexity via metal and carbonized organic functional groups.
2. The molecular structure of HAN in term of amount halogen type atom and the larger molecular of HAN molecule obtains more adsorption capacity and selectivity.

## 1.4 SCOPE OF STUDY

The scope of experiments and the related parameters were concluded as followed and reported in Fig. 1.1 and 1.2.

## 1. Adsorbents

This study was used 16 adsorbents including

- Pristine MOFs (ZIF-8(Zn), MIL-53(Al), MIL-88B(Fe), UiO-66(Zn) and HKUST-1(Cu))
- Carbonized MOFs (C-ZIF-8, C-MIL-53, C-MIL-88B(Fe), C-UiO-66 and C-HKUST-1)
- Washed carbonized MOFs (WC-ZIF-8, WC-MIL-53, WC-MIL-88B(Fe), WC-UiO-66, and WC-HKUST-1)
- Compared with commercial powder activated carbon (PAC Shirasaki-S10)

## 2. Adsorbates

The HANs involved in this paper as adsorbates including four species by following; Chloroacetonitrile (MCAN), Dichloroacetonitrile (DCAN), Bromoacetonitrile (MBAN) and Dibromoacetonitrile (DBAN)

## 3. Adsorption experiment

The adsorption experiments were investigated under batch experiment. Adsorption experiments were used tap water mixed with granular activated carbon (GAC) to remove background contaminant and co-existing DBPs as the solvent for all experiment. pH used tap water was at ~6.5-7.0. The temperature of all experiments was controlled at room temperature (at  $25^{\circ}\text{C} \pm 2$ ).

Adsorbents screening was investigated by using the same amount of each adsorbent with same initial concentration of HANs solution at designed mixing time. The comparison of batch adsorption capacity of each adsorbent

was done, and then three adsorbents that performed the highest HANs adsorption capacity were selected for the study of adsorption kinetics and adsorption isotherms.

Adsorption kinetic experiment was investigated by varying contact time from 0 to 1,560 minutes. The adsorption kinetic models were included pseudo-first-order, pseudo-second-order and the intraparticle diffusion model to describe the adsorption mechanisms.

Adsorption isotherm experiments were investigated by varying concentrations of HANs solution. The adsorption isotherm model i.e. Linear, Langmuir, Freundlich, BET, and Dubinin–Radushkevich (D-R) isotherm were calculated to determine adsorption capacities.

Selectivity adsorption experiment for four types of HANs on selected adsorbent in mixed HANs solution was investigated and compared with the single solution by adsorption capacity.

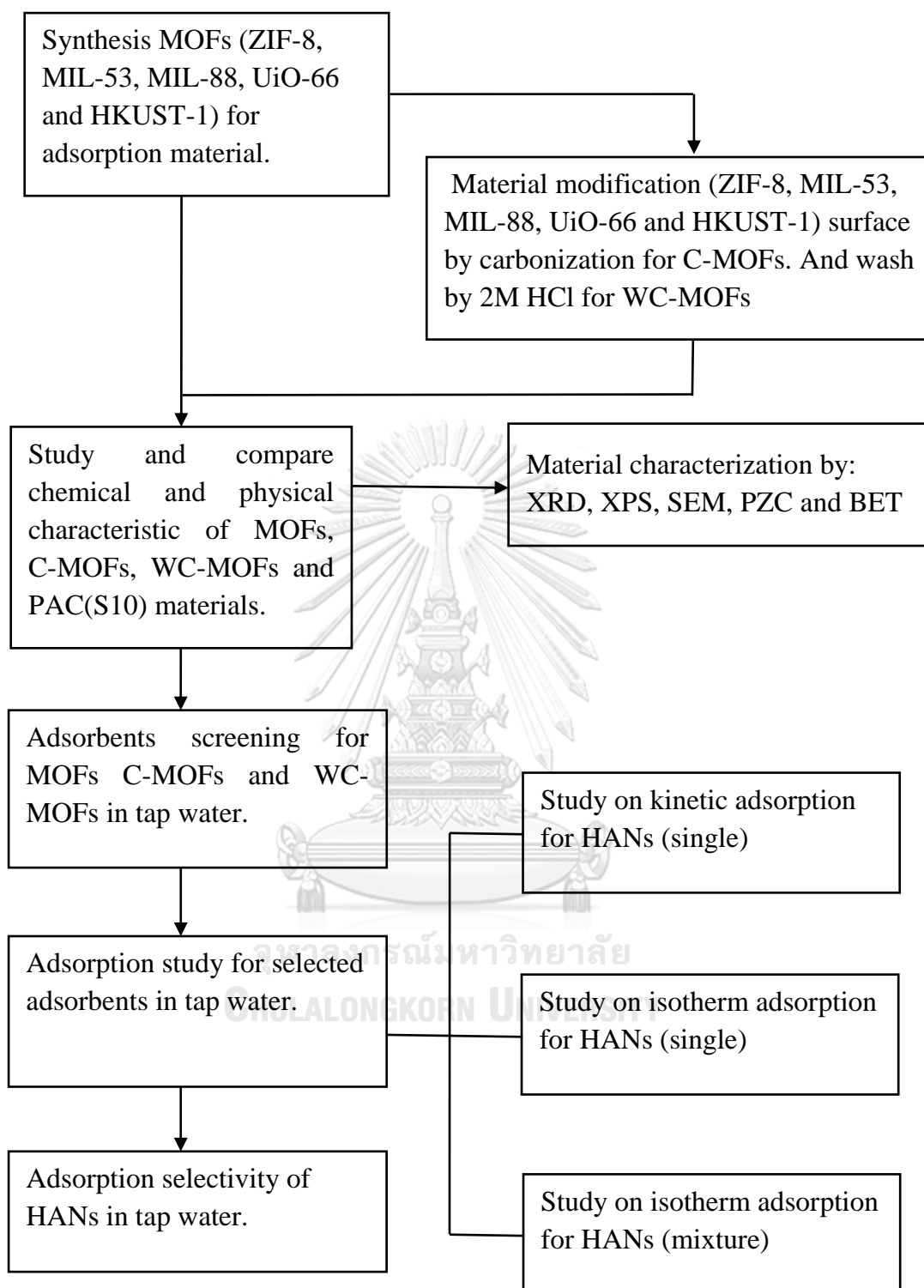


**Figure 1. 1** Flow chart for the scope of study.

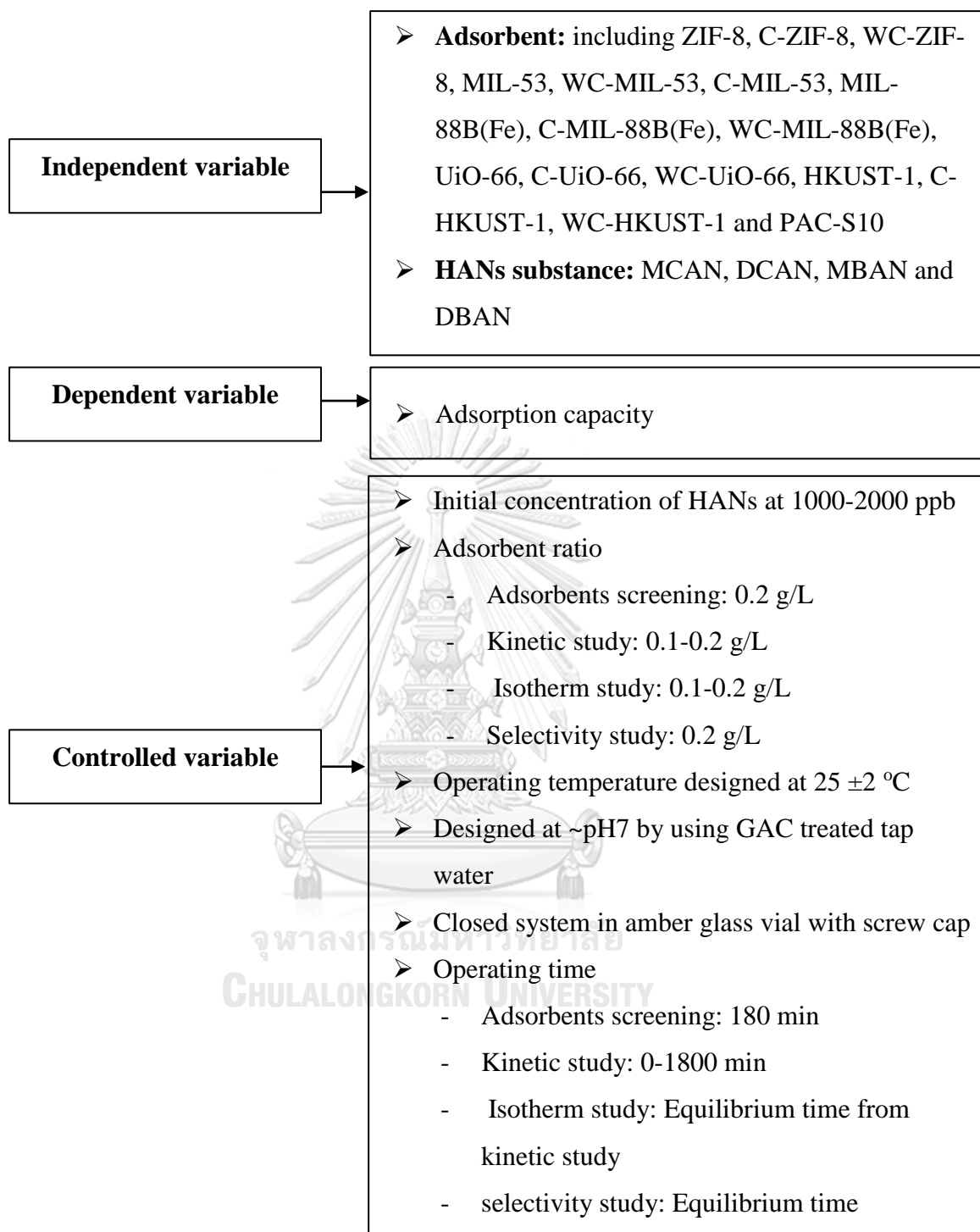


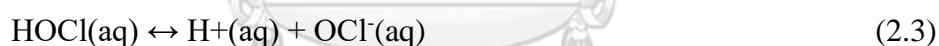
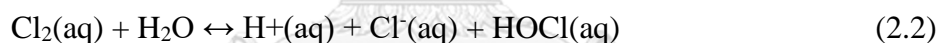
**Figure 1.2** Independent, dependent and controlled variables of the experiments

## CHAPTER II

### THEORETICAL BACKGROUND AND LITERATURE REVIEWS

#### 2.1 DISINFECTION BY-PRODUCT (DBPs)

The conventional water treatment plant has been designed to remove contaminants to supply high-quality water, i.e. coagulation and flocculation, sedimentation, filtration, and disinfection. For the disinfection process, chlorine is one of the most commonly used disinfectant in the disinfection process. Chlorine is very applicable and very effective for the deactivation of most microorganisms in water including pathogenic microorganisms. In addition, chlorine also a costly and easy method for disinfection of water. When using as disinfectant, chlorine may be dissolved in water by the following equilibrium reactions (Weiner, 2012)



From Figure 2.1, at pH below 7.5 (eq. 2.2), hypochlorous acid (HOCl) is the controlling dissolved chlorine species. Above pH 7.5 (eq. 2.3), chlorite anion ( $\text{OCl}^-$ ) is controlling. The energetic disinfection species,  $\text{Cl}_2$ , HOCl, and  $\text{OCl}^-$ , are the total free available chlorine, but chloride ion ( $\text{Cl}^-$ ) does not act as disinfectant. HOCl is the most efficient as a microorganisms killer because it can penetrate cell membranes of microorganisms easier than can  $\text{OCl}^-$ .



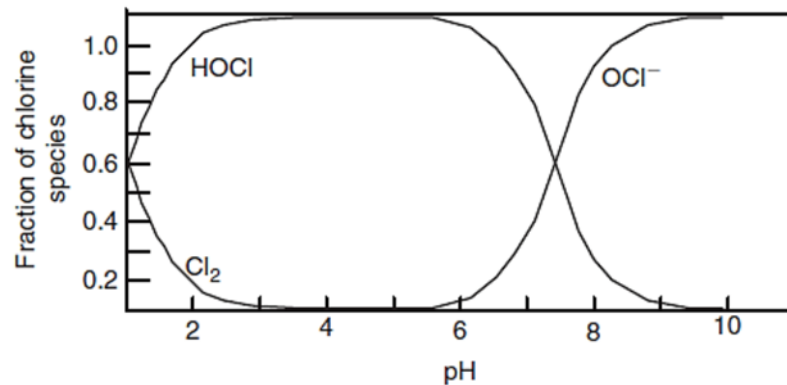


**Figure 2.1** Distribution diagram for dissolved chlorine species. (at pH 7.5,  $[\text{HOCl}] = [\text{OCl}^-]$ ) (Weiner, 2012)

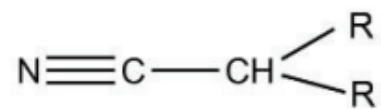
Unfortunately, Free chlorine radical,  $\text{Cl}^\cdot$ , can react with natural organic matter naturally occurring in water to form disinfection by-products (DBPs) that may cause health risks. On the other hand, when aqueous free chlorine reacts with natural organic matter (NOM), disinfection by-products (DBPs) can be formed in treated water. Epidemiological studies of DBPs show that potential health risks from DBPs include cancer and reproductive developmental effects, with bladder cancer, showing the most consistency in human epidemiologic studies from several countries. DBPs are several organic and inorganic compounds that had found in water. Although 600-700 of DBPs have been identified in water, there are few major halogenated DBPs which commonly study such as Trihalomethanes (THM), Haloacetic acids (HAAs). The summary of DBPs and their effect are shown in Table 1. (Gopal, Tripathy, Bersillon, & Dubey, 2007)

**Table 2.1** DBPs and its health effect

Class of DBPs	Compounds	Health effects
Trihalomethanes (THM)	Chloroform	Cancer, liver, kidney and reproductive effects
	Dibromochloromethane	Nervous system, liver, kidney and reproductive effects
	Bromodichloromethane	Cancer, liver, kidney and reproductive effects
	Bromoform	Cancer, liver, kidney and reproductive effects
Haloacetonitrile (HAN)	Trichloroacetonitrile	Cancer, mutagenic and clastogenic effects
Halogenated aldehydes and ketones	Formaldehyde	Mutagenic
Halophenol	2-Chlorophenol	Cancer and tumor promoter
Haloacetic acids (HAA)	Dichloroacetic acid	Cancer and reproductive and developmental effects
	Trichloroacetic acid	Liver, kidney, spleen and developmental effects

## 2.2 HALOACETONITRILES (HANs)

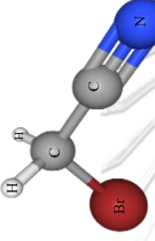
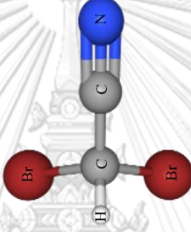
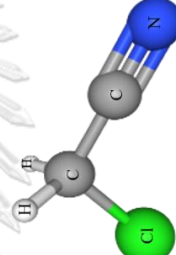
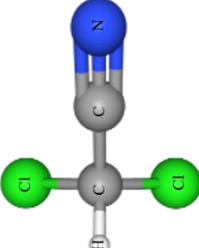
HANs are a relatively new class of nitrogenous disinfection by-products (N-DBPs), characterized by higher genotoxicity and cytotoxicity than the relatively THMs or HAAs. Many studies found that several factors, such as pH, temperature, disinfection doses, reaction time, and concentrations of halides are associated with the formation of HANs. HANs are from the chlorination in water usually shows in the formation of  $X_nCH_nCN$  as shown in Figure 2.1. This study considered four HANs substances, as shown in Table 2.2.



**Figure 2.2** The structure of HANs



Table 2.2 Properties of selected HANs substances

Name	Formula	Name	Structure (PubChem)	Molecular weight MW ( $\text{g}\cdot\text{mol}^{-1}$ )	Solubility (HSBD)( $\text{mg}\cdot\text{ml}^{-1}$ )
1. Bromoacetonitrile	$\text{C}_2\text{H}_2\text{BrN}$	MBAN		119.95	50-100
2. Dibromoacetonitrile	$\text{C}_2\text{HBr}_2\text{N}$	DBAN		198.84	9.6
3. Chloroacetonitrile	$\text{C}_2\text{H}_2\text{ClN}$	MCAN		75.5	$1 \times 10^5$
4. Dichloroacetonitrile	$\text{C}_2\text{HCl}_2\text{N}$	DCAN		109.94	33.5

Due to HANs routes of exposure are breathing (inhalation), eating or drinking (ingestion), or contact with the skin (dermal contact). The level of concern of the adverse health effects of these toxic agents is increasing with the increased level of compromised source waters used in the generation of drinking water from their treatment reagent, and new emerging DBP classes are entering the drinking water stream

Nowadays, there is no regulation of HANs contaminant in drinking water as THMs and HAAs. However, the World Health Organization (WHO) has set for the guideline for 3 HANs substances. DCAN and DBAN, which were shown in Table 2.3.

**Table 2.3** HANs guideline values for drinking-water quality (WHO, 2011)

HANs substances	Guideline value ( $\mu\text{gL}^{-1}$ )
DCAN (Dichloroacetonitriles)	20
DBAN (Dibromoacetonitriles)	70

Researchers (Plewa & Wagner, 2015) has used mammalian cell microplate-based assays and generated *in vitro*, systematic, analytical, comparative databases on the chronic cytotoxicity and genotoxicity of individual DBPs including for N-DBPs and they found that HANs were in the middle class of comparative chronic cytotoxicity in Chinese hamster ovary (CHO) cells (LC50).

Although there are many studies on the toxicity of HANs, the metabolic mechanism and direct influence of HANs to human health remain unclear because of most epidemiological studies, the DBP metric is the concentration of trihalomethanes (THMs) in drinking water. Few studies have compared to HANs or new types of emerging DBPs. Nevertheless, HANs still are in their high toxicity DBPs, which are harmful to humans, need for more study, and research in fields of risk assessment and reduction or elimination procedures. Therefore, this research has chosen HANs to study of adsorption by carbonized-MOFs.

The adverse effects could be investigated due to the simultaneous presence of HANs, even if at low concentrations. Wastewater plant design high-performance treatments to produce high-quality water supply, i.e. hybrid technologies, combinations of conventional and advanced treatments, are proving effective solutions to reach almost complete removal and improving the cost of processes. One of the treatment processes that can use for purification water is adsorption process which use appropriate adsorbent to adsorb pollutant in water even in low concentration.

### **2.3 METAL ORGANIC FRAMEWORKS (MOFs)**

From the review of Bin Li (Li et al., 2016), Metal–organic frameworks (MOFs), also known as coordination polymers, represent an interesting type of solid crystalline materials that can be straightforwardly self-assembled through the coordination of metal ions/clusters with organic linkers, which mimic the porous nature of zeolite materials. MOFs materials can succeed in the functions of both site, metal ions/clusters, and organic linkers. Hence MOFs can provide special properties such as electronic, magnetic, and optical properties of such inorganic and organic

building units to develop multifunctional materials. MOFs also can be used as gas storage and separation, optical materials, chemical sensing, catalysis, and biomedicine.

Considering the ability of MOFs for gas storage, researchers (Furukawa et al., 2010) have found that MOFs are efficiency material for H<sub>2</sub> storage by their extremely high porosities, pore-volume, and surface areas. Thus, MOFs are challenging to use for liquid storage in HANs adsorption process.

## **2.4 ADSORBENT IN THIS STUDY**

### **2.4.1 ZIF-8**

ZIF8 (Zeolitic Imidazolate Framework) is a metal-organic framework (MOF) made by zinc ions coordinated by four imidazolate rings in the same way as Si, and Al atoms are covalently joined by bridging oxygens in zeolites as the structure in Figure 2.2a. The sphere represents the pore size within the framework, which can be used for gas storage.

### **2.4.2 MIL-53 (Al)**

The MIL-53 materials family has recently attracted a lot of attention for gas adsorption (Boutin, A., 2009). This study considered to use MIL-53(Al) for HANs adsorption. A framework topology of MIL-53 is formed of unidimensional chains of corner-sharing Al(NO<sub>3</sub>)<sub>3</sub> octahedra linked by terephthalic acid ligands, which results in linear lozenge-shaped channels large enough to accommodate small guest molecules as shown in Figure 2.2b.

### 2.4.3 MIL-88B (Fe)

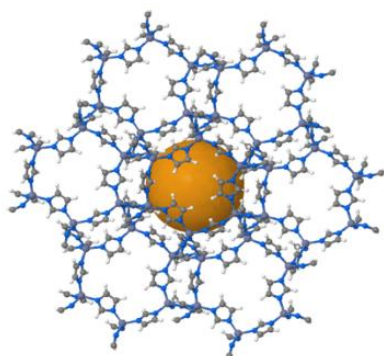
MIL-88B (Fe) frameworks (MIL = Matériaux de l'Institut Lavoisier/ Materials from the Lavoisier Institute) have been reported on their exceptionally large bulk, as shown in Figure 2.2c. The capacity of the MIL-88B's unit cell to reversibly swell and shrink under the influence of an external stimulus (temperature, pressure, chemical inclusion) without harming the framework topology. Such behavior is unusual for solid crystals and thus of great interest for selective adsorption of gases or solvents

### 2.4.4. UiO-66

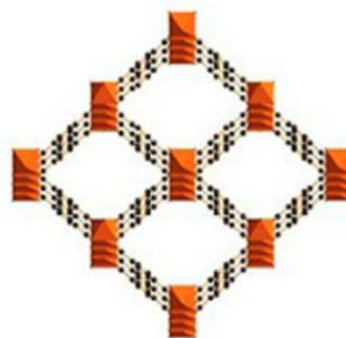
UiO-66 (University of Oslo) is a metal-organic framework made up of  $[\text{Zr}_6\text{O}_4(\text{OH})_4]$  clusters with 1,4-benzodicarboxylic acid struts. The orange sphere shows the primary pore size, and the green sphere shows the secondary pore size, both of which can be used for gas storage as shown in Figure 2.2d.

### 2.4.5. HKUST-1

HKUST-1 (Hong Kong University of Science and Technology), Figure 2.2e is a metal-organic framework (MOF) made up of copper nodes with Trimesic acid struts between them. The spheres represent the pore sizes within the framework, which can be used for gas storage.



(a)



(b)



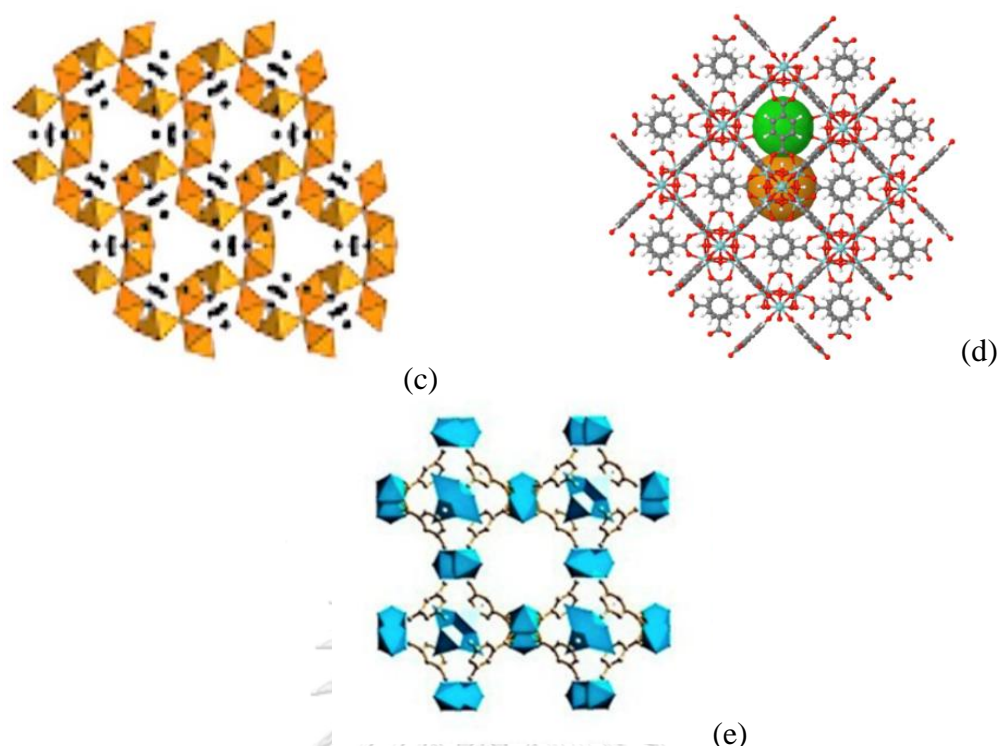


**Figure 2.3** MOFs structure; (a) ZIF-8(Zn), (b) MIL-53(Al), (c) MIL-88B (Fe), (d) UiO-66(Zr) and (e) HKUST-1(Cu).

## 2.5 ADSORPTION THEORY

### 2.5.1 ADSORPTION APPLICATION

In general, the adsorption process has been used as water purification technology. The adsorption process is widely used for many sources of water, i.e. industrial influent/effluent water, groundwater, water supply, and also in drinking water production. Adsorption method presents several advantages for water purification which is easy to use and operate and also has flexibility for many conditions, requires low energy, and has ability to regenerate the exhausted adsorbent. Overall, the performances of adsorption process depend on several internal and external factors including the type of adsorbent, selectivity of adsorbent, properties of target pollutant, concentration of target pollutant in water, operating condition, cost-

effectiveness plan and pollutant standard goals (Bonilla-Petriciolet, Mendoza-Castillo, & Reynel-Ávila, 2017)

### 2.5.2 ADSORPTION MECHANISM

For the adsorption mechanism, when a molecule attached to a surface, it can bind with either a chemical interaction (chemisorption) and/or physical interaction (physisorption). Chemisorption involves the formation of a chemical bond between the adsorbate and the surface. Physisorption involves weaker interactions relate to the polarization of the adsorbate and surface rather than electron transfer between them.

For HANs adsorption mechanism with inorganic adsorbents was studied by (Prarat, Ngamcharussrivichai, Khaodhiar, & Punyapalakul, 2011). They proposed the FT-IR analysis result to indicated that the adsorption mechanism involves a more complex interplay between an ion-dipole electrostatic interaction and chemisorption.

### 2.5.3 MODEL FOR ADSORPTION MECHANISM

#### Adsorption capacity

The adsorption capacity of adsorbent can calculate by the following equation.

$$q = \frac{(C_0 - C_e)}{M} \times V \quad (2.4)$$

$$\%removal = \left( \frac{C_0 - C_e}{C_0} \right) \times 100 \quad (2.5)$$

Where; q = Adsorption capacity (µg/g)

$C_0$  = Initial adsorbate concentration at equilibrium (µg/L)

$C_e$  = Final adsorbate concentration (µg/L)

M = Mass of adsorbent (g)

V = Volume of solution (L)

### Adsorption kinetic

Adsorption kinetic is used for describing the rate of adsorption reaction and always fitted with two classical models. First, pseudo-first-order model and second is pseudo-second-order model. The applicability of these kinetics models were determined by measuring the coefficients of determination ( $R^2$ ). High values of  $R^2$  indicate that the model is appropriate for the data (Safa & Bhatti, 2011).

#### A. Pseudo-first-order model

$$q_t = q_e(1 - \exp^{-k_1 t}) \quad (2.6)$$

$$\ln(q_e - q_t) = \ln q_e - k_1 t \quad (2.7)$$

$$\log(q_e - q_t) = \log q_e - \frac{k_1}{2.303} t \quad (2.8)$$

Where;  $q_t$  = Adsorption capacity ( $\mu\text{g/g}$ ) at time (min)  
 $q_e$  = Adsorption capacity ( $\mu\text{g/g}$ ) at equilibrium  
 $k_1$  = Pseudo first order rate constant, slope

#### B. Pseudo-second-order model

$$q_t = \frac{q_e^2 k_2 t}{1 + q_e k_2 t} \quad (2.9)$$

$$\frac{t}{q_t} = \frac{1}{k_2 q_e^2} + \frac{t}{q_e} \quad (2.10)$$

Where;  $q_t$  = Adsorption capacity ( $\mu\text{g/g}$ ) at time (min)  
 $q_e$  = Adsorption capacity ( $\mu\text{g/g}$ ) at equilibrium

$k_2$  = Pseudo second order rate constant, calculated slope from plot between  $t/q_t$  vs  $t$

### Adsorption isotherms

#### A. Freundlich's isotherm

$$q_e = K_F C_e^{1/n} \quad (2.11)$$

$$\log q_e = \log K_F + (1/n) \log C_e \quad (2.12)$$

Where;  $q_e$  = Adsorption capacity ( $\mu\text{g/g}$ ) at equilibrium

$K_F$  = The measure of sorption capacity

$1/n$  = Adsorption intensity

$C_e$  = Final concentration ( $\mu\text{g/L}$ )

$K_F$  and  $1/n$  can find from intercept and slope respectively of the linear plot of  $\log q_e$  vs  $\log C_e$

#### B. Langmuir's isotherm

$$q_e = \frac{q_m K_L C_e}{1 + K_L C_e} \quad (2.13)$$

Where;  $q_e$  = Adsorption capacity ( $\mu\text{g/g}$ ) at specific amount of adsorbent

$q_e$  = Adsorption capacity ( $\mu\text{g/g}$ ) at equilibrium

$q_m$  = Maximum amount adsorbate to form a monolayer ( $\mu\text{g/g}$ ) at equilibrium

$K_L$  = The Langmuir constant

$C_e$  = Final concentration ( $\mu\text{g/L}$ )

\*  $K_L$  and  $q_m$  can find from the liner plot of  $C_e/q_e$  vs  $C_e$

$$\frac{C_e}{q_e} = \frac{1}{K_L q_e} + \frac{1}{q_m} C_e \quad (2.14)$$

The Langmuir isotherm can be used to predict the affinity between adsorbate and adsorbent by using the dimensionless equilibrium parameter  $R_L$ , which showed in (2.15) equation.

$$R_L = \frac{1}{1 + K_L C_0} \quad (2.15)$$

Where;  $K_L$  = The Langmuir constant

$C_0$  = Initial concentration ( $\mu\text{g/L}$ )

\* If the value of  $R_L$  is between 0 to 1 for favorable adsorption, but  $R_L > 1$  for unfavorable adsorption. The value of  $R_L$  equal to 1 represents linear adsorption. The value of  $R_L$  equal to 0 showed that the adsorption process is irreversible.

### C. BET isotherm

When the initial adsorbed layer becomes a surface for further adsorption, instead of the isotherm stabilized in a saturated monolayer, the formation of multilayers can be expected. The most widely used isotherm for the multilayer adsorption was derived by Brunauer (Brunauer, Emmett, & Teller, 1938) and is called the BET isotherm.

$$q_e = \frac{q_{BET} k_1 C_e}{(1 - k_2 C_e)(1 - k_2 C_e + k_1 C_e)} \quad (2.16)$$

Where;  $q_t$  = Adsorption capacity ( $\mu\text{g/g}$ ) at time (min)

$q_e$  = Adsorption capacity at equilibrium ( $\mu\text{g/g}$ )

$C_e$  = Final concentration ( $\mu\text{g/L}$ )

$q_{\text{BET}}$  = The monolayer adsorption capacity ( $\mu\text{g/g}$ )

$k_1, k_2$  = The BET constants ( $\text{L}/\mu\text{g}$ ).

#### D. Dubinin–Radushkevich (D-R) Isotherm

The Dubinin–Radushkevich (D-R) isotherm model considers that adsorbent size is comparable to the micropore size, and the adsorption equilibrium relation for a given adsorbate–adsorbent combination can be expressed independently of temperature by using the adsorption potential ( $\varepsilon$ ),

$$\varepsilon = RT \ln \left( 1 + \frac{1}{C_e} \right) \quad (2.17)$$

The D-R isotherm assumes a Gaussian-type distribution for the characteristic curve and the model can be described by Eq.15 and sorption free energy can find by Eq. 16

$$q_e = q_{\text{max}} \exp(-\beta \varepsilon^2) \quad (2.18)$$

$$E = \frac{1}{(2\beta)^{1/2}} \quad (2.19)$$

Where;  $q_t$  = Adsorption capacity ( $\mu\text{g/g}$ ) at time (min)

$C_e$  = Final concentration ( $\mu\text{g/L}$ )

$q_e$  = Adsorption capacity at equilibrium ( $\mu\text{g/g}$ )

$\beta$  = The the mean sorption free energy ( $\text{kJ/mol}$ )

$\varepsilon$  = Adsorption potential

$E$  = Free energy ( $\text{kJ/mol}$ )

## 2.6. CARBONIZATION

There are many methods to improve, adapt or develop adsorption materials for more efficiency in each application. The carbon material is one of the most popular modified materials for adsorption. Thus, this research will select carbonization method to modify adsorbents for study kinetic, isotherm and capacity in adsorption application. The well-known carbon material is activated carbon, which produced from carbonization by heating in an inert atmosphere such as flue gas via dehydration and devolatilization of the carbon. Carbonization reduces the volatile content of the source material to under 20%. The black outcomes are unique and versatile adsorbents because they have a large surface area, highly microporous character, and a high degree of surface reactivity. They are universal adsorbents which can adsorb varying amounts of organic or inorganic compounds. The most widely used carbonized adsorbents have surface areas between 800 and 1500 m<sup>2</sup>/g.

### 2.6.1 CARBONIZATION ATMOSPHERE

For more studied for carbonization in 2018, Wang and his team (Wang et al., 2018) had studied pyrolysis in different atmospheres between N<sub>2</sub> and CO<sub>2</sub>. As a result, they found that in N<sub>2</sub> atmosphere, mass loss of this interval was mainly attributed to the thermal decomposition of minerals, so the residue after pyrolysis was char and ash, while in CO<sub>2</sub>, the char gasification by CO<sub>2</sub> occupied a more prominent role and therefore only ash remained. The semi-quantitative EDS results can be confirmed that the carbon content in the residue of N<sub>2</sub> atmosphere was 10.88 wt.% while that of CO<sub>2</sub> atmosphere was 3.3 wt.%.

Currently, in 2015, They (Bakhtiari et al., 2015) reported the study about the efficiency of the obtained MOF-derived nanoporous carbon (MOF-NC) particles as adsorbent for the removal of copper (Cu) ions from an aqueous solution. The sample was carbonized a tube furnace and was exposed to a flow of N<sub>2</sub> for an hour. After that, the furnace was heated to 800°C with a rate of 5 °C min<sup>-1</sup>, kept for 5 hrs and cooled down to room temperature.

In 2016, Chen and team (Shen, Chen, Chen, & Li, 2016) also used N<sub>2</sub> flow for simple one-step direct carbonization using the synthesized MOFs as precursors. The MOFs (0.200 g) was taken in a silica boat and then placed in a tube furnace and heated from room temperature to 800 °C under N<sub>2</sub> gas with a heating rate of 5 °C min<sup>-1</sup>. After reaching the target temperature (800 °C), the temperature was maintained at 800 °C for 5 hours, after that cooled down to room temperature with a cooling rate of 1 °C min<sup>-1</sup>. From both studies, carbonization with N<sub>2</sub> flow was select as method for material modification in this research.

### **2.6.2. CARBONIZATION TEMPERATURE**

Wancharop and team studied carbonized zeolitic imidazolate framework (ZIF-8) with different temperatures in the ranges of 600-1000 °C without adding external carbon sources. As a result, they concluded that ZIF-8 @900°C (Fig.3) showed the best capacity performance with surface area 1075 m<sup>2</sup>/g, which can be compared with ZIF-8@1000 °C that had 1110 m<sup>2</sup>g<sup>-1</sup>.



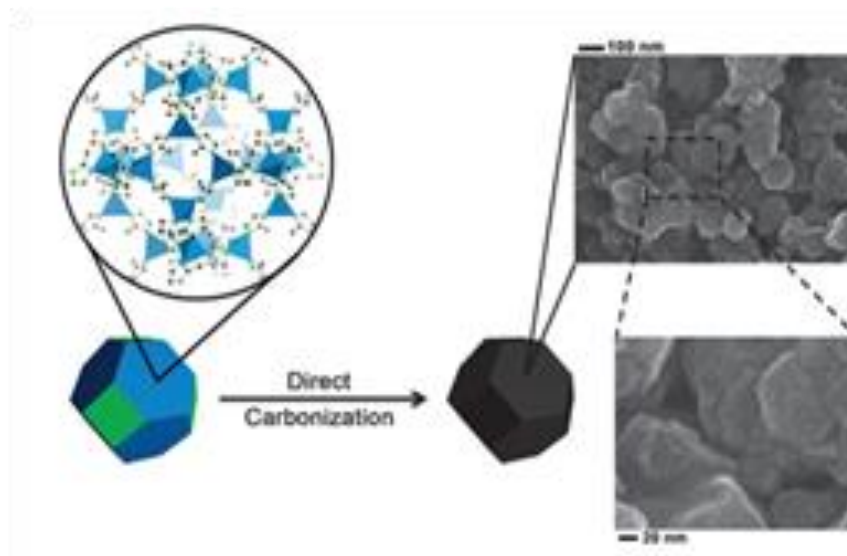


**Figure 2.4** ZIF-8 through direct carbonization

From ASC Nano journal (2014), They (S. Zhao et al., 2014) studied for MIL-88B pyrolyzed at different temperatures are used as the Oxygen Reduction Reaction (ORR) catalysts (the samples pyrolyzed at 700, 800, and 1000°C) suggesting that 900°C is the optimal pyrolysis temperature for obtaining highly active ORR catalysts.

This study (Young et al., 2016) also focused on nanoporous carbon materials prepared by direct carbonization of zeolitic imidazolate frameworks (ZIF-8) towards supercapacitor applications. Several types of nanoporous carbons have been prepared by varying the applied carbonization temperature. They demonstrated the effects of various factors (e.g., surface area, nitrogen content, degree of graphitization, and relative percentage of micropores) on the performance. The result showed that ZIF-8, which carbonized at 900 °C is the optimal carbonization temperature for ZIF-8, the highest surface area.

**Table 2.4** Surface areas, pore volumes, micropore volumes, and percentages of micropores for nanoporous carbons prepared at various temperatures

Temperature (°C)	$S$ ( $\text{m}^2 \text{g}^{-1}$ )	$V$ ( $\text{cm}^3 \text{g}^{-1}$ )	$V_{\text{micro}}$ ( $\text{cm}^3 \text{g}^{-1}$ )	$V_{\text{micro}}/V$ (%)
700	1032	0.80	0.329	41.1
800	1678	0.97	0.531	54.7
900	1823	1.40	0.551	39.4
1000	1591	0.89	0.595	66.7
AC	2370	1.38	0.987	71.5

Carbonized ZIF-8 can keep the polyhedron structure the same as ZIF-8, as shown in Figure 2.3, with high surface area, open-pore network of the carbon matrix, which can facilitate fast molecular diffusion of Cu ions in aqueous solutions with excellent adsorption performance. Their ZIF-8-NC showed an impressive saturation capacity for Cu ions compared with commercial activated carbons. From previous study, this research will use temperature for carbonization at 900°C for all MOFs material.

## CHAPTER III

### RESEARCH METHODOLOGY

#### 3.1. EQUIPMENTS AND MATERIALS

##### 3.1.1. EQUIPMENTS AND GLASSWARES

1. Beaker 25, 100, 250, 500 and 1,000 mL
2. Volumetric flask 25, 50, 100 and 1,000 mL
3. Amber glass bottle with screw cap 200 mL
4. Amber Duran glass bottle with screw cap 250 and 500 mL
5. Duran glass bottle with screw cap 250 and 500 mL
6. Amber glass vial 40 mL with silicone/PETE septa cap
7. Amber glass vial 2 mL with septa cap
8. Teflon-lined stainless-steel autoclave
9. Glass funnel 40 mm
10. Stainless steel spatula
11. Test tube rack 28 mm
12. Thermometer
13. Magnetic bar
14. Porcelain dish
15. Forceps
16. Centrifuge tube
17. Buchner funnel and flask
18. Desiccator
19. PETE cylinder 10 mL
20. Nylon filter 25  $\mu$ m
21. Auto pipette tips
22. Stirring rod
23. Vortex
24. Magnetic stirrer
25. Rotary shaker
26. Fume hood
27. GC/ECD
28. Oven
29. Nitrogen flow furnace
30. Centrifuge

### 3.1.2. CHEMICAL

1. HCL 37%
2. NaOH 8 M
3.  $\text{Zn}(\text{NO}_3)_2 \cdot 6\text{H}_2\text{O}$
4. 2-methylimidazole
5.  $\text{Al}(\text{NO}_3)_3$
6. DMF
7. Acetone
8. Methanol
9. Ethanol
10.  $\text{FeCl}_3 \cdot 6\text{H}_2\text{O}$
11. Terephthalic acid
12.  $\text{ZrCl}_4$
13. Acetic acid
14.  $\text{Cu}(\text{NO}_3)_2 \cdot \text{H}_2\text{O}$
15. Trimesic
16.  $\text{Na}_2\text{SO}_4$
18. MTBE
19. DI water
20.  $\text{KH}_2\text{PO}_4$
21.  $\text{K}_2\text{HPO}_4$
22. HANs compound (MCAN, DCAN, MBAN and DBAN)



## 3.2. MATERIALS SYNTHESIS

### 3.2.1. ZIF-8, C-ZIF-8 and WC-ZIF-8

#### A. ZIF-8

ZIF-8, synthesized in a purely aqueous system. Zinc nitrate hexahydrate ( $\text{Zn}(\text{NO}_3)_2 \cdot 6\text{H}_2\text{O}$ ) (5 mmol) and 2-methylimidazole (mIm) (40 mmol) are dissolved in separate 100 mL portions of methanol. The two clear solutions are combined and stirred rapidly for 1 h, during which time the combined solution became cloudy due to the precipitation of nanoparticles (NPs) of ZIF-8. The ZIF-8 colloid is separated from the solution by three times of centrifugation at 5000 rpm for 15 min and resuspension of the nanoparticles in DI water, filtrate by GF/C filter, and the product is further dried at room temperature in a desiccator with reduced pressure (Tian et al., 2014).

#### B. C-ZIF-8 and WC-ZIF-8

The product of ZIF-8 is added through the direct carbonization under nitrogen flow for 1 hour at 900 °C, with heating rate at 10 °C min<sup>-1</sup>, without any pre-treatments. Wash carbonized ZIF-8 by 2 M HCL and dried at 120 °C. Finally, washed carbonized ZIF-8 was produced.

### 3.2.2. MIL-53(Al), C-MIL-53(Al) and WC-MIL-53(Al)

#### A. MIL-53(Al)

MIL-53(Al), A solution containing 8 mmol aliquot of  $\text{Al}(\text{NO}_3)_3$ , 4 mmol 1,4-benzenedicarboxylic acid, and 8 mmol sodium hydroxide are mixed in a 100 mL distilled water at room temperature for 24 hour. The pore of materials are activated by DMF solvent exchange at 150 °C for 24 hours by transferred to a Teflon lined stainless steel autoclave. The synthesized light-yellow MIL-53(Al) solid is washed

with methanol to remove the DMF solvent from the pores of the material. And sticky cloudy product was oven at 150 °C for 24 hours. After that the light-yellow powder product is dried at 105 °C for 24 hours (Sánchez-Sánchez et al., 2015)

#### B. C-MIL-53(Al) and WC-MIL-53(Al)

The product of MIL-53 (Al) is added through the direct carbonization under nitrogen flow for 1 hour at 900 °C, with heating rate at 10 °C min<sup>-1</sup>, without any pre-treatments. Wash carbonized MIL-53 (Al) by 2 M HCL and dried at 105 °C. Finally, washed carbonized MIL-53 (Al) were produced.

### 3.2.3. MIL-88B (Fe), C-MIL-88B (Fe), WC-MIL-88B (Fe)

#### A. MIL-88B (Fe)

The synthesis method was adapted from (Gholizadeh Khasevani & Gholami, 2018) and Nanotech's method. A 1.5 mmol of FeCl<sub>3</sub> 6H<sub>2</sub>O and 1.5 mmol 1,4-benzenedicarboxylic acid are dissolved in 30 mL DMF then stirred with a magnetic stirrer for 30 minutes. The mixture is kept in autoclave Teflon liner and heated in oven at 110 °C for 24 hours. The product is isolated by centrifugation. Wash the product by fresh methanol for 12 hours for 3 times, dried at 105 °C for 12 hours.

#### B. C-MIL-88B (Fe) and WC-MIL-88B (Fe)

The product of MIL-88(Fe) is added through the direct carbonization under nitrogen flow for 1 hour at 900 °C, with heating rate at 10 °C min<sup>-1</sup>, without any pre-treatments. Wash carbonized MIL-88B(Fe) by 2 M HCL and dried at 105 °C. Finally, washed carbonized MIL-88 (Fe) were produced.

### 3.2.4. UiO-66 (Zr), C-UiO-66 (Zr) and WC-UiO-66 (Zr)

#### A. UiO-66 (Zr)

The synthesis of UiO-66(Zr) is carried out by 1.5 mmol of  $ZrCl_4$  and 1.5 mmol of 1,4-benzenedicarboxylic acid were dissolved in 30 mL DMF, then add 19.3 mL acetic acid and stirred with a magnetic stirrer for 30 minutes. The mixture is placed in Teflon-lined autoclave and heated in oven at 140 °C for 24 hours. The product was isolated by centrifugation. Wash the product by fresh methanol for 12 hours for three times, dried at 105 °C for 12 hours (Jin & Yang, 2017)

#### B. C-UiO-66 (Zr) and WC-UiO-66 (Zr)

The product of UiO-66(Zr) is added through the direct carbonization under nitrogen flow for 1 hour at 900 °C without any pre-treatments. Wash carbonized UiO-66 (Zr) by 2 M HCL and dried at 105 °C. Finally, washed carbonized UiO-66 (Zr) was produced.

### 3.2.5. HKUST-1, C-HKUST-1, and WC-HKUST-1

#### A. HKUST-1

0.875 g of  $Cu(NO_3)_2 \cdot H_2O$  are dissolved in 12 mL of DI water, and 0.42 g of Trimesic are dissolved in 12 mL of ethanol. Subsequently, both solutions were mixed, kept under stirring with magnetic stirrer of 60 min and then placed in Teflon-lined autoclave at 120 °C in oven for 16 hours. Finally, turquoise crystals are collected and dried at 120 °C for 10 hours. (Chiericatti, Basilico, Basilico, & Zamaro, 2012; Lin, Adhikari, Ku, Chiang, & Kuo, 2012)

#### B. C-HKUST and WC-HKUST-1

The product of HKUST-1 is added through the direct carbonization under nitrogen flow for 1 hour (at temperature ranges of 600–900 °C) without any pre-treatments. Wash carbonized HKUST-1 by 2 M HCL and dried at 105 °C. Finally, washed carbonized HKUST-1 was produced.

### 3.2.6. Powder activated carbon (PAC)

Shirasagi S10 powder activated carbon in this study was bought from Japan EnviroChemicals, Ltd. (JEC).

### 3.3. ADSORBENT CHARACTERIZATION

Synthesized adsorbents were characterized the properties by the following methods. X-ray Powder Diffraction (XRD) was applied to prove the quality of synthesized MOFs with the references by phase identification of crystalline structure. The equipment used in this study was SmartLab X-Ray Diffractometer, Rigaku. The X-ray photoelectron spectroscopy (XPS) spectra were acquired by using a Kratos/Axis ultra DLD spectrometer to determine surface composition of materials. The texture of adsorbents were observed by scanning electron microscopy (SEM) with S-4800, Hitachi. Surface areas of adsorbents were measured by physical gas adsorption of surface area analyzer, Autosorb-1, Quantachrome. Fourier transform infrared spectrometer (FT-IR) based analysis of the adsorbent surface was performed to investigate the active surface functional groups. The batch equilibrium method of acid-base titration was applied for measuring point of zero charge (PZC) of synthesized adsorbents.

### 3.4. REAGENT PREPARATION

#### 3.4.1. Phosphate buffer

Phosphate buffer stock was prepared by mixture of 10 g of potassium phosphate ( $\text{KH}_2\text{PO}_4$ ) and 5.8 g of dipotassium phosphate ( $\text{K}_2\text{HPO}_4$ ), then stirring for 1 hour in 100 mL of DI water; both buffer salts should be in granular form and of ACS grade or better. After that the solution was kept in bottle with screw cap for dilution.



Fresh phosphate buffer was diluted from 10 mL phosphate buffer stock into 1000 mL of DI water for 0.01 M phosphate buffer.

### 3.4.2. Distilled water reagent

Reagent water was defined as purified water, which does not contain any measurable quantities of any target analytes or any other interfering species. This research used DI water 18  $\Omega$  from Elga purelab ultra machine.

### 3.4.3. Tap water reagent

DBPs background of tap water was adsorbed by mixing 1000 mL of tap water with 10 g of GAC for 30 minutes. After filtrate GAC from tap water by GF/C filter, tap water was measured organic carbon by UV-VIS spectrophotometer at wavelength 254 nm and total organic carbon analyzer (TOC). The organic carbon in tap water was detected in very low concentration <0.002 mg carbon/L. The existing of HANs substances in tap water was also investigated by using GC/ECD. The treated tap water was used for all experiments in this study.

## 3.5. ADSORBATE PREPARATION

HANs sample were prepared by using four chemicals as followed:

Bromoacetonitrile (MBAN) Alfa Aesa, CAS:590-17-0

Dibromoacetonitrile (DBAN) Alfa Aesa, CAS: 3252-43-5

Chloroacetonitrile (MCAN) Alfa Aesa, CAS: 545-06-2

Dichloroacetonitrile (DCAN) Sigma-Aldrich, CAS: 3018-12-0

Each chemical was diluted in acetone by calculated volume for stock of 500 ppm. After that, stock of each chemical was dilute with treated tap water to designed concentration for fresh initial concentration.

### 3.6. ADSORBENTS PREPARATION

Adsorbents were kept in the desiccator all the time. Before adsorption activities, every adsorbent was dehumidified by drying at 105°C for 3 hours.

### 3.7. POINT OF ZERO CHARGE STUDY

The pH at point of zero charge (pH<sub>pzc</sub>) was determined by loading 0.1 g of sample into 50 mL of tap water with different initial pH value. HCl (0.01 M) and NaOH (0.01 M) was used to adjust the range between 2 and 12. The mixtures were shaken at room temperature for 24 h and the final pH was measured using a pH meter. The pH<sub>pzc</sub> value was evaluated at the point at which the initial pH value equals to the final pH.

### 3.8. ADSORBENT SCREENING

A stock solution of each HANs was prepared under batch experiment at initial concentration of 1000 ppb in treated tap water at the indicated pH. In adsorbent screening study, 0.010 g. of adsorbents (ZIF-8(Zn), C-ZIF-8, WC-ZIF-8, MIL-53(Al), C-MIL-53, WC-MIL-53, MIL-88B (Fe), C-MIL-88B, WC-MIL-88B, UiO-66(Zr), C-UiO-66, WC-UiO-66, HKUST-1(Cu), C-HKUST-, WC-HKUST-1 and PAC S10)) and 50 mL of each HANs solutions were mixed in a 200 mL amber glass bottle with screw cap. The adsorption study will be continuing by shaking in rotary shaker at 200 rpm (25±2 °C). After reaching designed time, a solid part was withdrawn and filtered by 0.22 µm nylon syringe filter. Then the remaining was kept for the extraction by the EPA method 551.1.

### **3.9. ADSORPTION KINETIC STUDY**

Adsorption on the prepared samples was carried out in batch experiments. Adsorption kinetic study was varied contact time for adsorption at from 0 to 1800 min with 0.005-0.01 g of adsorbent and 50 mL of 1000-2000 ppb HANs solution (MCAN, DCAN, MBAN, and DBAN) with adsorbed tap water. Therefore, shaking in a 200 mL amber glass bottle with screw cap. The adsorption study was continuing by shaking in rotary shaker at 200 rpm ( $25\pm 2$  °C). After reaching equilibrium time, a solid part was withdrawn and filtered through 0.22  $\mu$ m nylon syringe filter. Then the remaining is kept for the extraction by the EPA method 551.1.

### **3.10. ADSORPTION ISOTHERM STUDY (SINGLE SOLUTE)**

Adsorption isotherm study was varied initial concentration for adsorption at 5, 10, 25, 50, 100 and 500 ppb. with 0.01 g of adsorbent and 50 mL of 1ppm single HANs solution in adsorbed tap water. Therefore, shaking in a 200 mL amber glass bottle with screw cap. The adsorption study was continuing by shaking in rotary shaker at 200 rpm ( $25\pm 2$  °C). After reaching equilibrium time, a solid part was withdrawn and filtered through 0.22  $\mu$ m nylon syringe filter. Then the remaining was kept for the extraction by the EPA method 551.1.

### **3.11. ADSORPTION ISOTHERM STUDY (MIXED SOLUTE)**

Adsorption isotherm study was varied initial concentration with 0.01 g of adsorbent and 50 mL of mixed four-HANs solution in adsorbed tap water. Therefore, and shaking in a 200 mL amber glass bottle with screw cap. The adsorption study was continuing by shaking in rotary shaker at 200 rpm ( $25\pm 2$  °C). After reaching equilibrium time, a solid part was withdrawn and filtered through 0.22  $\mu$ m nylon

syringe filter. Then the remaining was kept for the extraction by the EPA method 551.1., and the result was compared with single solute study.

### **3.12. EXTRACTION AND ANALYTICAL METHODS**

#### **3.12.1. HANs extraction**

HANs was extracted according to the EPA method 551.1. Sample was extracted by liquid-liquid extraction. A 25 mL of sample was filled in the 40 mL amber glass vial with screw cap and silicone septum. After that 5 g. of Na<sub>2</sub>SO<sub>4</sub> was added and mixed by vortex for 2 minutes, then 2.5 mL of MTBE was added and mixed by vortex for 3 minutes. The solution is standing for 5 minutes for separation, 1 mL of organic layer was transferred to glass amber GC vial with septum crimping cap and analyze by GC/ECD.

#### **3.12.2. GC/ECD setting**

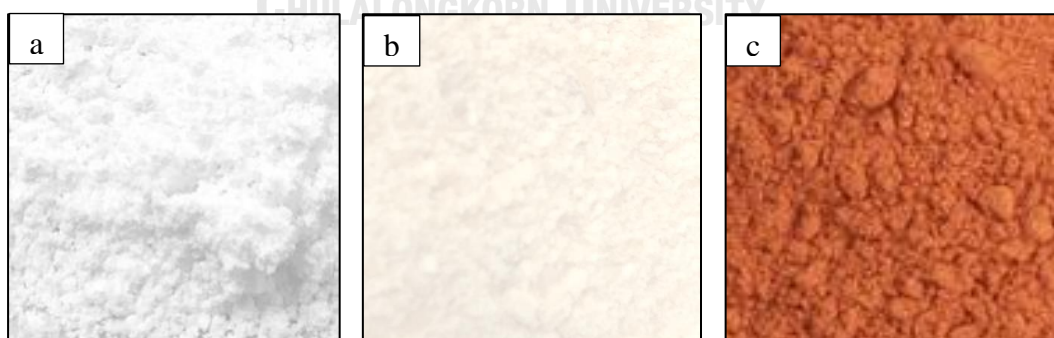
GC/ECD was set with HP-1 column Serial No US4760541H from Agilent Technologies System. Nitrogen and helium act as carrier gases with back split inlet, ratio 100:1 and flow 150 mL/min at 200°C with pressure 7.38 psi. Oven was set at 45°C at initial, ramp1 at 150°C for 2 min, and post-run at 200°C for 1 min. The detector was set at 260°C with N<sub>2</sub> makeup flow at 45°C.

## CHAPTER IV

### MATERIALS CHARACTERIZATION RESULTS

#### 4.1 INTRODUCTION

In this study, each Metal-Organic Frameworks (MOFs) were synthesized, then were modified by direct carbonization (pyrolysis) under nitrogen flow. The carbonized MOFs were washed by acid solution to clean the surface. The conventional MOFs, carbonized MOFs (C-MOFs) and washed carbonized MOFs (WC-MOFs) were used as the adsorbents to investigate the effects of different physicochemical characteristics on the adsorption capacities for HANs compared to the commercial PAC. Hence, the physicochemical characteristics of all synthesized adsorbents were investigated, including; XRD, FTIR, SEM, N<sub>2</sub> adsorption/desorption isotherm (BET), and XPS. The characterized data were combined with adsorption experiment results to study the relationships between physicochemical characteristics and adsorption phenomena of HANs. The appearance of the synthesized materials are shown in Figure 4.1



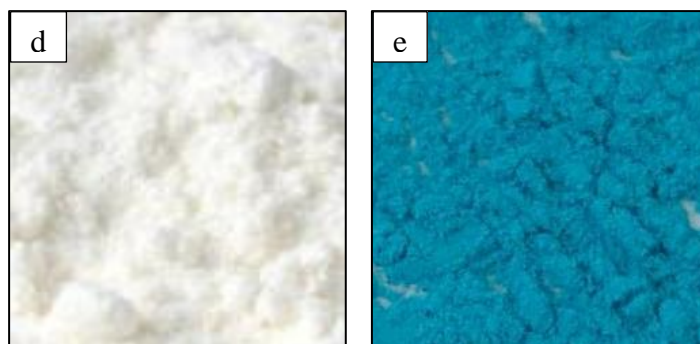


**Figure 4.1** Appearance of the synthesized adsorbents (a) ZIF-8(Zn), (b) MIL-53 (Al), (c) MIL-88B (Fe), (d) UiO-66(Zr) and (e) HKUST-1(Cu)

#### 4.2 SURFACE FUNCTIONAL GROUP ANALYSIS BY FTIR

Fourier-transform infrared spectroscopy was used to identify surface functional groups of all synthesized MOFs and WC-MOFs i.e. ZIF-8(Zn), MIL-53 (Al), UiO-66(Zr), MIL-88B (Fe), HKUST-1(Cu), WC-ZIF-8, WC-MIL-53, WC-UiO-66, WC-MIL-88B and WC-HKUST-1 as shown in Figure 4.2. The characteristic band of ZIF-8 (Figure 4.2(a)) at  $2,926\text{ cm}^{-1}$  was associated with the aromatic C–H asymmetric stretching vibrations. Bands at  $675\text{ cm}^{-1}$  and  $760\text{ cm}^{-1}$  could be assigned as C–H bending mode, respectively. Whereas band at  $1145\text{ cm}^{-1}$  and  $1,485\text{ cm}^{-1}$  were derived from aromatic C–N stretching mode and C–N stretch vibration, respectively. Similarly, the bands at  $995\text{ cm}^{-1}$  could be assigned as C–N bending vibration. The band at  $1300\text{--}1460\text{ cm}^{-1}$  was for the entire ring stretching regions. The band at  $1,561\text{ cm}^{-1}$  were identified for O–H bending vibration. And band at  $694\text{ cm}^{-1}$  was due to the ring out of plane bending vibration of the Hmim. (Y. Zhang, Jia, & Hou, 2018). Most of the bands in ZIF-8 was disappeared in WC-ZIF-8. The band at  $1,544\text{ cm}^{-1}$  and  $1,216\text{ cm}^{-1}$  were identified for N–H bending vibration and aromatic C–N stretching

mode, respectively. The region weak peak at 3,400-3,900 could referred to C–H bonding.

According to MIL-53(Al) (Figure 4.2(b)), the bending O–H bands of the hydroxyl groups was also visible at 994  $\text{cm}^{-1}$  (F. Zhang et al., 2012). The band 751  $\text{cm}^{-1}$  and 836  $\text{cm}^{-1}$  were assigned to C–H wagging and C=O bending. The bands at 1,018  $\text{cm}^{-1}$  and 1,068  $\text{cm}^{-1}$  were identified as C–H stretching. The –C=O symmetric stretching was from band 1,408  $\text{cm}^{-1}$  and C=N bending from bands at 1,507  $\text{cm}^{-1}$  and 1,578  $\text{cm}^{-1}$  (Do, Hoang, & Kaliaguine, 2011) Similarly, WC-MIL-53 (Al) had a weak band at 3,350 which stand for N–H bending vibration

The bands 747  $\text{cm}^{-1}$  in MIL-88B (Fe) (Figure 4.2(c)) were assigned to C–H bending of the benzene ring (H. Zhang et al., 2019). The sharp peaks appeared at 1596  $\text{cm}^{-1}$ , and 1503  $\text{cm}^{-1}$  are related to the C=O asymmetric and symmetric stretching vibrations, respectively. This shows the presence of terephthalic ligands in MIL-88B (Fe) structure. Also, the band at 1659  $\text{cm}^{-1}$  is attributed to the C=O stretching vibration (Mahmoodi et al., 2019) The band at 1,380 could be assigned to symmetric stretching of carboxyl group (Gholizadeh Khasevani & Gholami, 2018) The region weak peak at 3,565-3,900 could referred to C–H and C–H bonding. This vibrational peak was associated with the bending vibration of the C–H bond observed at 2,916  $\text{cm}^{-1}$  in WC-MIL-88B (Fe) (An, Cheng, Wang, Wang, & Lin, 2016)

In UiO-66 (Figure 4.2(d)), typical bands representing the O–C–O asymmetric stretching in the terephthalic ligand are also seen at 1566  $\text{cm}^{-1}$ . The small bands at 1506  $\text{cm}^{-1}$  and 1391  $\text{cm}^{-1}$  represent the vibration of a benzene ring. The peak at 746

$\text{cm}^{-1}$  was due to  $-\text{OH}$  and  $\text{C}-\text{H}$  vibrations in the terephthalic ligand.(Ivanchikova et al., 2014) The strong  $\text{C}-\text{O}$  stretching at  $1,101 \text{ cm}^{-1}$  was found in WC-UiO-66.

For HKUST-1(Cu) (Figure 4.2(e)), band at  $1702 \text{ cm}^{-1}$  corresponds to stretching vibration of  $\text{C}=\text{O}$  acid ligands, indicated the deprotonation process occurred in  $\text{C}=\text{O}$  bond. The band at  $1,364 \text{ cm}^{-1}$  and  $1442 \text{ cm}^{-1}$  was attributed to  $\text{C}-\text{O}$  of trimesic and the band at  $728 \text{ cm}^{-1}$  was attributed to  $\text{Cu}-\text{O}$  bonding. (L. Zhao et al., 2019) The abroad band around  $3,400 \text{ cm}^{-1}$  could be attributed to  $\text{O}-\text{H}$  stretching.





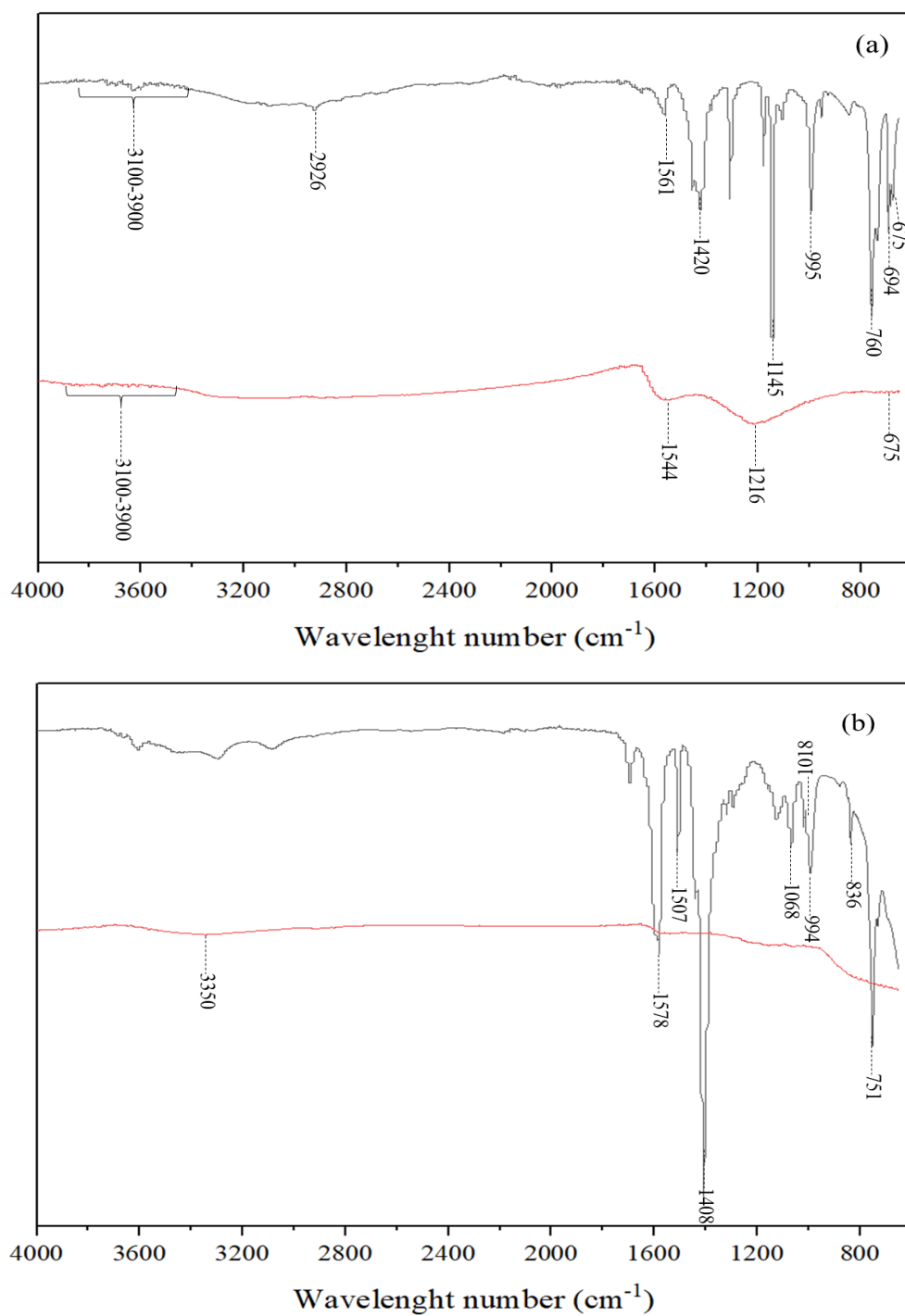


**Figure 4.2** FTIR spectra of MOFs (up) and WC-MOFs (down); (a) ZIF-8(Zn) and WC-ZIF-8; (b) MIL-53(Al) and WC-MIL-53

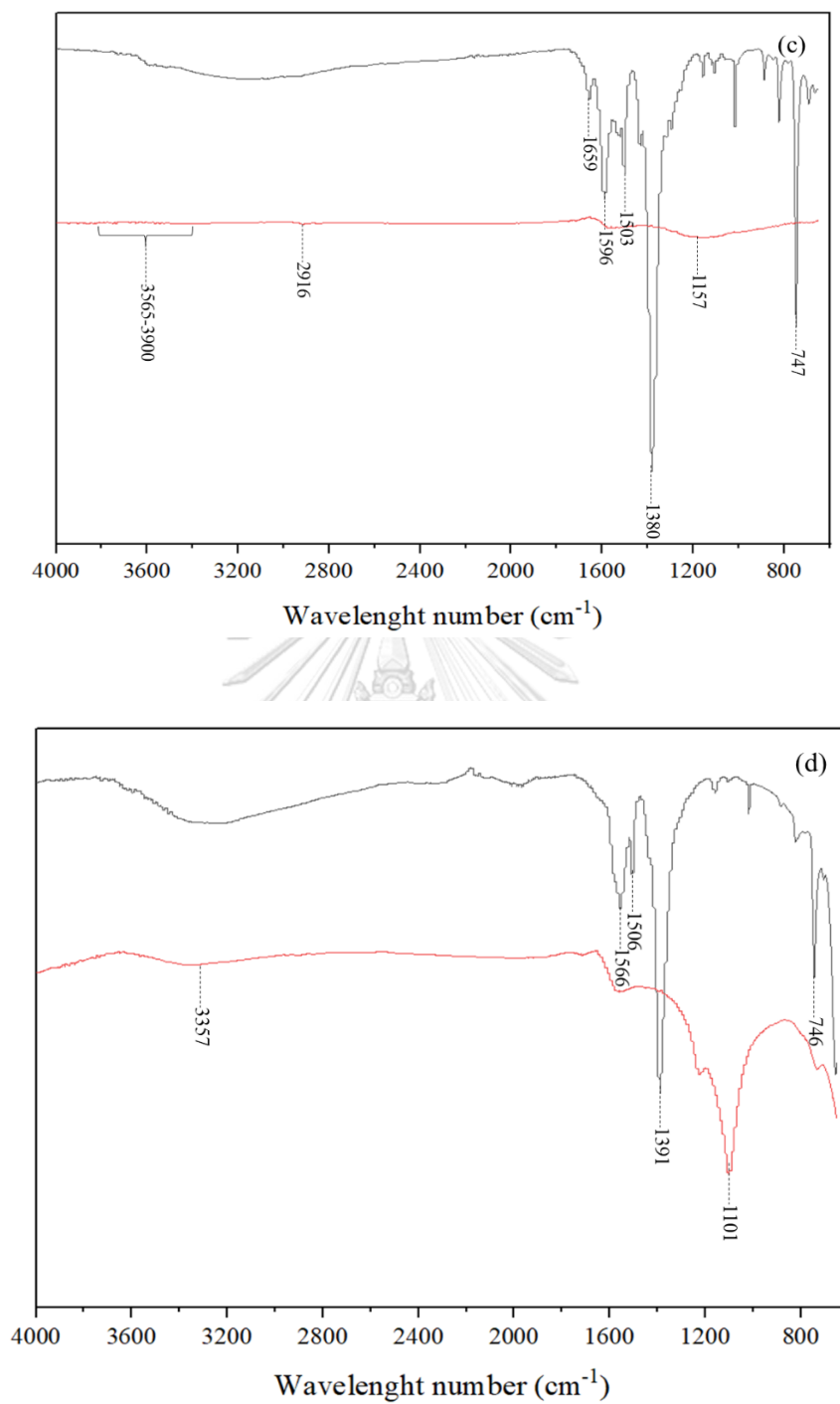


**Figure 4.3** FTIR spectra of MOFs (up) and WC-MOFs (down); (c) MIL-88B (Fe) and WC-MIL-88B; (d) UiO-66(Zr) and WC-Uio-66

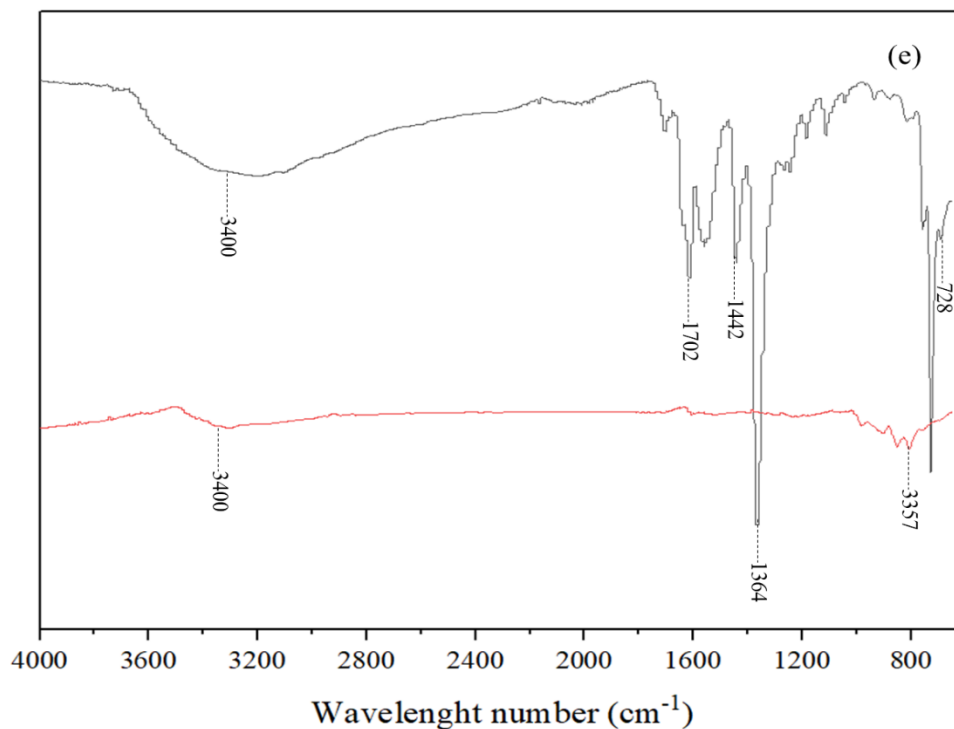


**Figure 4.4** FTIR spectra of MOFs (up) and WC-MOFs (down); (e) HKUST-1(Cu) and WC-HKUST-1.

### 4.3 POWDER X-RAY DIFFRACTION– POWDER-XRD

The powder XRD pattern of the synthesized MOFs and C-MOFs were showed in Figure 4.3. The crystallographic structure of the synthesized MOFs and C-MOFs were characterized by powder x-ray diffraction (XRD) using a Rigaku, SmartLab diffractometer in transmission geometry using CuK $\alpha$  radiation at 40 kV and 30 mA. The data were acquired at scan speed 1.0000 deg/min and step width 0.0100 deg. From Figure 4.2(a), comparing between ZIF-8 stimulation pattern (from ICDD and COD; Diffraction database) and synthesized ZIF-8 was agreed well with ICDD database. C-ZIF-8 has the soft and round peak around 26° which can refer to carbon crystalline structure i.e. graphene and graphite (Ilkiv et al., 2014)

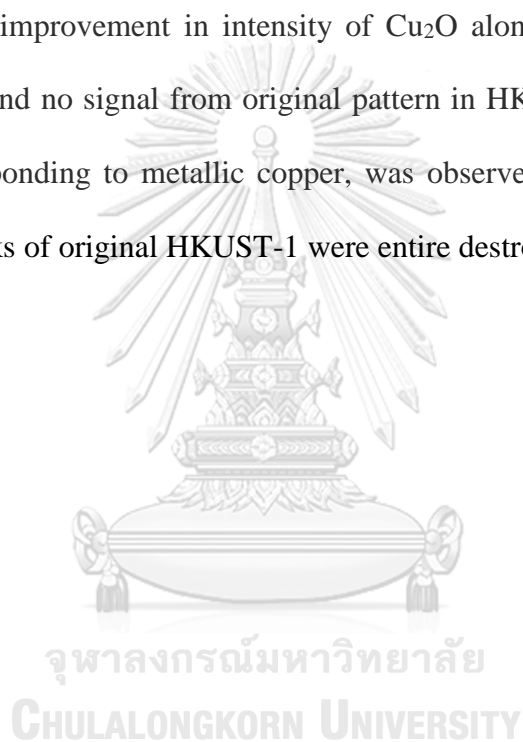
The MIL-53(Al) XRD found the strongest diffraction peaks of the MIL-53(Al) structure at  $8.8^\circ$  and framework was also characterized by the specific peaks at  $10.9$ ,  $12.8$ , and  $22.0^\circ$  as in good agreement with that of the previous report of MIL-53 (Al) pattern (Sánchez-Sánchez et al., 2015). The peak at  $27^\circ$  can be assigned to Al peak. C-MIL-53 (Al) has weak and round peaks at  $32^\circ$  and  $45.5^\circ$  which can interpret for Al residue peak (T et al., 2018)

Figure 4.2(c) shows the main peaks of the MIL-88B(Fe) synthesized by the conventional route with DMF as the solvent that was agreed well with pattern from this study (Hou et al., 2018). The next step after carbonization of the framework at  $900^\circ\text{C}$ . The strongest peak was found at  $44.5^\circ$  and followed by peak at  $43.5^\circ$  might be assumed as a metallic compound in structure.

The X-ray diffraction (XRD) patterns of the synthesized UiO66 and stimulated UiO-66 are exhibited in Figure 4.2 (d). It is clearly shown that diffraction peaks are well indexed to other works (at peak  $7^\circ$  and  $8.5^\circ$ ), which indicated the MOF was successfully synthesized. Whereas, C-UiO-66 framework is unstable due to carbonization at high temperatures. Thus, it can't maintain an original degree of crystallinity. The patterns in Figure 4.2 (d) showed that the crystallinity of C-UiO-66 was almost changed, which manifested high temperature have destroyed the structure of the framework (Jin & Yang, 2017; Luan et al., 2015).

XRD pattern of the synthesized HKUST-1 (Figure 4.2(e)) was in good agreement with the stimulated HKUST pattern, indicating the successful synthesis of HKUST-1(L. Zhao et al., 2019). While the synthesized HKUST-1 showed stronger intensities of diffraction peaks than the stimulation. The results of intensities could

confirm the well preserved MOFs structure (Maleki, Hayati, Naghizadeh, & Joo, 2015). The XRD pattern of HKUST-1 and C-HKUST-1 are shown in **Figure 4.3 (e)**. The peaks are appeared at  $2\theta$ ,  $36.4^\circ$  on C-HKUST, which matching the reflection from the (111) planes of  $\text{Cu}_2\text{O}$  (Lin et al., 2012). No diffraction peaks for phosphorus or graphitic carbon species were observed in C-HKUST-1, since the carbon has low content in the products or poor degree of crystallinity. When the temperature increased, a high improvement in intensity of  $\text{Cu}_2\text{O}$  along the (111) direction was highly observed, and no signal from original pattern in HKUST-1. Peaks shift at  $44^\circ$  and  $50.3^\circ$ , corresponding to metallic copper, was observed. This result can assume that the frameworks of original HKUST-1 were entire destroyed at  $900^\circ\text{C}$ .



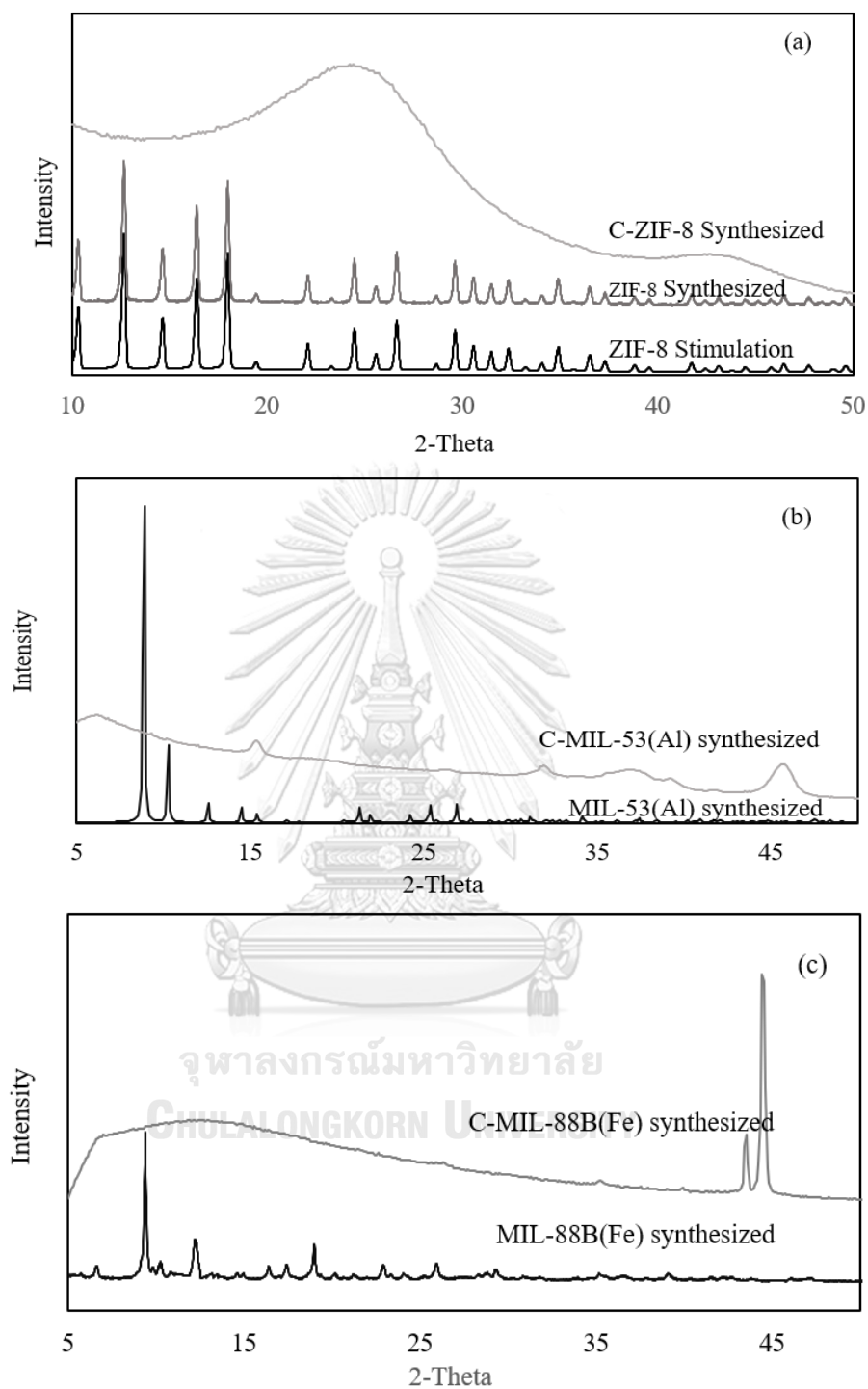


**Figure 4.5** XRD pattern of MOFs and C-MOFs; (a) ZIF-8(Zn) and C-ZIF-8; (b) MIL-53(Al) and C-MIL-53; (c) MIL-88B(Fe) and C-MIL-88B

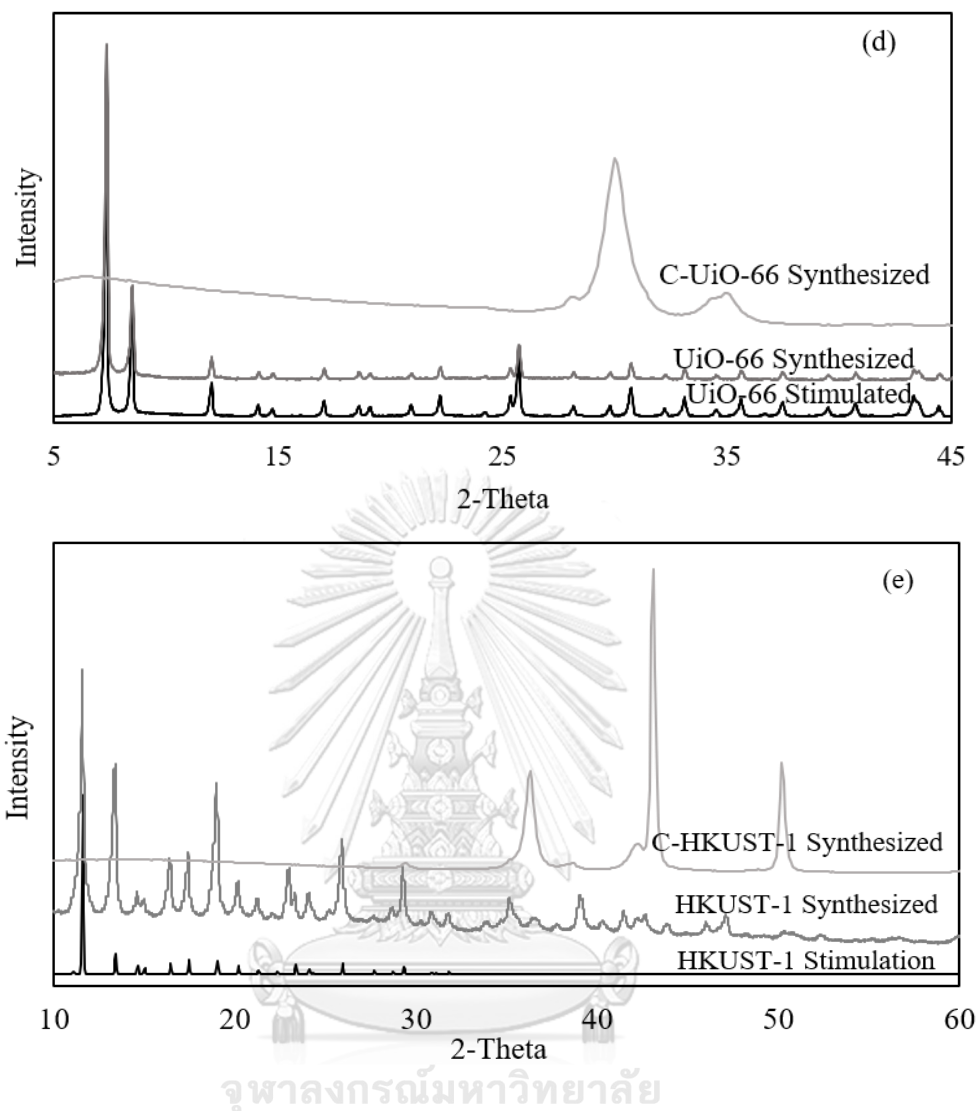


**Figure 4.6** XRD pattern of MOFs and C-MOFs; (d) UiO-66(Zr) and C-UiO-66; and (e) HKUST-1(Cu) and C-HKUST-1.

### 4.3 SCANNING ELECTRON MICROSCOPE AND ENERGY DISPERSIVE X-RAY SPECTROMETER (SEM-EDS)

The morphologies of MOFs, C-MOFs, and WC-MOFs were observed by using scanning electron microscope and energy dispersive x-ray spectrometer (SEM-EDS) with JEOL InTouchScope™ series SEMs, JSM-IT500HR and Hitachi, S-4800.

The images of materials are shown in Figure 4.3 (a1-a3) of the obtained ZIF-8 and parent particles. The average particle sizes are 1  $\mu\text{m}$ . These images reveal the

formation of ZIF-8 with polyhedron morphology with a smooth surface. (Bakhtiari et al., 2015). Thus, the carbonization at 900°C does not change the morphology, but the surface was rougher than ZIF-8 might be from by-product and residue from carbonization. As a result, after washed C-ZIF-8 by acid solution, the surface became same as original ZIF-8. During the carbonization, a network of nanocarbon is formed through the thermal decomposition of ZIF-8 which acts both as sacrificial template and carbon precursor.

According to the SEM results in **Figure 4.3 (b1-b3)**, all MIL-53(Al) type materials were synthesized in a nanoscale form. The MIL-53(Al) sample is composed of elongated elliptical nanocrystals with sizes up to 500 nm, and width can be greater than 100 nm (Isaeva et al., 2019; Sánchez-Sánchez et al., 2015) that. According to the irregular shape of these particles. There were difficult to estimated size and morphology among MOF, C-MOF, and WC-MOF.

From the SEM images, the synthesized MIL-88B (Fe) has random size of approximately 0.5-5  $\mu\text{m}$  with hexagonal rod-like morphology with uniform random size distribution. (Ma et al., 2013). After carbonization the morphology of small-size MIL-88B (Fe) was destroyed. Even some large-size MIL-88B (Fe) is stable, but the surface was rougher and after wash by acid solution the surface was all most disappeared.

UiO-66 from solvothermal synthesis reveals sharp edges with an octahedral shape with average diameters of approximately 1-3  $\mu\text{m}$ . The surface is quite smooth.(Lee, Kim, Kang, & Cohen, 2015). After carbonization the morphology was not changed but the surface was cover by by-product and residue from carbonization.



And the particle adhered together. Although wash by acid solution, the particle still adhered as a group of particles.

HKUST-1 in Figure 4.3 (e1) has an octahedral shape with average diameters of approximately 5-15  $\mu\text{m}$ . Solvothermal synthesis generally produces crystals of cubic shape with sharp edges and smooth surface uniform particle size and has visible pore at surface. However, when it was carbonized at 900°C, the morphologies of the particle surface are totally different. C-HKUST in Figure 4.3 (e2) and WC-HKUST in Figure 4.3 (e3) showed the same octahedral structure with the appearance of few particles over the surface but surface became rougher and was taken by number of small particles. This could indicate the transformation of HKUST-1

The **Table 4.1** are summarized the element quantitative from EDS analysis. All materials similarly show higher carbon (C) mass portion after carbonization at 900 °C and lower of substrate metal percentage.

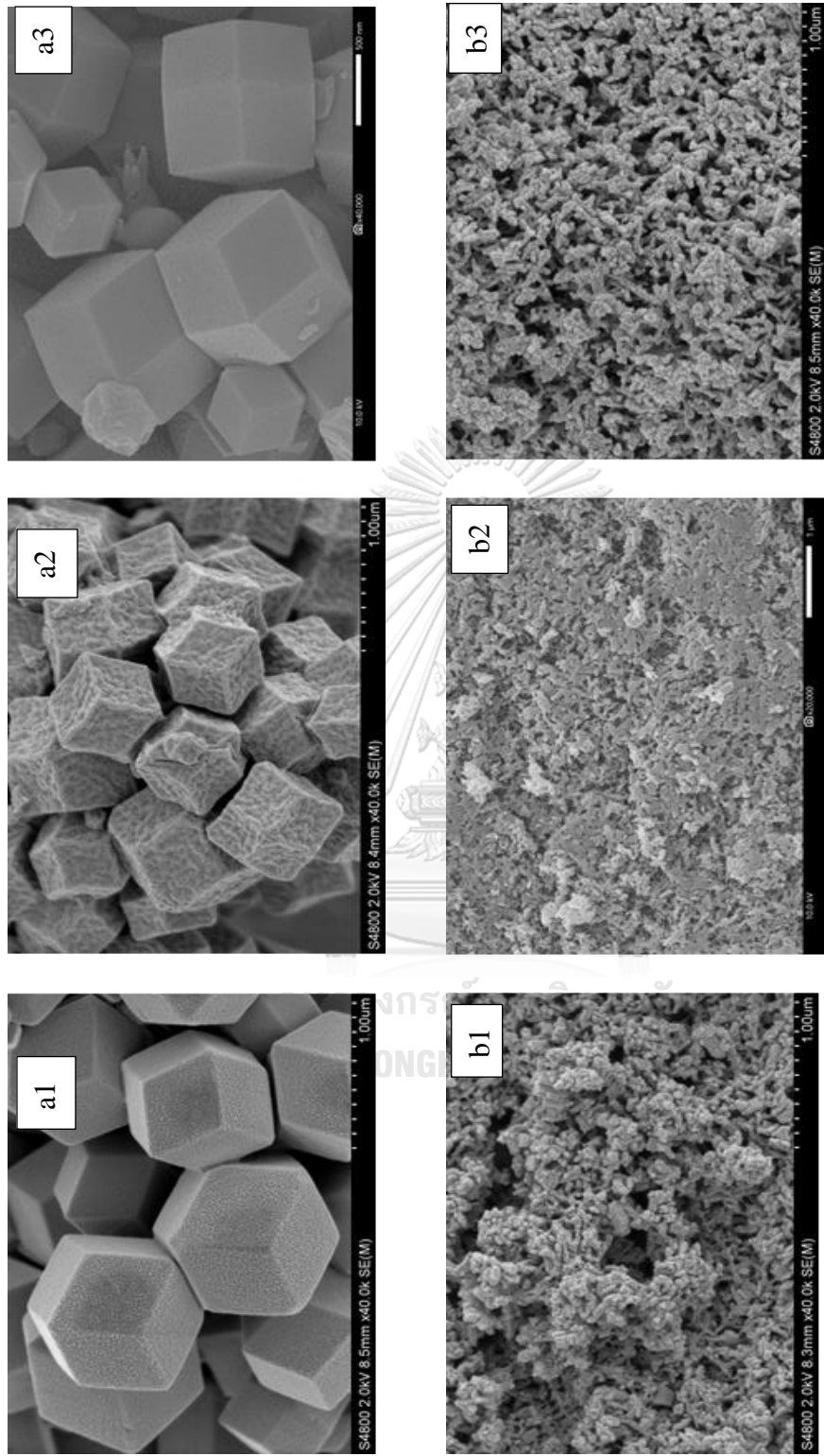


**Figure 4.7** SEM images of (a1) ZIF-8(Zn), (a2) C-ZIF-8 and (a3) WC-ZIF-8; (b1) MIL-53 (Al), (b2) C-MIL-53 and (b3) WC-MIL-53

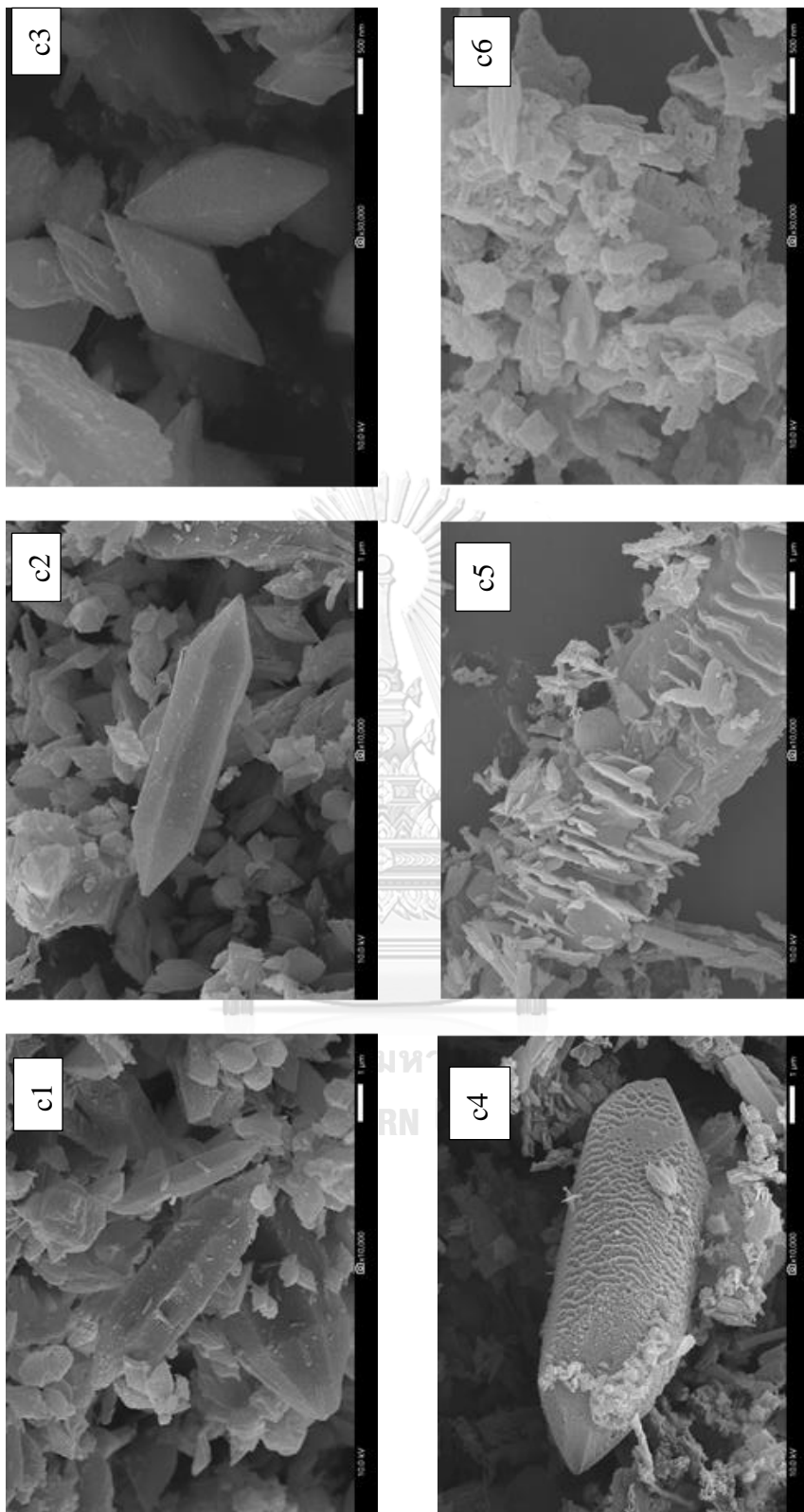


**Figure 4.8** SEM images of (c1-c3) MIL-88B(Fe) and (c4) C-MIL-88B

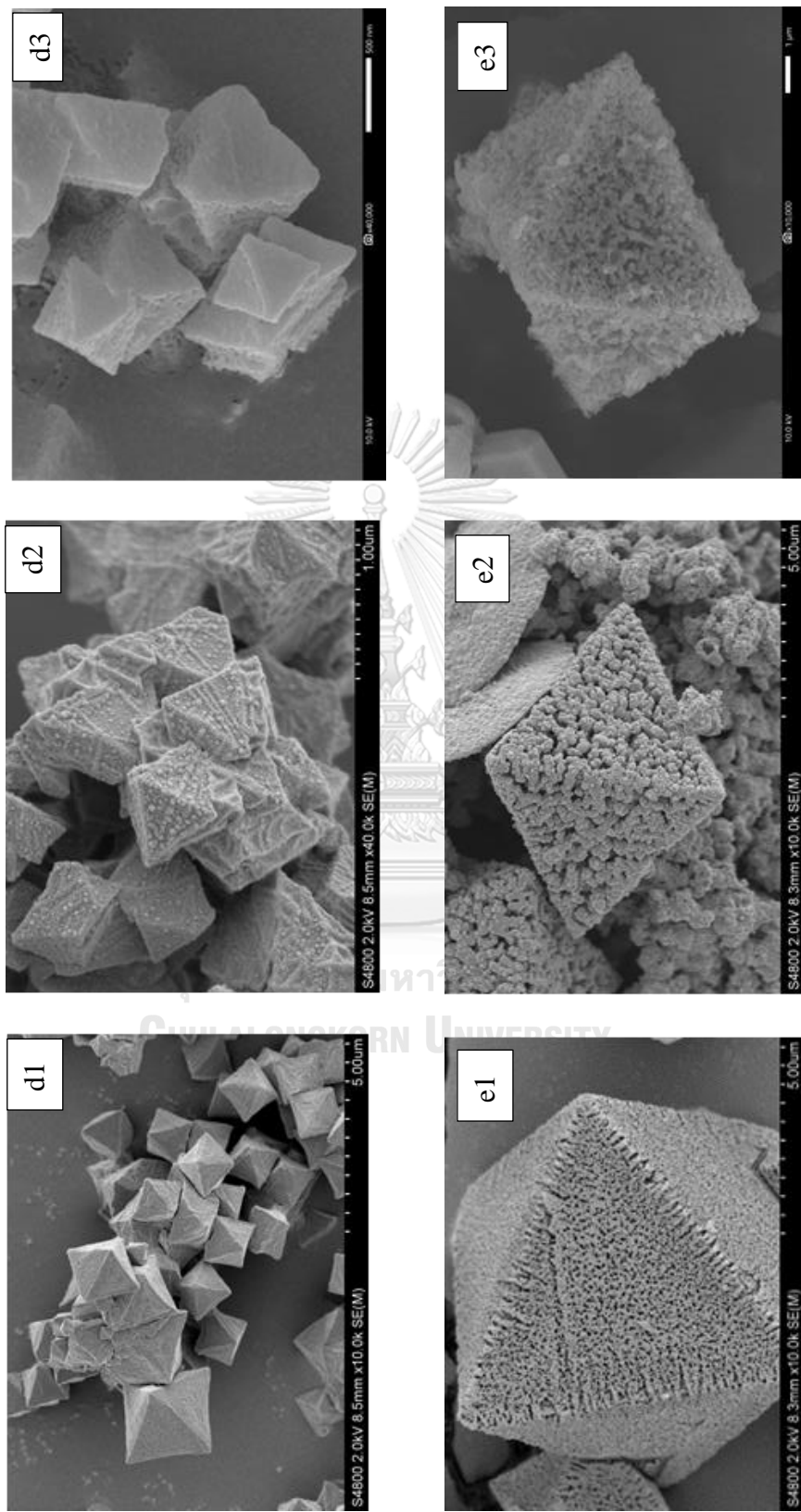


**Figure 4.9** SEM images of (d2) C-UiO-66 and (d3) WC-UiO-66; and (e1) HKUST-1(Cu), (e2) C-HKUST-1 and (e3) C-HKUST-1

**Table 4.1** EDS element data analysis

Parent	Element	Conventional MOFs		Carbonized MOFs		Wash-carbonized MOFs	
		Atomic (%)	Mass (%)	Atomic (%)	Mass (%)	Atomic (%)	Mass (%)
<b>ZIF-8</b>	C	59.02	45.77	74.24	62.63	63.57	72.14
	N	27.89	22.22	14.24	14.01	21.15	20.58
	O	8.23	8.5	8.52	0.39	6.37	5.43
	Zn	4.86	20.51	3.06	0.29	8.91	1.86
<b>MIL-53 (Al)</b>	C	31.83	22.14	37.37	27.55	51.89	39.47
	O	45.98	41.77	46.37	45.53	31.18	31.59
	Al	23.09	36.09	16.26	16.26	16.93	28.94
<b>MIL-88B (Fe)</b>	C	69.18	50.24	83.01	76.78	88.58	83.71
	O	21.59	20.88	16.27	20.04	10.81	13.60
	Fe	7.23	24.43	0.53	2.29	0.61	2.68
<b>UiO-66</b>	C	52.14	24.3	54.49	28.68	68.73	46.52
	O	32.1	19.92	55.68	21.72	25.3	22.81
	Zr	15.76	55.76	31.65	49.6	5.97	30.67
<b>HKUST-1</b>	C	57.66	30.75	26.35	7.53	74.42	48.49
	O	23.76	16.88	16.64	6.33	7.74	6.72
	Cl	0.04	0.07	0.07	0.05	10.95	21.06
	Cu	18.54	52.3	56.94	86.08	6.89	23.73

#### 4.4. PORE AND SURFACE AREA ANALYSIS

The presence surface, pore size, and pore size distribution of MOFs, C-MOFs, and WC-MOFs were observed by using, Quantachrome® ASiQwin™- automated gas sorption analyzer. Before operation, sample was degassed at 50-250 °C for 3 h to remove any contaminant that may be present at the surface. Surface area, pore diameter, pore volume, and pore size distribution were determined by nitrogen adsorption-desorption isotherm. The surface area (BET) was calculated according to Brunner-Eller-Teller (BET) equation using N<sub>2</sub> adsorption isotherm data. Pore diameter, pore volume, and pore size distribution were calculated according to Barrett-Joyner-Halenda (BJH) equation. Figure 4.4 exhibited the nitrogen adsorption-

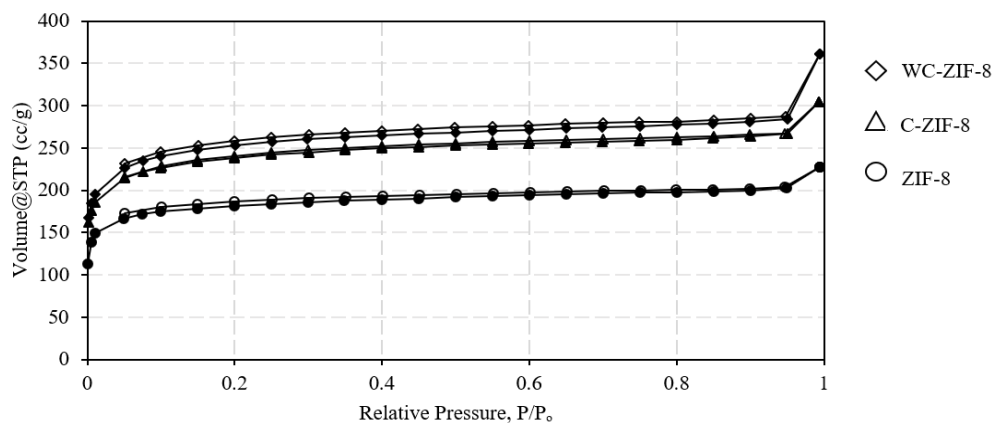
desorption isotherm of material. The Table 4.2 is concluding the pore and surface area analysis.

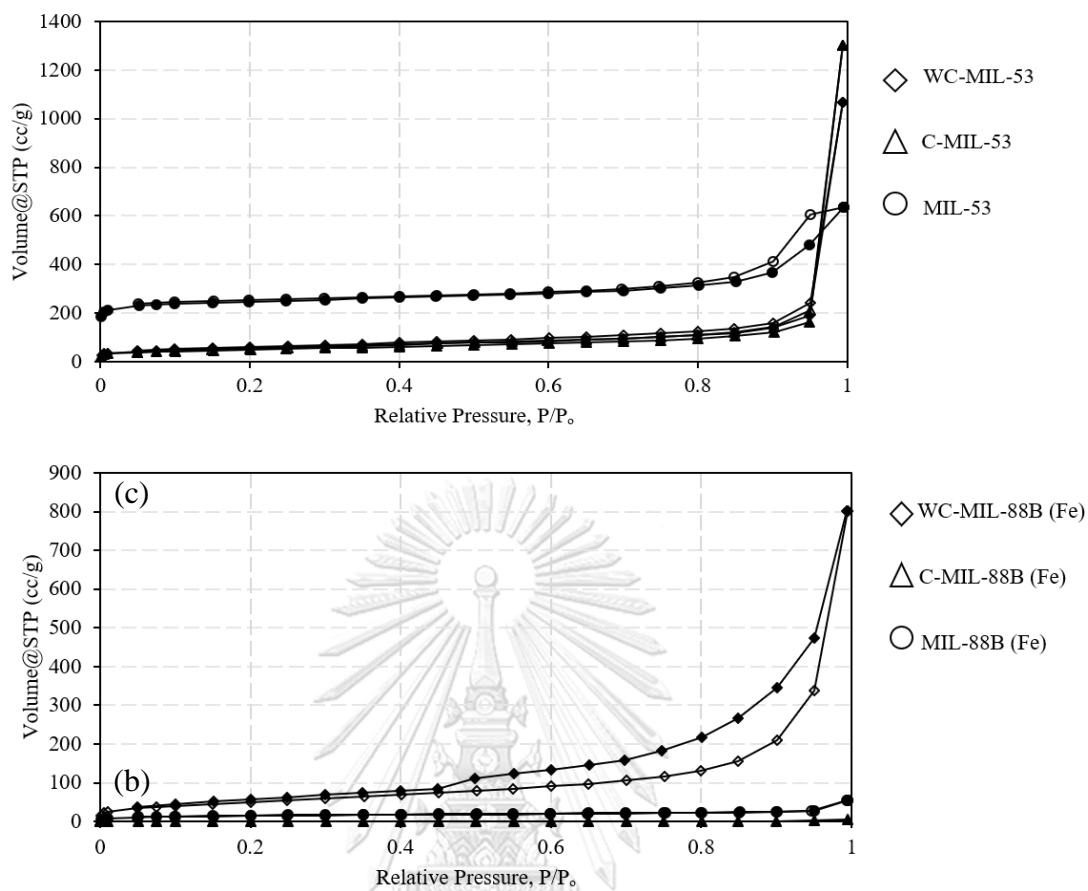
The surface properties of ZIF-8(Zn) were improved by carbonization. According to the N<sub>2</sub> adsorption isotherm, the surface area was getting high from 561.37 m<sup>2</sup>/g to 742.17 m<sup>2</sup>/g after carbonization as shown in Figure 4.4 (a). Moreover, after washing C-ZIF-8 by acid solution, surface area was reached 790.35 m<sup>2</sup>/g. The pore size distribution of ZIF-8(Zn) are in the range of microporous material. Similarly, MIL-88B(Fe) also shows the improvement of carbonization and acid wash, which the surface area was raised from 50.971 m<sup>2</sup>/g to 189.37 m<sup>2</sup>/g, as in Figure 4.4 (c). In addition, pore volume of WC-MIL-88B (Fe) also raised from 0.00818 cc/g up to 1.24 cc/g. As shown in **Figure 4.7** pore radius was expanded from below 10 Å to 20-30 Å. Thus, pore size and pore volume were increased.

Although ZIF-8 and MIL-88B (Fe) were improved by carbonization and acid wash, the rest of adsorbent are lost the surface properties. For instance, the surface area of UiO-66 was much more reduce from 1043.9 m<sup>2</sup>/g to 155.8 m<sup>2</sup>/g after acid washed, similarly to pore volume. HKUST-1 also destroyed by carbonization and acid washed toward the increasing mean pore radius while the pore volume is decreasing that might be from pore collapse. The assumption was supported by SEM images of HKUST-1 from **Figure 4.3 (e2-e3)** which show the collapse surface and pore.

**Table 4.2** Surface area and pore characteristic of synthesized adsorbents.

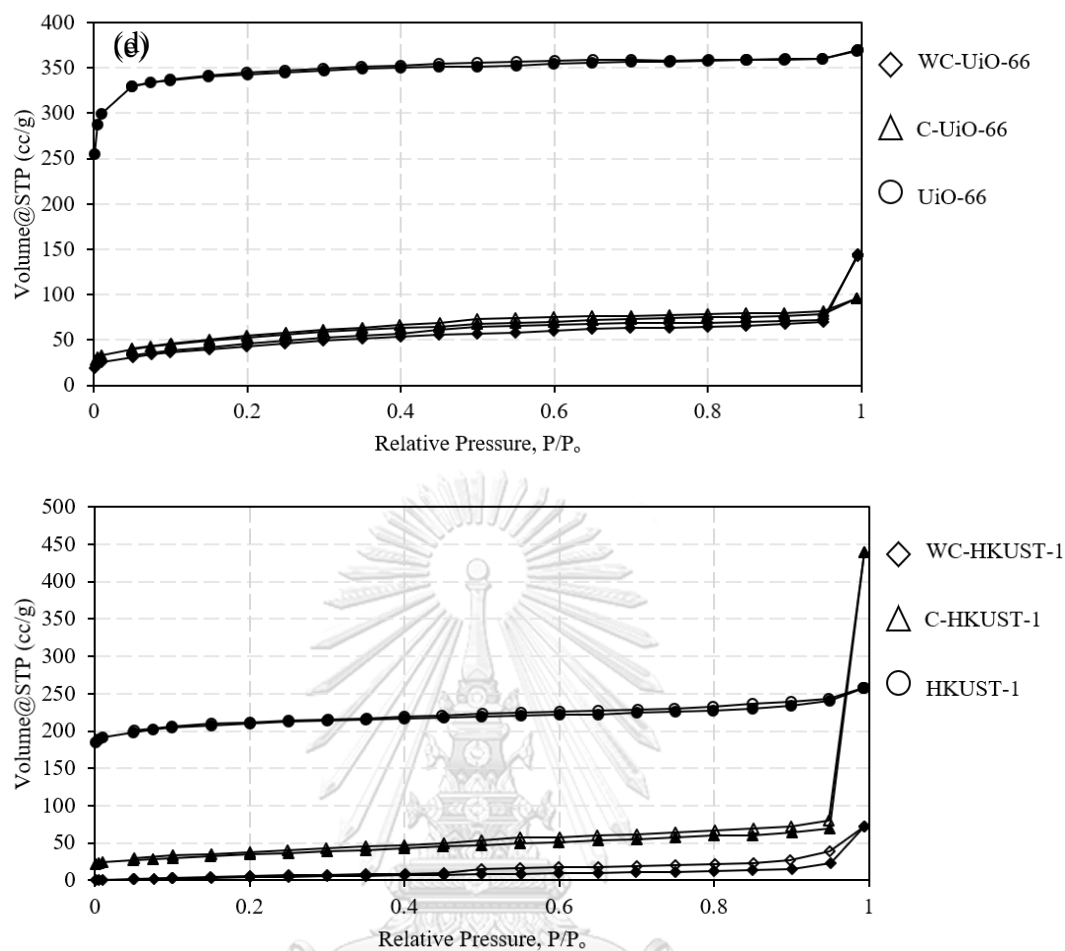
material	BET			BJH			Degas Temp (°C)
	surface area	pore radius	pore volume	surface area	pore radius	pore volume	
	m <sup>2</sup> /g	Å	cc/g	m <sup>2</sup> /g	Å	cc/g	
ZIF-8(Zn)	561.3	12.5	0.3524	1390.6	3.89	0.406	50
MIL53(Al)	768.2	25.6	0.9843	1170.4	3.92	0.900	100
MIL-88B(Fe)	50.9	33.9	0.0864	101.25	3.89	0.095	100
UiO-66(Zn)	1043.9	10.9	0.5720	1781.4	3.90	0.472	100
HKUST-1(Cu)	645.7	12.3	0.3985	323.6	3.94	0.171	100
CZIF-8	742.1	12.6	0.4708	1108.2	4.00	0.417	250
CMIL53	168.7	33.94	2.0130	317.1	3.89	2.034	250
CMIL-88B	2.2	71.1	0.0081	3.65	13.69	0.009	250
CUiO-66	183.6	16.2	0.1491	262.4	4.01	0.155	250
CHKUST-1	119.1	33.63	0.6802	116.2	3.96	0.671	250
WCZIF-8	790.3	14.1	0.5580	1268.6	3.96	0.522	250
WCMIL53	195.0	33.94	1.6510	342.1	3.97	1.675	250
WCMIL-88B	189.3	131	1.2400	366.4	3.90	1.283	250
WCUiO-66	155.8	28.7	0.2239	268.1	3.92	0.243	250
WCHKUST-1	20.5	33.69	0.1124	31.7	15.2	0.188	250



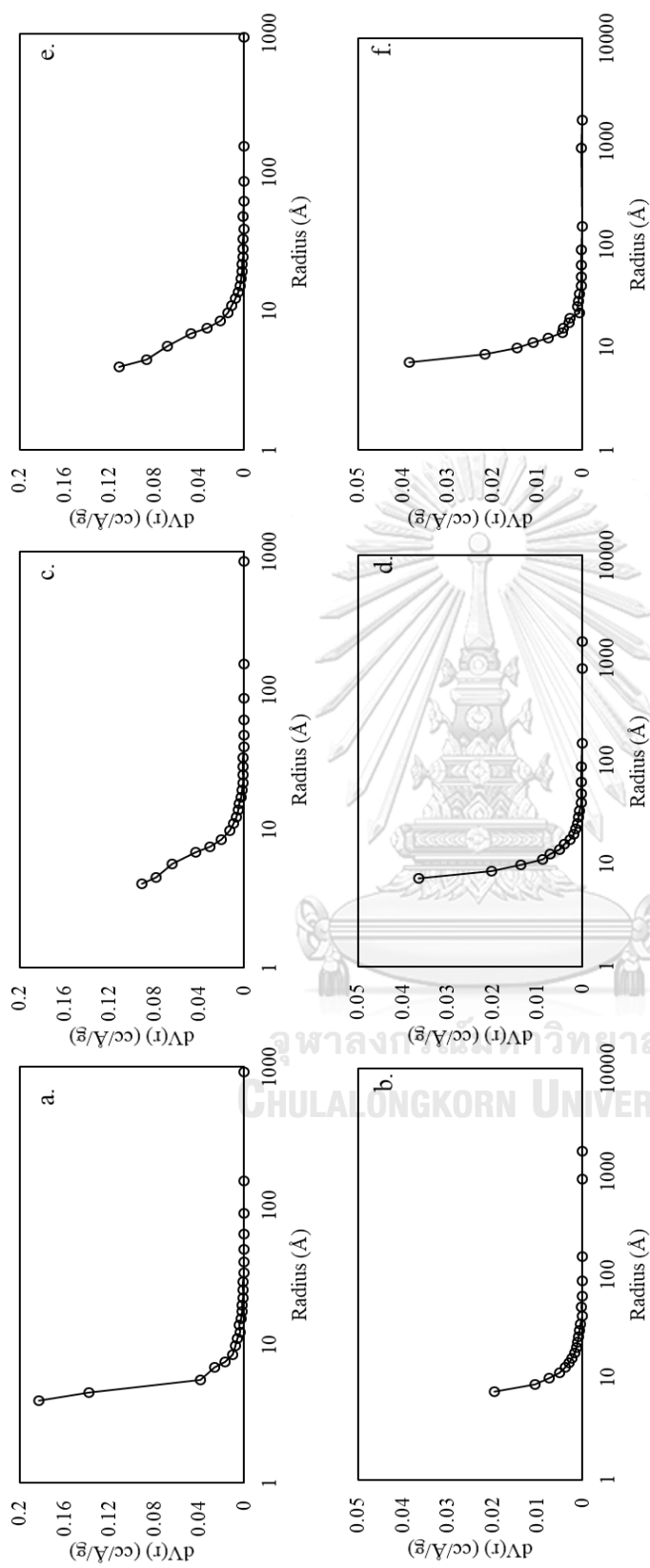


**Figure 4.10** Nitrogen sorption isotherm of MOFs C-MOFs and WC-MOFs; (a) ZIF-8(Zn), C-ZIF-8 and WC-ZIF-8; (b) MIL-53(Al) C-MIL53 and WC-MIL-53 ; (c) MIL-88B (Fe), C-MIL-88B and WC-MIL-88B

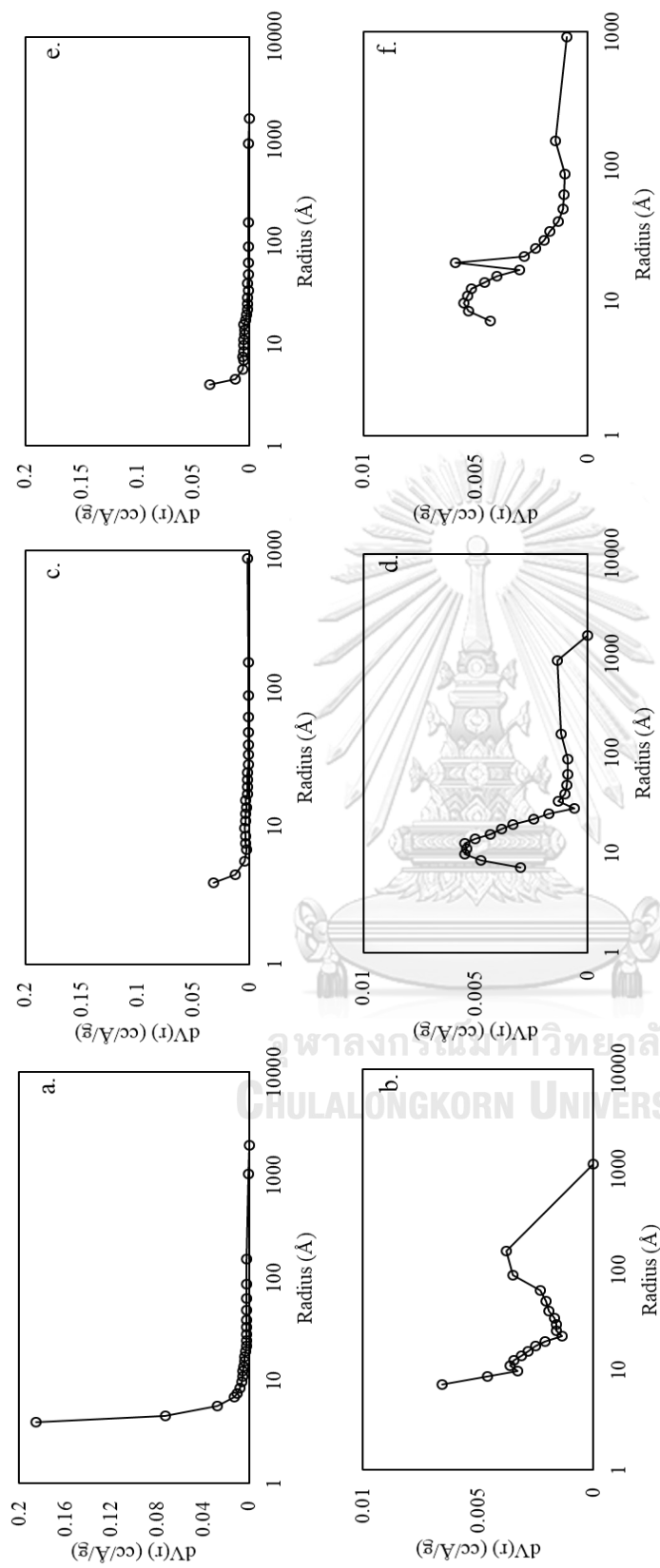




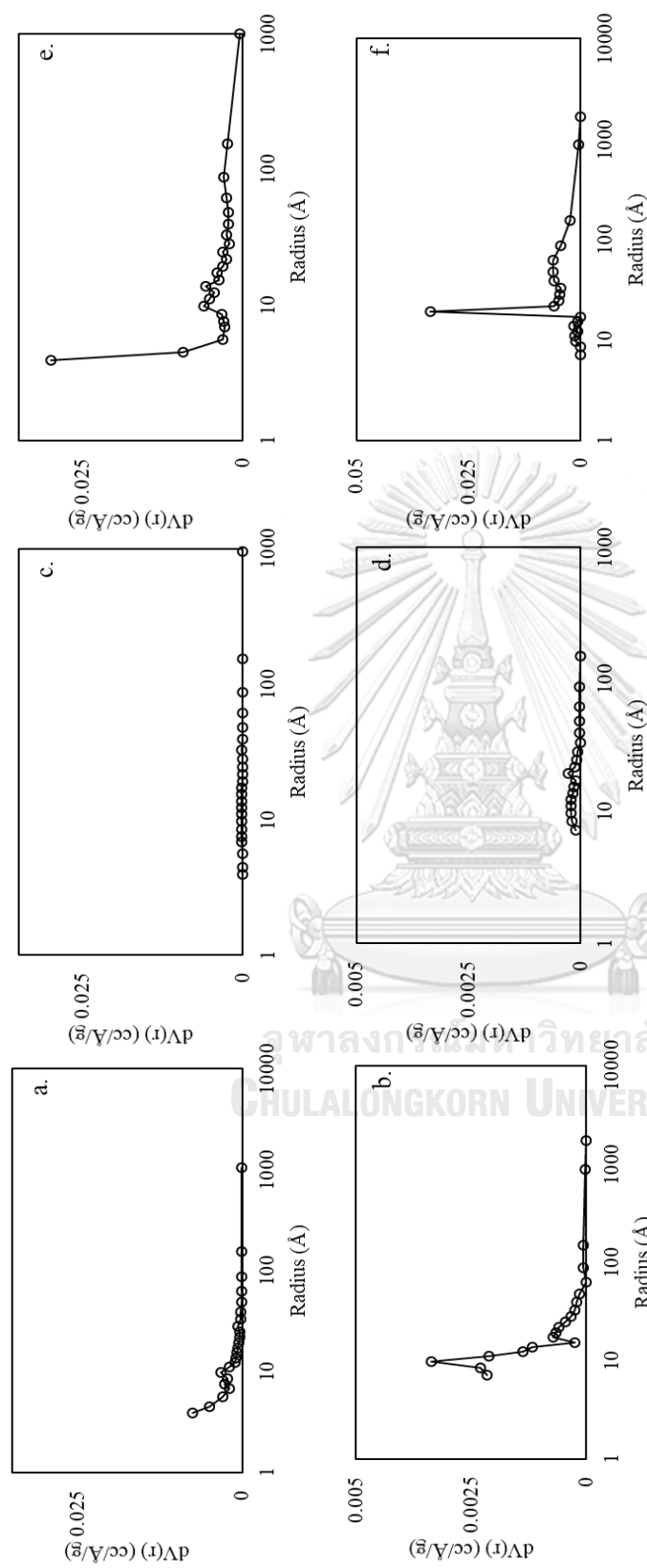
**Figure 4.11** Nitrogen sorption isotherm of MOFs C-MOFs and WC-MOFs; (d) UiO-66 (Zr), C-UiO-66 and WC-UiO-66; and (e) HKUST-1(Cu), C-HKUST-1 and WC-HKUST-1 at 77 ° K. Opened and closed symbols are represented the nitrogen adsorption and desorption.



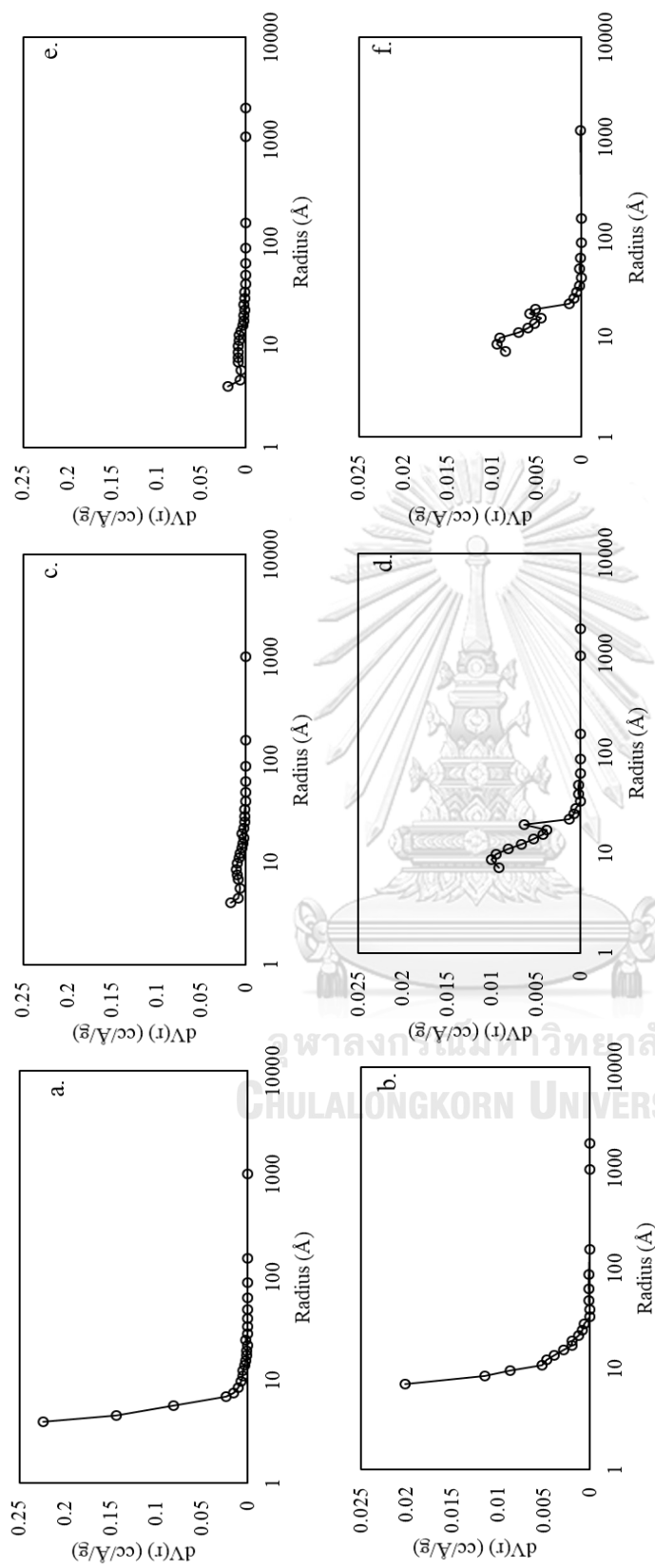
**Figure 4.12** BJH pore size distributions derived from sorption isotherm of (a) adsorption ZIF-8(Zn), (b) desorption ZIF-8(Zn), (c) adsorption C-ZIF-8, (d) desorption C-ZIF-8, (e) adsorption WC-ZIF-8 and (f) desorption WC-ZIF-8



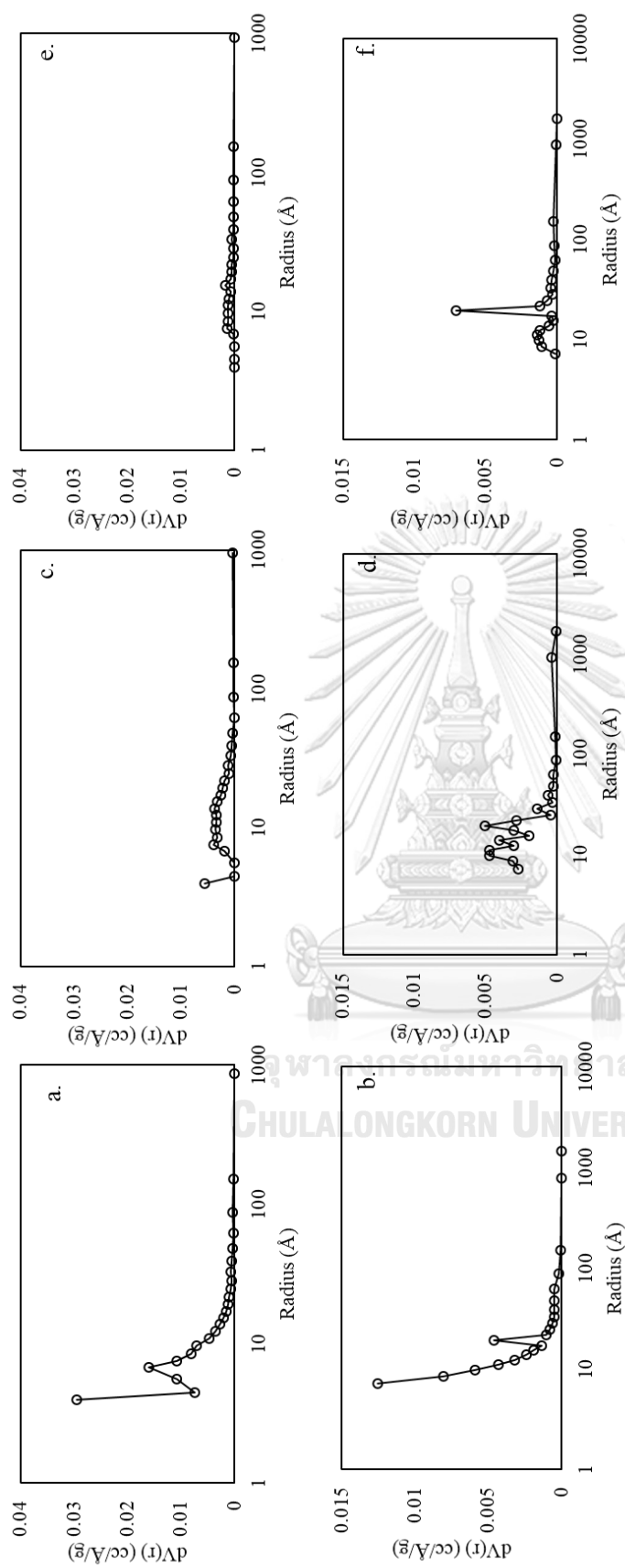
**Figure 4.13** BJH pore size distributions derived from sorption isotherm of (a) adsorption MIL-53(Al), (b) desorption MIL-53(Al), (c) adsorption C- MIL-53, (d) desorption C- MIL-53, (e) adsorption WC- MIL-53 and (f) desorption WC- MIL-53.



**Figure 4.14** BJH pore size distributions derived from sorption isotherm of (a) adsorption MIL-88B(Fe), (b) desorption MIL-88B(Fe), (c) adsorption C-MIL-88B, (d) desorption C-MIL-88B, (e) adsorption WC-MIL-88B, and (f) desorption WC-MIL-88B.



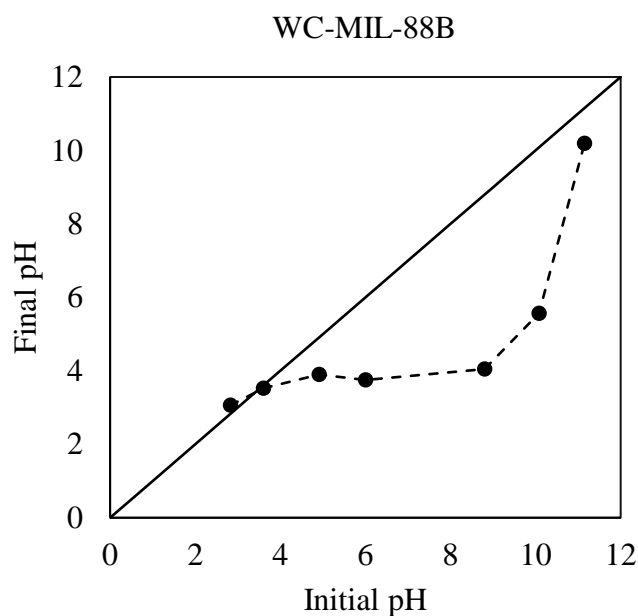
**Figure 4.15** BJH pore size distributions derived from sorption isotherm of (a) adsorption UiO-66(Zr), (b) desorption UiO-66(Zr), (c) adsorption WC-UiO-66, (d) desorption WC-UiO-66 and (e) adsorption WC-UiO-66 and (f) desorption WC-UiO-66.



**Figure 4.16** BJH pore size distributions derived from sorption isotherm of (a) adsorption HKUST-1(Cu), (b) desorption HKUST-1(Cu), (c) adsorption C- HKUST-1, (d) desorption C- HKUST-1, (e) adsorption WC- HKUST-1 and (f) desorption WC- HKUST-1.

#### 4.5 POINT OF ZERO CHARGE (PZC)

The pH of treated tap water was adjusted to the range between 2 and 12 by adding either 0.01M of HCl or 0.01M of NaOH. The 0.1 g of adsorbent was added to 50 ml of the tap water. After the pH stabilized (after shaking for 24 h), the final pH was recorded. The graphs of final pH versus initial pH were used to determine the points at which the initial and final pH values were equal. As shown in Figure 4.10, this point was taken as pHzpc. In this study, pHzpc of WC-MIL-88B (Fe), WC-ZIF-8 and PAC S10 were found to be 4, 3 and 8



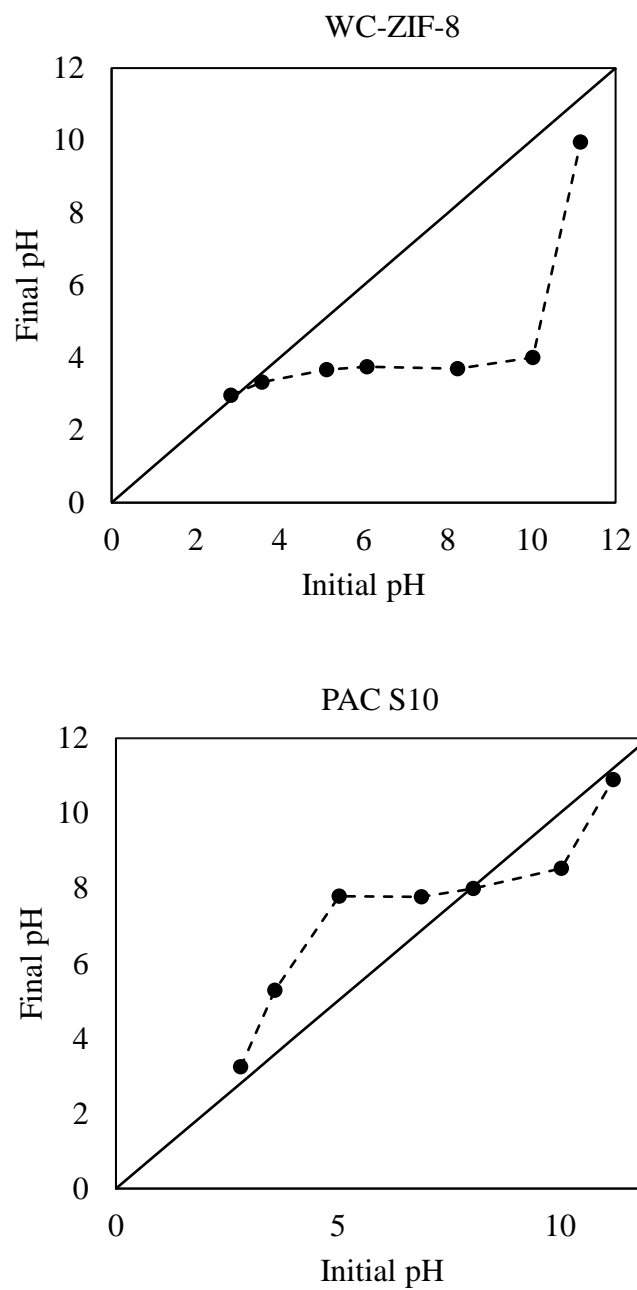


**Figure 4.17** Point of zero charges (pH<sub>zpc</sub>) of WC-MIL-88B (Fe), WC-ZIF-8 and PAC S10.



## CHAPTER V

### ADSORPTION EXPERIMENT RESULTS

#### 5.1 INTRODUCTION

Adsorption on the synthesized adsorbents was carried out in batch experiments. The adsorption capacity of these materials (ZIF-8(Zn),C-ZIF-8, WC-ZIF-8, MIL-53(Al), C-MIL-53, WC-MIL-53, MIL-88B(Fe), C-MIL-88B, WC-MIL-88B, UiO-66(Zr), C-UiO-66, WC-UiO-66, HKUST-1(Cu), HKUST-, C-HKUST-1, and PAC S10) were evaluated by adsorption of a HANs aqueous mixture. The adsorption study was started with the screening of adsorbent for selecting the most appropriate adsorbents to be the representative for further adsorptive studies such as adsorption kinetic, adsorption isotherm and adsorption selectivity.

#### 5.2. ADSORBENT SCREENING

The results of the adsorbent screening in each HANs are shown in Figure 5.1 in terms of removal percentages. First, MCAN removal percentages were slightly low for all adsorbents (approximately 0-10.3%). WC-MIL88B (Fe) shows the highest removal percentage, followed by MIL-53 (Al) and ZIF-8 at only 10.3%, 9.4%, and 8.3%, respectively. Comparing with PAC S10, these synthesized materials still show higher adsorption potential. For DCAN, WC-MIL88B surprisingly shown a quite high adsorption capacity at 97.7% and following by WC-ZIF-8 at 37.9%, while PAC S10 showed four times lower adsorption capacity than WC-MIL88B. Like MCAN, all adsorbents showed low adsorption capacity of MBAN, but slightly higher at 18.2% (WC-ZIF-8), 17.9% (WC-MIL-88B) and 9.8% for PAC S10. All washed carbonized shows high potential to adsorbed DBAN, especially WC-MIL-88B, WC-ZIF-8, and

PAC S10, which showed removal percentage at 99.1, 85.7, and 86.6 percent, respectively. According to the adsorption screening results, WC-MIL-88B (Fe), WC-ZIF-8 and PAC S10 were selected as the representative adsorbents for adsorption kinetic, isotherm and selectivity for 4-HANs

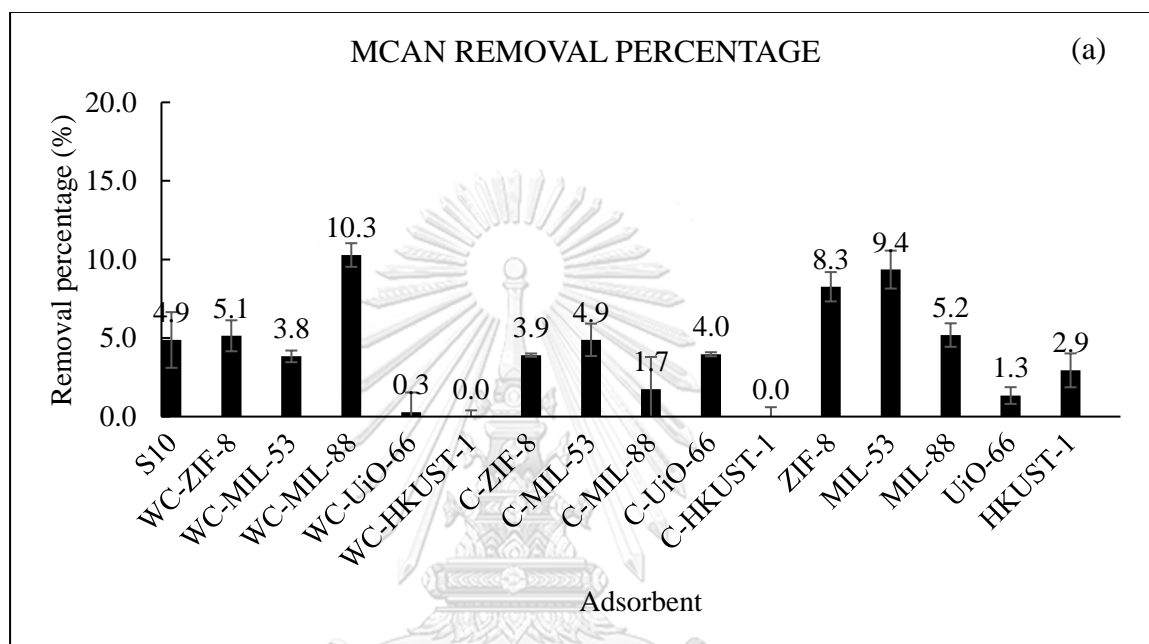


**Figure 5.1** Adsorbent screening of (a) MCAN at 1000 ppb with 0.2 g/L of adsorbent at 25 °C in tap water.

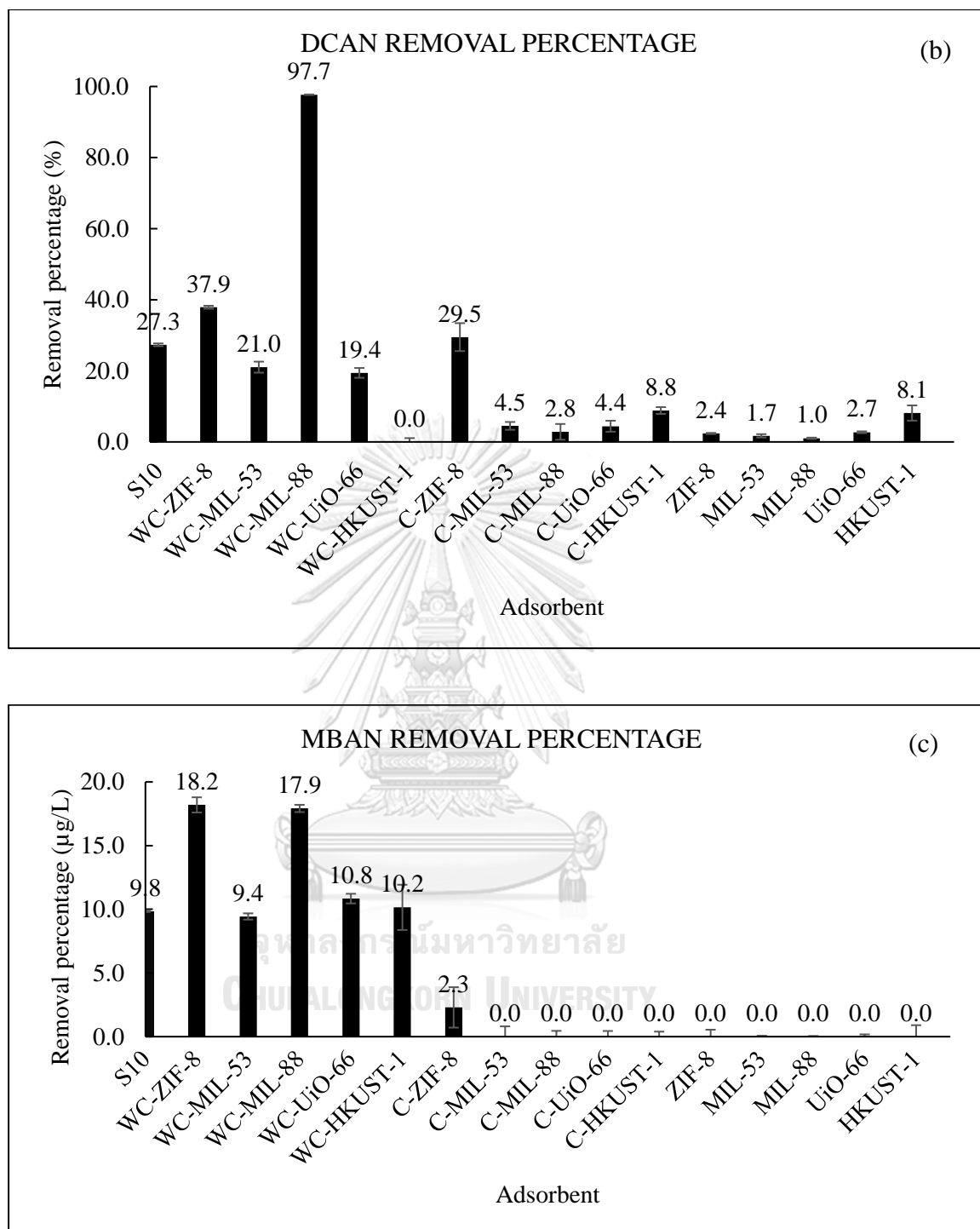


**Figure 5.2** Adsorbent screening of (b) DCAN and (c) MBAN at 1000 ppb with 0.2 g/L of adsorbent at 25 °C in tap water.

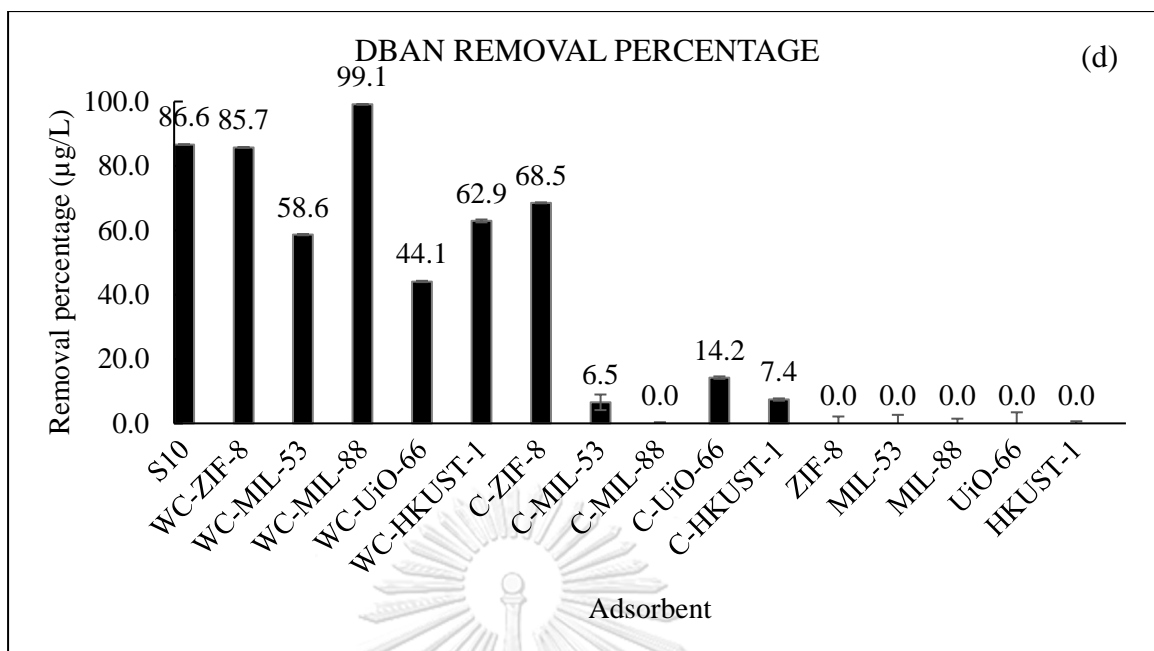


**Figure 5.3** Adsorbent screening of (d) DBAN at 1000 ppb with 0.2 g/L of adsorbent at 25 °C in tap water.

### 5.3. ADSORPTION KINETIC

From the kinetic analysis, the solute uptake rate and rate-limiting step, which controls the time required for completion of adsorption reaction was investigated. The objective of this kinetic study was focused on the analysis of the kinetics of the adsorption process with different kinds of adsorbent and adsorbate. The pseudo-first-order and pseudo-second-order adsorption kinetic models were employed to determine the adsorption order and rate constant of adsorption between HANs substance and carbonized MOFs in aqueous solution.

The kinetic adsorption experiments were carried out by withdrawing and analyzing the samples at the designed time until the consecutive residual HANs concentrations became closer. The kinetic data for the adsorption of WC-MIL-88B (Fe), WC-ZIF-8 and PAC S10 with MCAN, DCAN, MBAN, and DBAN were fitted

with the well-known kinetic models namely pseudo-first-order model and pseudo-second-order model.

Kinetic curves for HANs adsorption on the carbonized adsorbents are shown in Figure 5.3. Note that the kinetic data of adsorption are plotted with a different Y-axis scale to due to the much difference adsorption capacities. A large amount of DCAN was adsorbed over all adsorbents, but WC-MIL-88B(Fe) was reached the equilibrium within a short contact time (2 hours) whereas WC-ZIF-8 and PAC S10 can reach the equilibrium nearly to 24 hours. In addition, DBAN has the same trend for all adsorbents, but for WC-ZIF-8 and PAC S10 can reach the equilibrium faster than in DCAN adsorption.

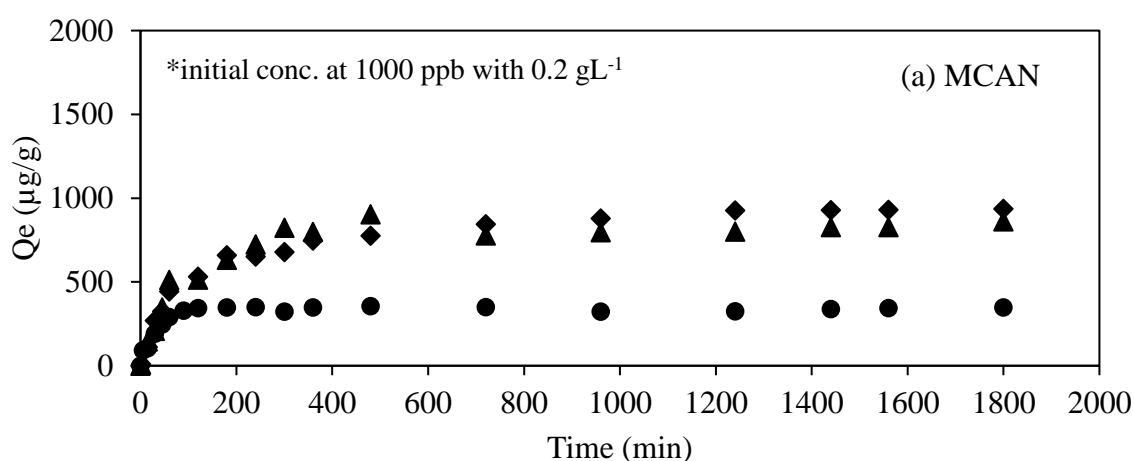
For MCAN adsorption in Figure 5.2 (a), PAC S10 reached equilibrium around 2 hours. The adsorption capacity of PAC S10 is slightly low compared with WC-MIL-88B, which shows the highest MCAN adsorption capacity and followed by WC-ZIF-8. WC-MIL-88B (Fe) and WC-ZIF-8 can reach the equilibrium at 8-9 hours.

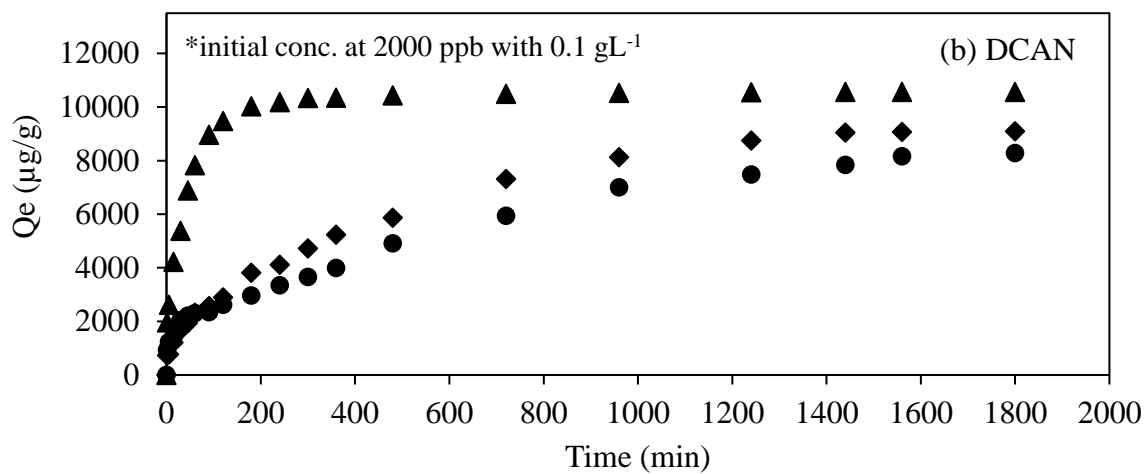
Similarly, PAC S10 shows the lowest MBAN adsorption capacity. The WC-MIL-88B (Fe) had the highest adsorption capacity for MBAN followed by WC-ZIF-8 (as shown in Figure 5.2 (c)). Adsorption rates of MBAN on all adsorbents were very slow compared with the other HANs, which might relate to the lowest hydrophobicity of MBAN (as shown in Table 2.2). The equilibriums can be reached after 20 hrs. However, WC-MIL-88 performed the highest adsorption rate for MBAN followed by WC-ZIF-8 and PAC S10 had the slowest adsorption rate.

Comparing between di-halogenic HANs (Di-HANs) and mono-halogenic HANs (Mono-HANs), the adsorption capacity was much different. Di-HANs can

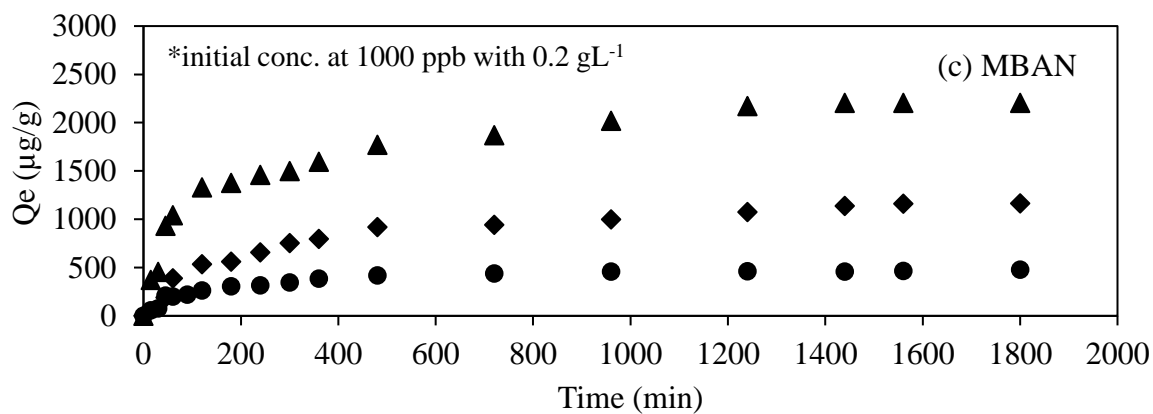
adsorb more than 4 times of mono-HANs. According to Table 5.3, the water solubility of HANs might affect the adsorption, and the large molecule of HANs (DBAN and DCAN) had more adsorbed capacity than the smaller molecule. Besides, from Table 5.3, the charge of H atom in HANs are ordered from DBAN>DCAN>MBAN>MCAN as the same order of adsorption capacity.

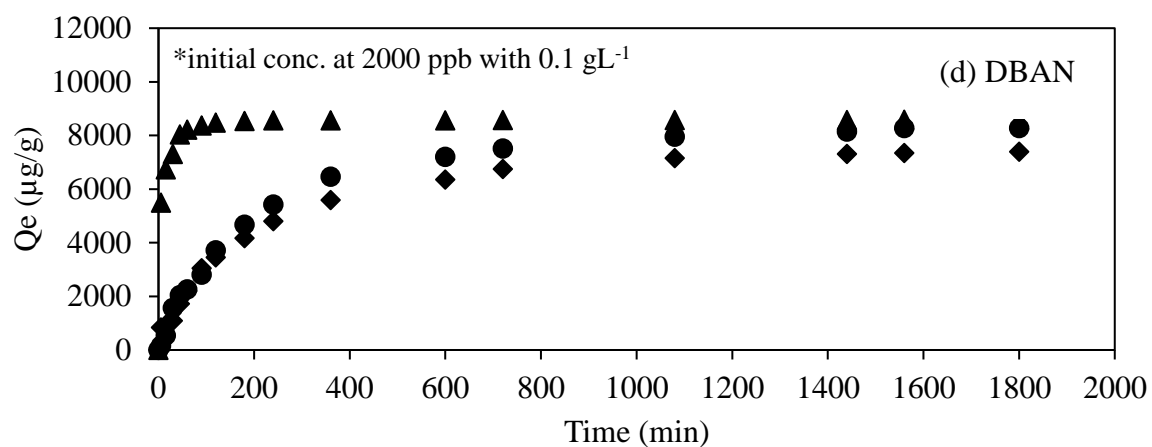
To describe the adsorption phenomena, two models for kinetic study were employed. The fitting results show that the pseudo-second-order model well fits the data more than pseudo-first-order (as shown by the kinetic parameters in Table 5.1), with the higher  $R^2$ . According to pseudo-second-order model, the driving force is the concentration of HANs in the solution which can interact with the active site on the porous carbonized MOFs, thus the removal of HANs from a solution is due to interactions between the two phases. Therefore, the pseudo-second-order model is more suitable to describe the adsorption kinetics of HANs on these porous carbonized MOFs.



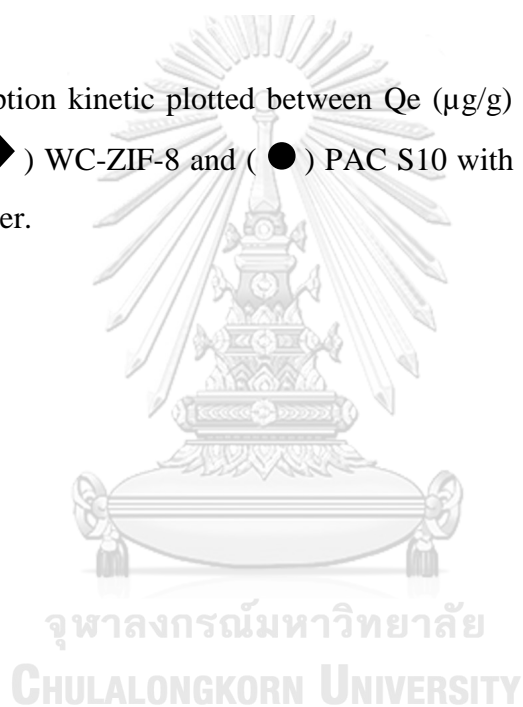


**Figure 5.4** Adsorption kinetic plotted between  $Q_e$  ( $\mu\text{g/g}$ ) versus time of (▲) WC-MIL-88B (Fe), (◆) WC-ZIF-8 and (●) PAC S10 with (a) MCAN and (b) DCAN at 25 °C in tap water.

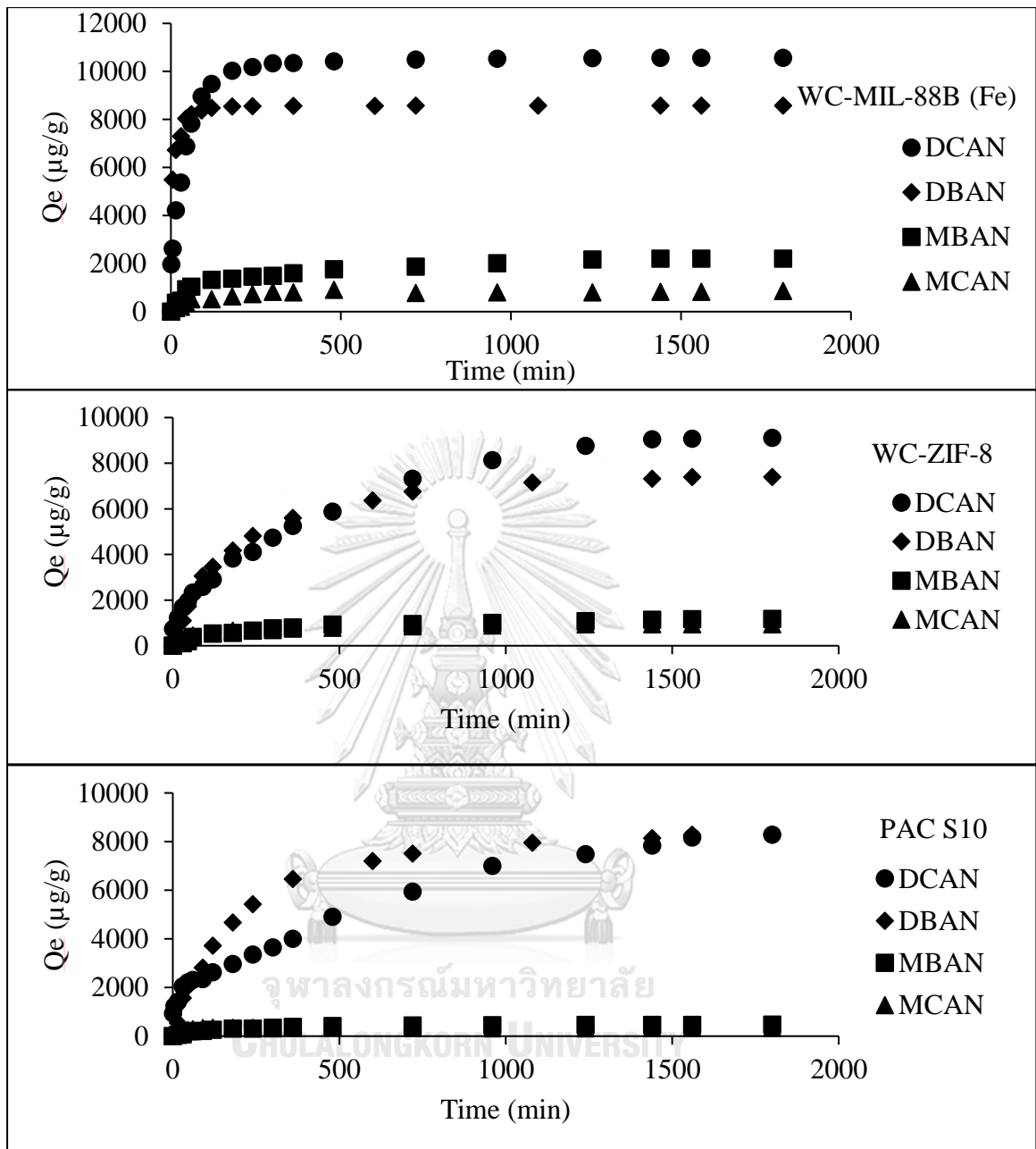




**Figure 5.5** Adsorption kinetic plotted between  $Q_e$  ( $\mu\text{g/g}$ ) versus time of (▲) WC-MIL-88B (Fe), (◆) WC-ZIF-8 and (●) PAC S10 with (c) MBAN and (d) DBAN at 25 °C in tap water.



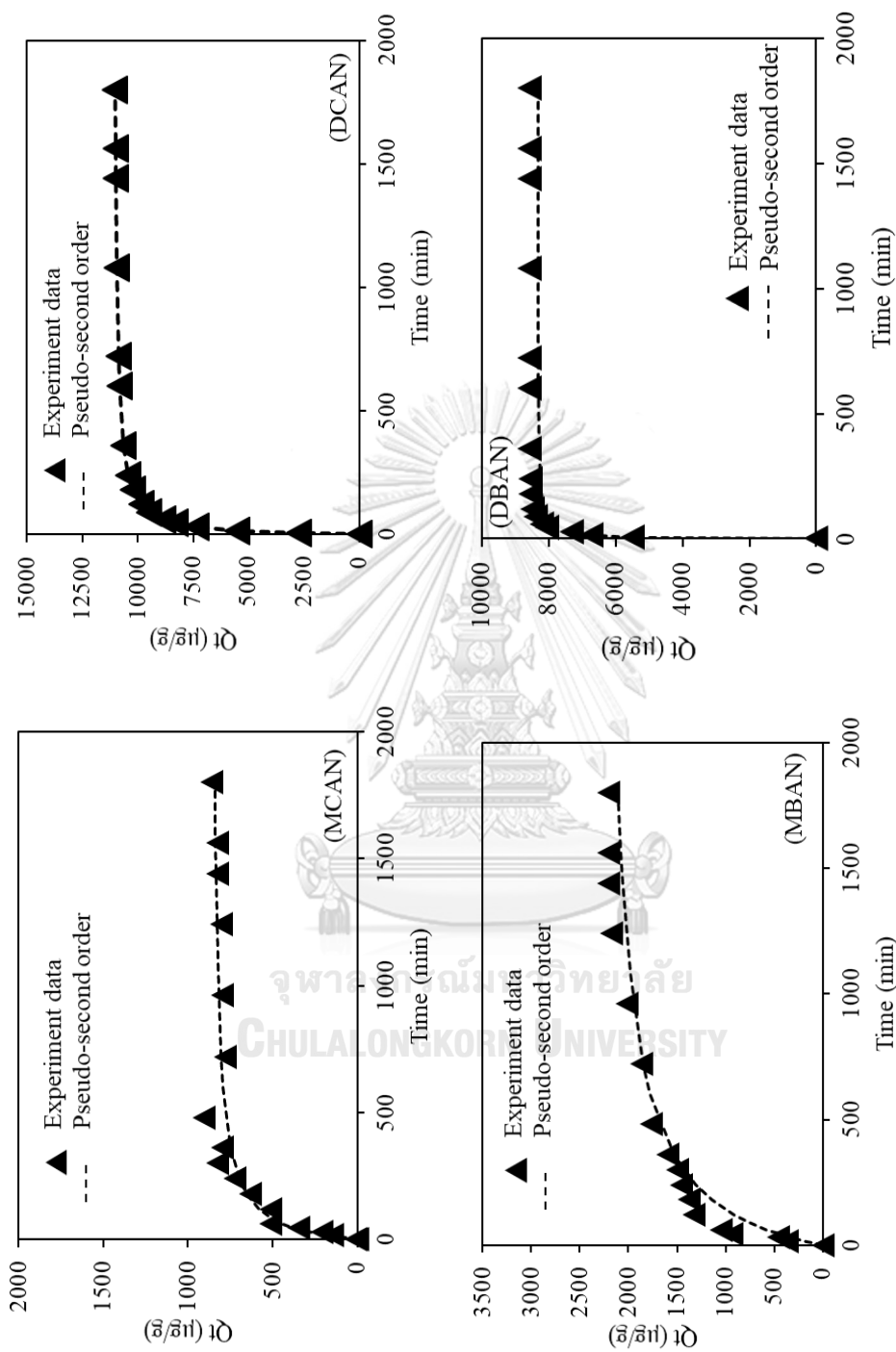




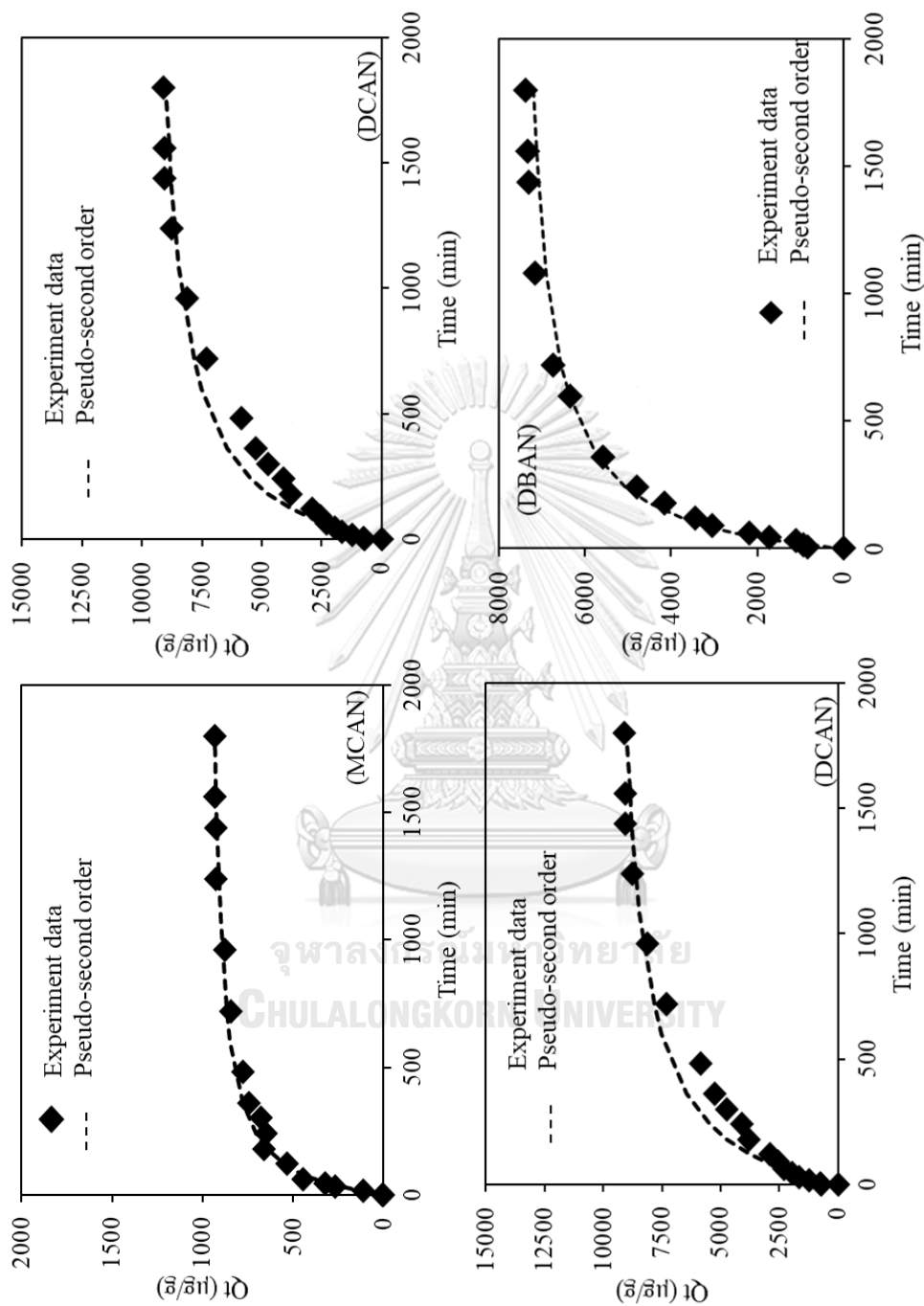
**Figure 5.6** Adsorption kinetic plot between  $Q_e$  ( $\mu\text{g/g}$ ) versus time of WC-MIL-88B (Fe), WC-ZIF-8 and PAC S10 with four HANs at 25 °C in tap water

Table 5.1 Kinetic adsorption parameters

ADSORBENT	PSEUDO-FIRST ORDER			PSEUDO-SECOND ORDER			Q <sub>e, exp</sub> μg/g	Q <sub>e, cal</sub> μg/g	ADSORPTION RATE (μg/g/h)
	R <sup>2</sup>	K <sub>1</sub>	R <sup>2</sup>	R <sup>2</sup>	K <sub>2</sub>	R <sup>2</sup>			
<b>DCAN</b>	WC-MIL-88B	0.9409	0.0022	0.9999	0.0009	0.0009	10559	10558.9	100343.2
	WC-ZIF-8	0.8753	0.0022	0.9699	0.0001	0.0001	9045.5	9038.5	8182.1
	PAC S10	0.858	0.0021	0.9474	0.0001	0.0001	7841.6	7834.6	6149.1
<b>DBAN</b>	WC-MIL-88B	0.7639	0.0018	1.0000	0.0001	0.0001	8579.4	8572.5	7360.7
	WC-ZIF-8	0.9516	0.0023	0.9944	0.0001	0.0001	7306.9	7299.9	5339.1
	PAC S10	0.9502	0.0023	0.9919	0.0001	0.0001	8142.5	8135.6	6630.2
<b>MCAN</b>	WC-MIL-88B	0.5927	0.0025	0.9961	0.0012	0.0012	826.5	825.9	819.7
	WC-ZIF-8	0.9607	0.0018	0.9975	0.001	0.001	927.7	927.0	860.7
	PAC S10	0.1368	0.0001	0.9985	0.0029	0.0029	338.6	338.4	332.6
<b>MBAN</b>	WC-MIL-88B	0.7432	0.0022	0.9944	0.0004	0.0004	2202.5	2200.7	1940.4
	WC-ZIF-8	0.8890	0.0017	0.9888	0.0008	0.0008	1135.2	1134.3	1030.9
	PAC S10	0.9218	0.0017	0.9932	0.0020	0.0020	457.4	457.9	418.4



**Figure 5.7** Comparison of the predicted and experimental data for equilibrium adsorption of four HANs on WC-MIL-88B.



**Figure 5.8** Comparison of the predicted and experimental data for equilibrium adsorption of four HANs on WC-ZIF-8

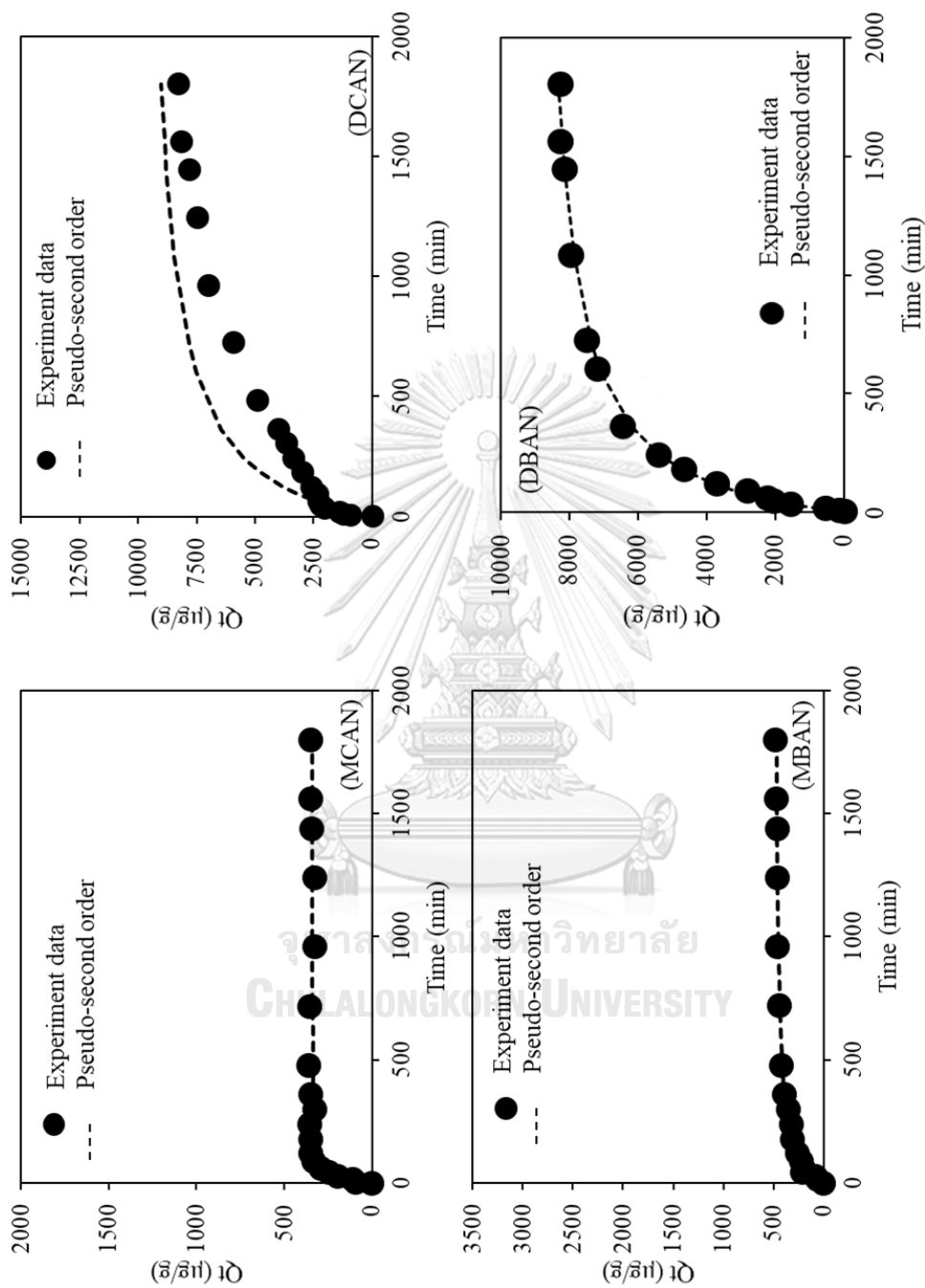


**Figure 5.9** Comparison of the predicted and experimental data for equilibrium adsorption of four HANs on PAC S10.

#### 5.4. ADSORPTION ISOTHERM (SINGLE SOLUTE)

This study investigated the effects of the surface functional group, porosity, and structures of carbonized material on the HANs adsorption isotherms. The isotherm models, linear, Langmuir and Freundlich isotherm models, were employed to determine the adsorption capacities. Towards a better understanding of the adsorption mechanism, the adsorptive interactions between the surface of adsorbents, surface charge and HAN molecular structures were determined.

According to the isotherm study for a single solute solution, the adsorption parameters were fitted with linear, Langmuir and Freundlich isotherm models as shown in Table 5.2. Adsorption isotherm of MCAN and DBAN on all three adsorbents are fitted well with Langmuir adsorption isotherm, accordingly with IUPAC adsorption classification as shown in Figure 5.7. The adsorption isotherms of MCAN and DBAN on all three adsorbents were classified in type I, which consistent with the results of micropore distribution from the surface analysis. For DCAN, adsorption on WC-MIL-88B was very high, and the linear model can be fitted well to the adsorption capacity due to the maximum capacity of WC-MIL-88B cannot be reached in the studied equilibrium concentration range (0-500 ppb).

From obtained adsorption isotherms and surface area of WC-ZIF-8 (790 m<sup>2</sup>/g) that was higher than WC-MIL-88B (189 m<sup>2</sup>/g) (as shown in Table 4.2) and comparable with PAC S10 (about 900 m<sup>2</sup>/g), which mean that surface area might not be the main factor for adsorption of four HANs on the carbonaceous surfaces. WC-MIL-88B, which has lowest surface area, had highest potential to interact with the HANs compared with WC-ZIF-8 and PAC S10.

The adsorption capacities of MCAN on carbonized MOFs (WC-MIL-88B and WC-ZIF-8) were higher than PAC. This might be caused by the effect of Metal oxide (Zn and Fe) embedded in the graphenic structure after carbonization that might enhance the adsorption capacity of MCAN. The presence of metal oxide might enhance the hydrogen bonding between N atom in MCAN, which has the highest hydrophilicity and hydroxyl groups on the surface of WC-MIL-88B and WC-ZIF-8.

Surprisingly, adsorption of DCAN on WC-MIL-88 which has the lowest surface and porosity was remarkably higher than WC-ZIF-8 and PAC. The presence of iron species on the surface should be suitable for interact with DCAN than Zn species and PAC. However, the adsorption capacities of WC-ZIF-8 and PAC were not different.

As same as MCAN, MBAN can be adsorbed by WC-MIL-88B and WC-ZIF-8 better than PAC; however, it was still much lower than DCAN adsorbed on WC-MIL-88B.

For DBAN, adsorption capacities of WC-MIL-88B and PAC were detected that higher than WC-ZIF-8. The lowest value of water solubility of DBAN might support the adsorption capacity of PAC which has the highest hydrophobicity.

The surface charge also has the effects for the HANs adsorption. Through, surface charge data of the adsorbents showed that the WC-ZIF8 and WC-MIL-88B (Fe) had more negatively charged at the adsorption pH, which is at a pH higher than adsorbents  $pH_{pzc}$ . The charge of the H-atom in the HANs molecule (from Table 5.2), is more positive compared with other atoms in HANs molecular structure. Thus, the negative surface charges of WC-ZIF8 and WC-MIL-88B could be electrostatically

attracted by the positive dipole of the H-atom in HANs molecules and deprotonated metal oxide groups (Me-O<sup>-</sup>) via ion-dipole electrostatic interaction.

At tap water pH (6-7), in addition, the surface of PAC S10 is positively charged based on  $pH_{pzc}$  at 8. Hence, the adsorbed molecule of HANs on PAC S10 should interact via the C and N atom, which had higher negative dipole moment than H and Halogen atom of the molecules (Table 5.2). Moreover, the combination of various interactions (such as hydrogen bonding, hydrophobicity, etc.) is supposed to be the main reason for HANs adsorption on PAC S10 (especially for DBAN) caused by its complex surface functional groups.

Adsorption mechanism for HANs adsorption on carbonized materials depend on the physico-chemical characteristic of materials and HANs substance which are including; physical adsorption from the weak forces such as electrostatic interactions and Van der Waals forces on the surface. Ion-dipole electrostatic interaction and H-bonding also effect to adsorption mechanism from HANs molecule. In addition, the strong chemical bonds such as covalent bonds might form between the surface of carbonized materials and the adsorbed HANs molecules in chemical adsorption (Panida Prarat, et al, 2011)



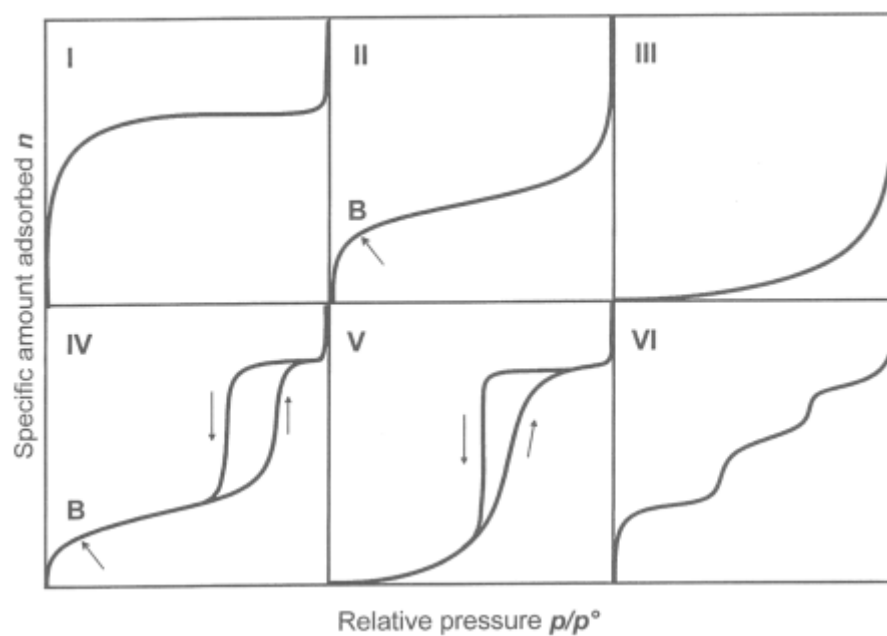


**Figure 5.10** IUPAC classification of adsorption (reference: IUPAC,1985)

**Table 5.2** HANs molecular dipole moment analysis

		<b>Charges <sup>a</sup></b>					
<b>MCAN</b>		<b>MBAN</b>		<b>DCAN</b>		<b>DBAN</b>	
C(1)	-0.1304	C(1)	-0.1205	C(1)	-0.1254	C(1)	-0.1089
C(2)	-0.1323	C(2)	-0.2513	C(2)	-0.0239	C(2)	-0.2460
N(3)	-0.0537	N(3)	-0.0542	N(3)	-0.0177	N(3)	-0.0219
Cl(4)	-0.0838	Br(4)	+0.0094	Cl(4)	-0.0362	Br(4)	+0.0633
H(5)	+0.2002	H(5)	+0.2083	Cl(5)	-0.0364	Br(5)	+0.0632
H(6)	+0.2002	H(6)	+0.2083	H(6)	+0.2399	H(6)	+0.2504

<sup>a</sup> Reference: Panida Prarat, et al, 2011

**Table 5.3** HANs molecular size

Parameters	HANs				
	MCAN	MBAN	DCAN <sup>a</sup>	DBAN	TCAN
MW (g mol <sup>-1</sup> )	75.50	119.95	109.94	198.85	144.39
Width (Å <sup>o</sup> )	2.43	2.52	2.89	2.52	2.90
Length (Å <sup>o</sup> )	3.10	3.15	3.61	3.75	3.60

<sup>a</sup> Reference: Panida Prarat, et al, 2011

**Table 5.4** Adsorption isotherm parameters

	Model	parameter	adsorbent		
			WC-MIL-88	WC-ZIF-8	PAC
MCAN	Langmuir	R <sup>2</sup>	0.9815	0.9447	0.9941
		Q <sub>m</sub> , μg/g	399.4	680.4	1441.4
		K <sub>L</sub> , L/ μg	0.1072	0.0437	0.0145
	Freudlich	R <sup>2</sup>	0.9024	0.8124	0.9645
		n	0.6367	0.4704	0.408
		K <sub>F</sub> , L/ μg	0.5462	0.3197	0.2653
linear	R <sup>2</sup>	0.7559	0.6147	0.7415	
	K <sub>p</sub>	1.8489	1.376	1.658	

	Model	parameter	adsorbent		
			WC-MIL-88	WC-ZIF-8	PAC
DCAN	Langmuir	R <sup>2</sup>	0.7352	0.9283	0.8444
		Q <sub>m</sub> , μg/g	112064.1	29952.7	106362
		K <sub>L</sub> , L/ μg	0.0014	0.0035	0.0006
	Freudlich	R <sup>2</sup>	0.7681	0.7376	0.9395
		n	0.32046	0.4378	0.41307
		K <sub>F</sub> , L/ μg	1.1438	0.2358	0.0941
linear	R <sup>2</sup>	0.8293	0.526	0.9194	
	K <sub>p</sub>	9.8523	8.6754	5.4203	

	Model	parameter	adsorbent		
			WC-MIL-88	WC-ZIF-8	PAC
MBAN	Langmuir	$R^2$	0.8291	0.7764	0.977
		$Q_m, \mu\text{g/g}$	3456.2	1296.2	751.7
		$K_L, \text{L}/\mu\text{g}$	0.0134	0.018	0.0164
	Freudlich	$R^2$	0.8986	0.905	0.832
		n	0.343292	0.49804	0.561079
		$K_F, \text{L}/\mu\text{g}$	0.2884	0.4126	0.2118
linear	$R^2$	0.9155	0.9155	0.6153	
	$K_p$	3.6376	5.5218	1.4518	

	Model	parameter	adsorbent		
			WC-MIL-88	WC-ZIF-8	PAC
DBAN	Langmuir	$R^2$	0.8576	0.7676	0.9028
		$Q_m, \mu\text{g/g}$	14271071.3	104918.3	66211184.2
		$K_L, \text{L}/\mu\text{g}$	0.0002	0.0021	0.0001
	Freudlich	$R^2$	0.8476	0.686	0.6561
		n	0.19135	0.3665	0.1043
		$K_F, \text{L}/\mu\text{g}$	0.2582	0.2174	0.2298
linear	$R^2$	0.835	0.716	0.447	
	$K_p$	228.04	20.252	121.01	

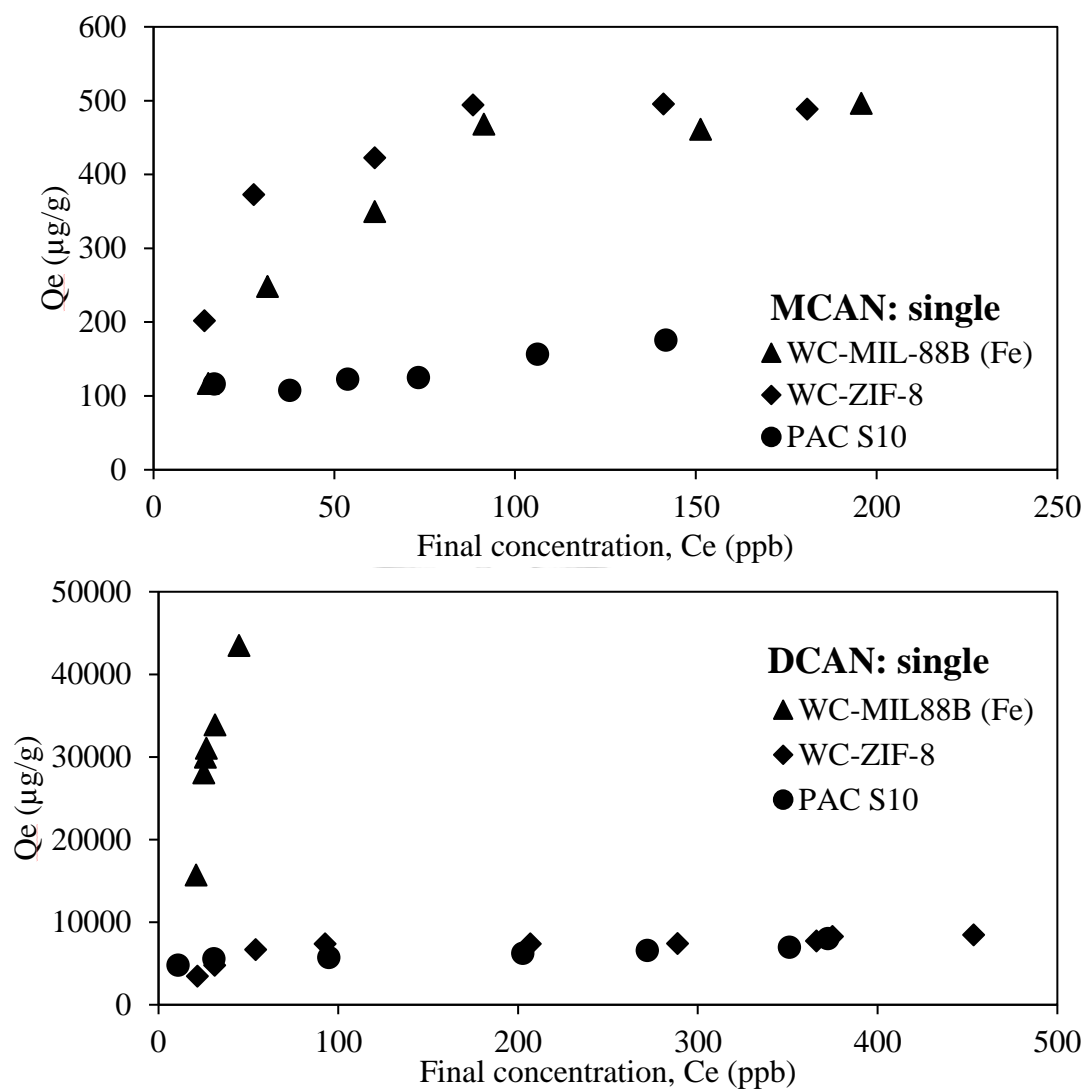


**Figure 5.11** Adsorption isotherms of MCAN and DCAN (in single solute) on WC-MIL-88B, WC-ZIF-8 and PAC S10 at 25 °C in tap water.

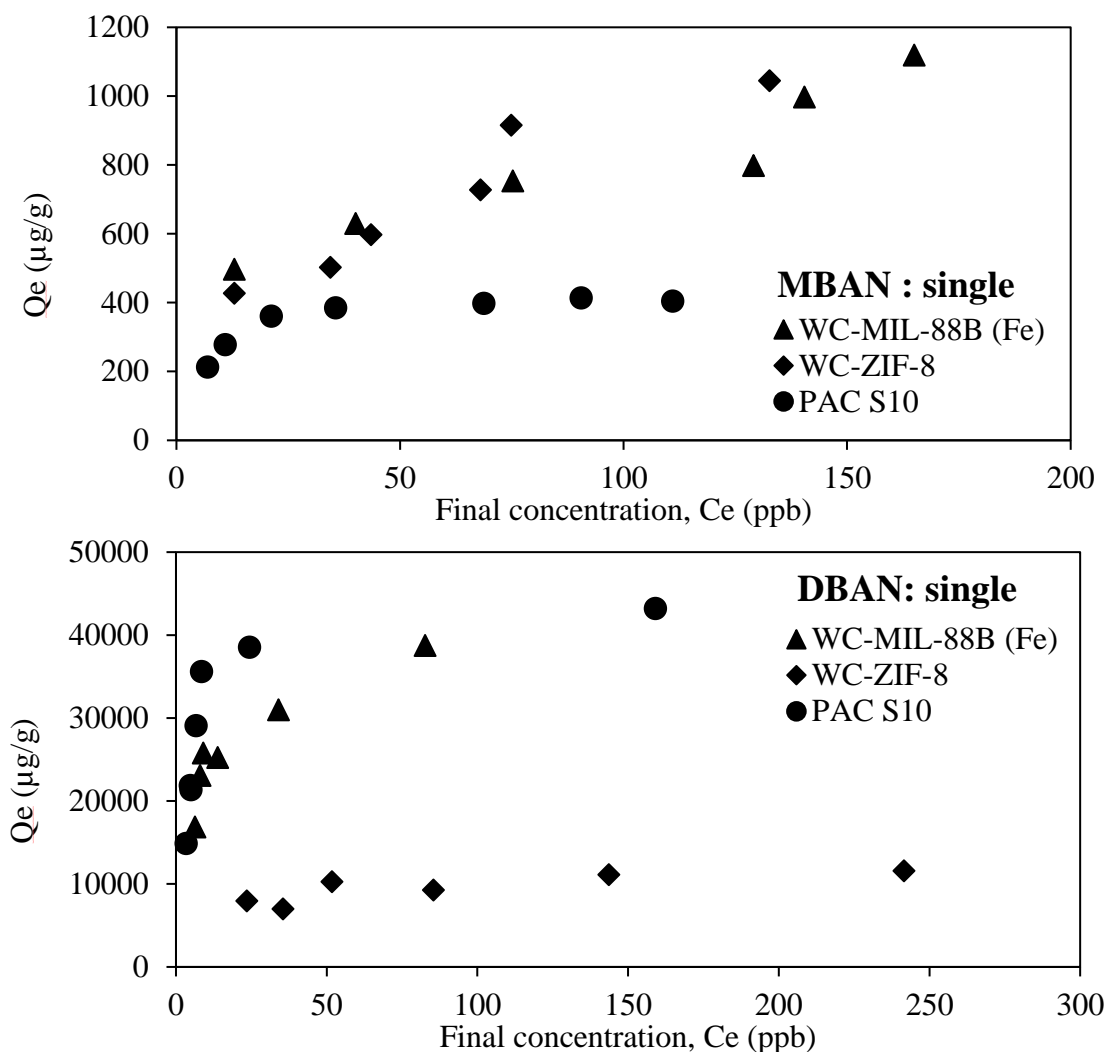


**Figure 5.12** Adsorption isotherms of MBAN and DBAN (in single solute) on WC-MIL-88B, WC-ZIF-8 and PAC S10 at 25 °C in tap water.

### 5.5. ADSORPTION SELECTIVITY (IN MIXED SOLUTE)

A comparison of adsorption capacities (shown in Figure 5.8) was included the adsorption isotherms of four HANs in single-solute solution and mixed-solute solution on WC-MIL-88B, WC-ZIF-8, and PAC S10. From Figure 5.8 (a), WC-MIL-88B could adsorb dihalogenic HANs (DCAN and DBAN) with very high capacities but exhibited low adsorption capacities for mono-halogenic HANs (MCAN and MBAN). This might be caused by the hydrophobic interaction which can be discussed

by water solubilities of di-halogenic HANs (as shown in Table 2.2) that are very low compared with the mono-halogenic HANs. Moreover, WC-ZIF-8 and PAC S10 (Figure 5.8 c,e) also shown the same trend in single-solute adsorption which can support the effect of hydrophobicity interaction of HANs on carbonized surfaces. However, PAC S10 exhibited lower adsorption capacity of DCAN (Figure 5.8e) lower than WC-ZIF-8 and WC-MIL-66B, which means that the surface of PAC S10 is sensitive to the hydrophobicity of DCAN than the others.

Figure 5.8 (b) reported the adsorption capacities of mixed HANs on WC-MIL-88B, which shown the same trend and sequence with the case of single-solute solution. Moreover, active surface of WC-MIL-88B seems to be enough for adsorption of mixed four HANs in equilibrium concentration range of 0-100 ppb. However, MCAN and MBAN in mixed-solute solution seem to have lower capacity by WC-MIL-88B (Fe) than in single-solute solution.

Adsorption isotherms of WC-ZIF-8 in Figure 5.8 (c) and (d) revealed the same trend with WC-MIL-88B. According to the obtained data shown in Figure 5.8, di-halogenic HANs, which had higher molecular weight and more atom of halogen group, are adsorbed well more than mono-HANs on all adsorbents. In addition, bromo-HANs had higher adsorption capacity than chloro-HANs, might due to the stronger charge in molecule. Thus, these results indicated the pattern of HANs adsorption which preference order as DBAN, DCAN, MBAN and MCAN, similarly to the order for single solute adsorption.

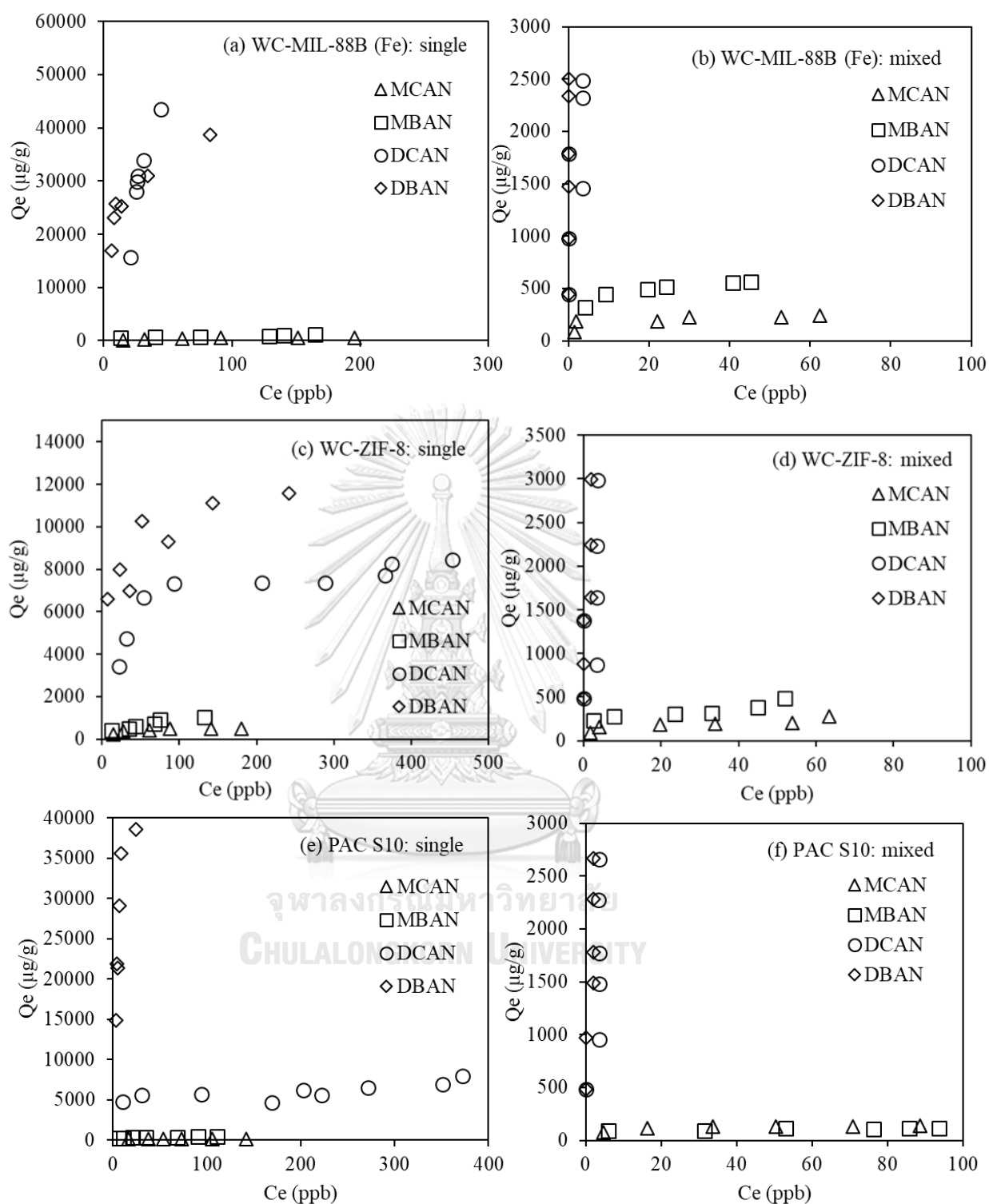


**Figure 5.13** Adsorption isotherms of WC-MIL-88B, WC-ZIF-8 and PAC S10 for four HANs in single-solute and mixed -solute in tap water at 25 °C.

## 5.6 SURFACE ELEMENT ANALYSIS BY X-RAY PHOTOELECTRON SPECTROSCOPY (XPS)

According to the EDS data reported in Table 4.1, the data could reveal only the mass and atomic percentage of each element. XPS was employed for further study to evaluate the feasible element which can bond with DCAN. In this study, 0.1 g of WC-ZIF-8 and WC-MIL-88B were used as representative carbonized MOFs which were mixed in 3,000 ppb DCAN solution, after adsorption was reached the equilibrium, the adsorbents were separated and dried at 60°C then keep in desiccator until tested by XPS; Pre-WC-MOFs stand for virgin carbonized MOFs and Post-WC-MOFs stand for DCAN adsorbed carbonized MOFs.

**Figure 5.9 (right)** shows the C 1s XPS spectra of post-WC-MOFs at varying charged and discharged states. For comparison, the pre-WC-MOFs were measured in the same procedure are illustrated in **Figure 5.9 (left)**. In general, the C 1s spectra of carbonized material displayed 4-5 peaks with binding energies of 284.6 eV, 285.6 eV, 286.7, 288.1 and 289.6 eV, with error in the binding energies of  $\pm 0.2-1$  eV. In the C 1s spectrum of the pre-WC-ZIF-8, all peaks shift at a little higher binding energy comparing with post-WC-ZIF-8. The peak at 284.6 eV, 285.6 eV, 286.7, 288.1 and 289.6 eV are observed which is responsible for the C=C/C-C, C=O, C-N, O-C=O and C=N.

C 1s XPS spectra of pre-MIL-88B (Fe) exhibits similar 4 peak without peak at binding energy 288.1 eV which are carbonyl group (O-C=O) but the carbonyl peak is appeared in post MIL-88B (Fe) at binding 288.78 eV.



According to the similar peak for both pre and post WC-MOFs, also the peak percentage which quite same after adsorption, the carbonaceous species on the surfaces might not directly participate in DCAN adsorption.

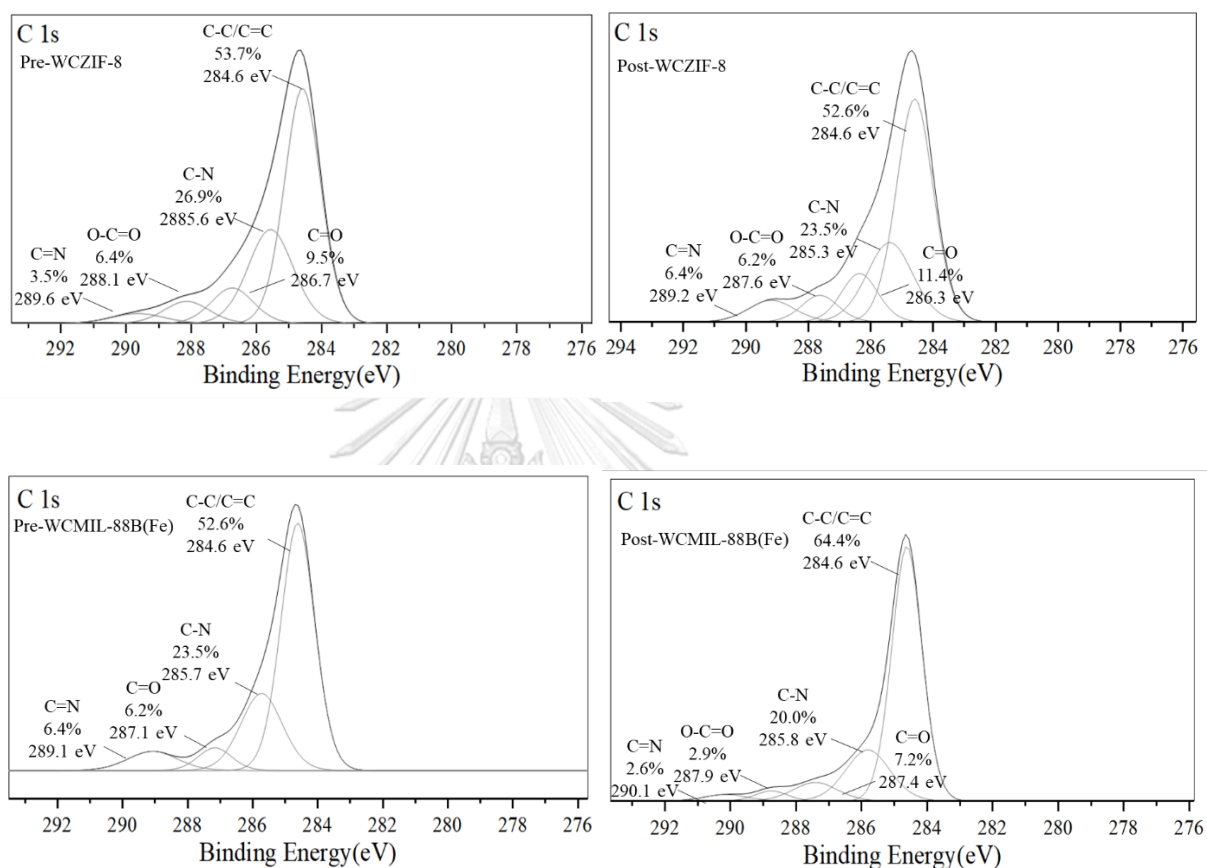


**Figure 5.14** C 1s XPS spectra of pre- and post-WC-ZIF-8 and WC-MIL-88B.

O 1s spectra were analyzed at binding energy 530 eV to 535 eV. For all materials could identify similar three peaks (as shown in Figure 5.10). Oxygen atom that bond in metal oxide complex can be identified at around binding energy 530.5 eV. In case of WC-ZIF-8 and WC-MIL-88B, the bonding are attributed to Zn-O and Fe-O, respectively. Binding energy at 532 eV and 533eV may contribute to the carbon species with C=O or O-C=O bonds that are a part of carboxylic or carbonyl functional groups. Considering the peak percentage after adsorption, both WC-ZIF-8 and WC-MIL-88B (Fe) showed the decreasing of the peak for O-C=O (at 533.9 ev.),

resulting the increase of C=O peak (at 53.21 ev.). This might be assumed that that can assume DCAN might interact with the adsorbents via O-C=O groups by ion-dipole electrostatic interaction.

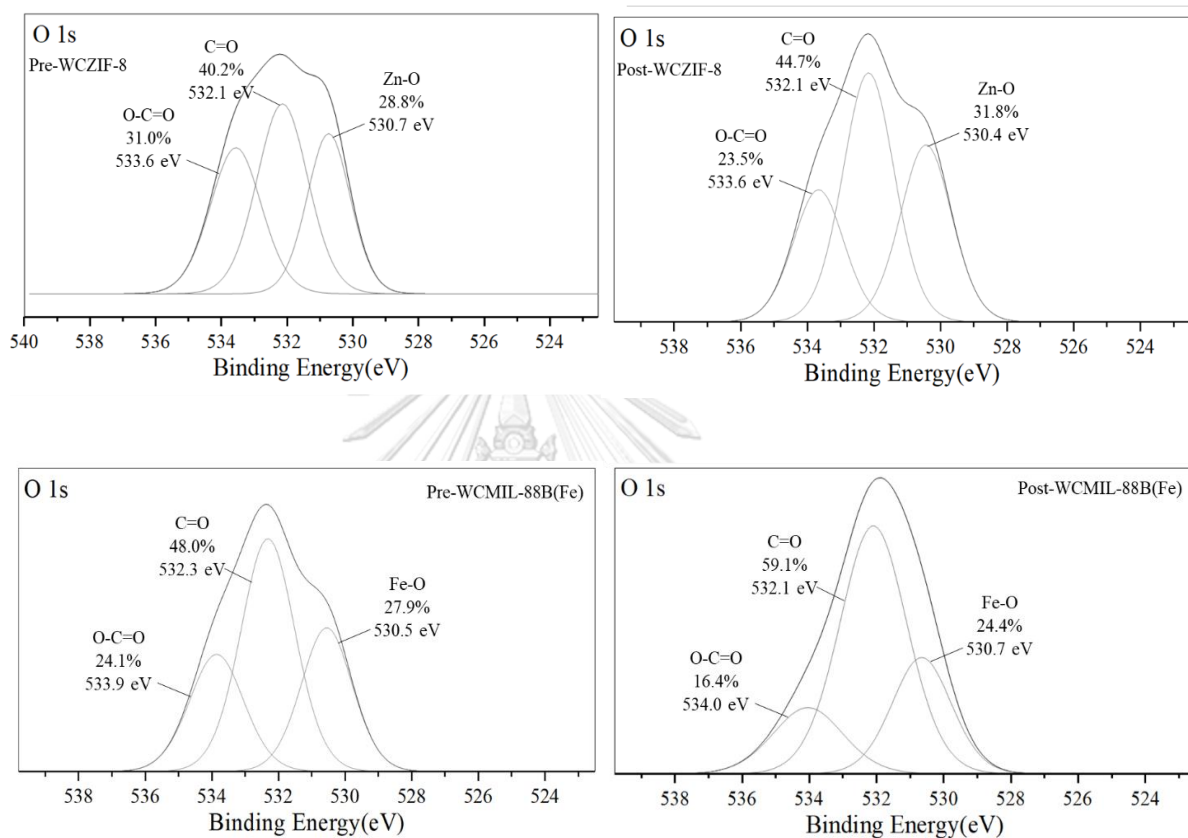


**Figure 5.15** O 1s XPS spectra of pre and post WC-ZIF-8 and WC-MIL-88B.

Zn 2p spectra of WC-ZIF-8 are shown in **Figure 5.10**. Zn 2p has 2 orbital including Zn 2p<sub>1/2</sub> and Zn 2p<sub>3/2</sub> which show at binding energy 1,021 eV and 1.045 eV, respectively. Zn–O bond was detected at 1,021 eV in both pre and post WC-ZIF-8 and have the similar peak percentage at 59-60%. The results of the Zn species in peak fitted could assumed that Zn species are not significant impact to the DCAN adsorption.

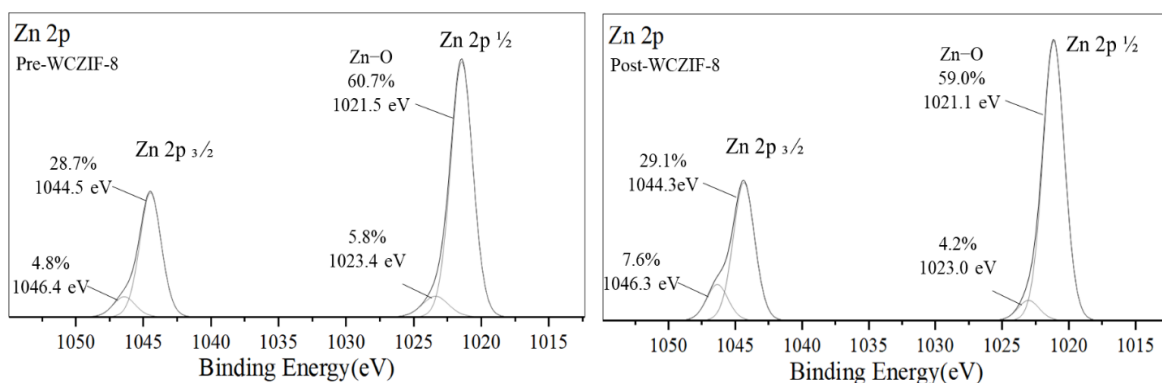


**Figure 5.16** Zn 2p XPS spectra of pre and post WC-ZIF-8

As shown in Figure 5.12, Fe 2p spectra at the peak 707.5eV of pre-WC-MIL-88B (Fe) can be attributed to zero-valence Fe, the other signals of 711.6 eV, 725.0 eV and shake-up satellite Fe at 720.2 eV are also observed. After adsorption, the peak located at around 710.0eV are appear. This peak could be attributed to Fe in the Fe-N<sub>x</sub> configuration. Thus, the results could assume than post-WC-MIL-88B (Fe) has Fe-N<sub>x</sub> bonding from N atom of DCAN.

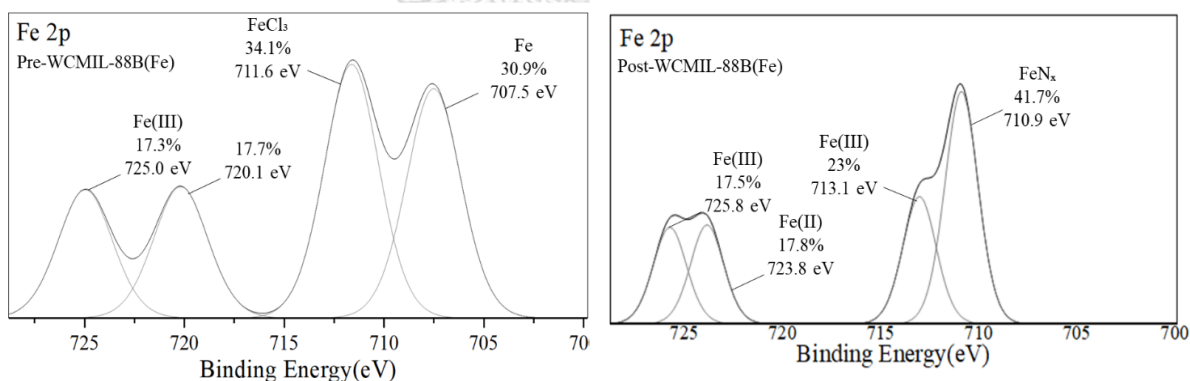


**Figure 5.17** Fe 2p XPS spectra of pre and post WC-MIL-88B.

The N 1s spectra of WC-ZIF-8 in Figure 5.13, three types of nitrogen spectra are deconvoluted. The presence of peaks located at 398.2 eV, 399.6±2 eV, and 401.0±3 eV can be attributed to the formation of C-NH<sub>2</sub>, C-N=C and graphitic N, respectively, with slightly C-N=C bonding changed. N species in WC-ZIF-8 might be formed by the substrate which has zinc nitrate hexahydrate and after carbonization N

atom became graphitic N. Whereas, pre-MIL-88B (Fe) could not detect N species. After adsorption, 3 peaks were observed at 399.1 eV, 401.2 eV and 402.7 eV and identified as Fe-N<sub>x</sub>, graphitic N and C-NH<sub>3</sub>. The observed peak can attribute the assumption that WC-MIL-88B can adsorb DCAN via the interaction between Fe complex and N atom on DCAN.

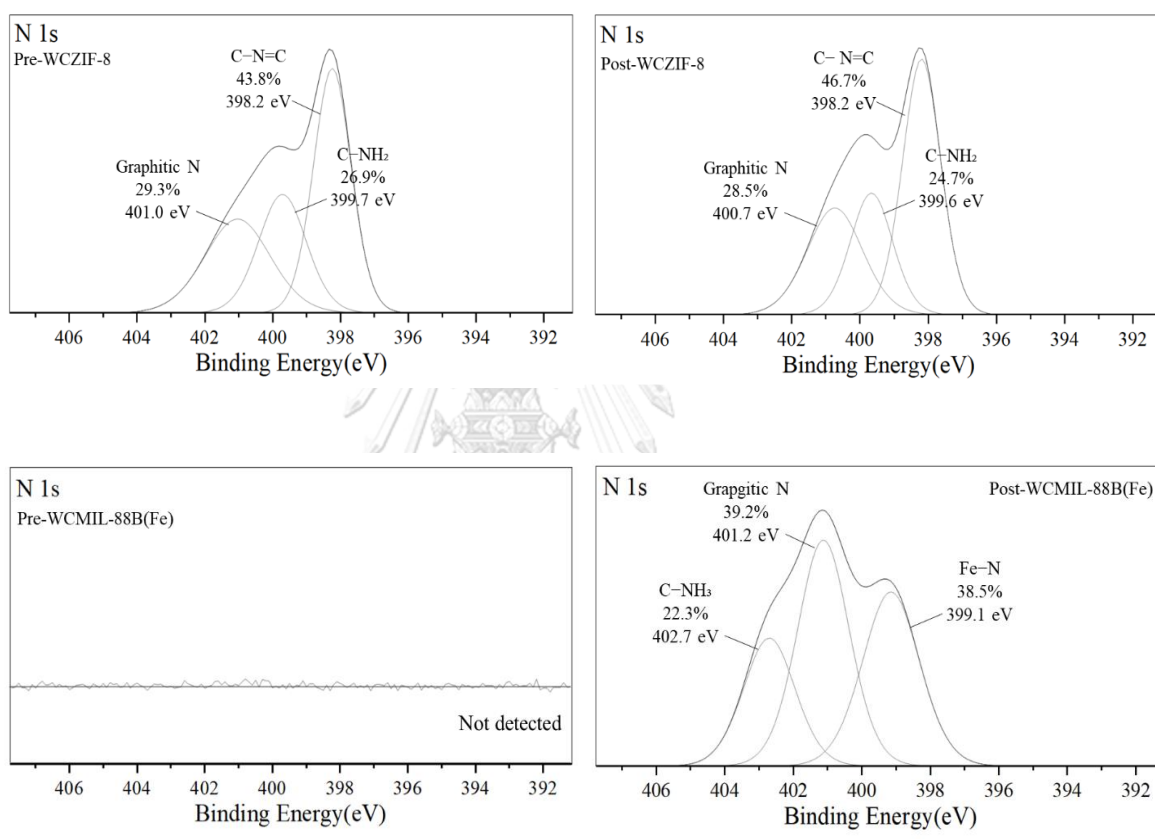


**Figure 5.18** N 1s XPS spectra of pre and post WC-ZIF-8 and WC-MIL-88B (Fe)

Cl 2p spectra was observed in pre-WC-MOFs, that might be the signal from the residual HCl used in the acid washing step and could not be washed out by DI water. The observed peaks were  $197.6 \pm 0.2$  eV,  $199.0 \pm 0.7$  eV and  $200 \pm 0.1$  eV, which are contributed to Cl<sup>-</sup>. For WC-MIL-88B(Fe), the presence of Cl<sup>-</sup> at peaks at  $199.5 \pm 2$  and  $200.2 \pm 3$  eV can be also indicated to the chloride ion in FeCl<sub>2</sub>, and the peaks

located at 200.4 eV and 201.7 eV can be attributed to C–Cl. The prominent Cl peaks at  $198.2\pm 0.2$  eV and  $199.7\pm 0.2$  eV can be attributed to chlorine intercalated between the graphite layers. After DCAN adsorption, significantly changed of Cl 2p spectra cannot be detected, which mean that the Cl<sup>-</sup> atom in both adsorbents and DCAN might not be the main active functional group for the adsorption.

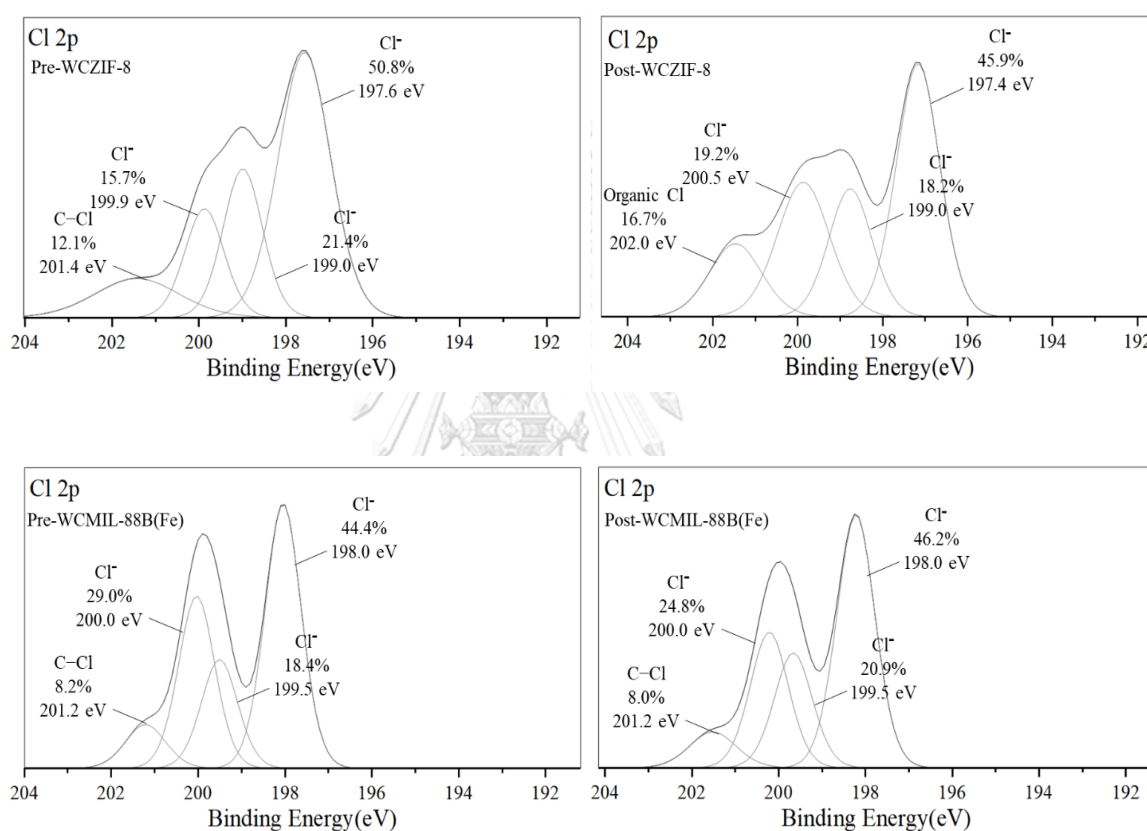


**Figure 5.19** Cl 2p XPS spectra of pre and post WC-ZIF-8 and WC-MIL-88B.

## 5.7 DEGRADATION OF HANs

During the experiment, the changing of HANs concentration in tap water was observed and it was found that HANs species can be degraded gradually by the time. The degradation might be caused by hydrolysis reaction between HANs and water, photodegradation or evaporation to the ambient. However, the amber bottle with a screw cap was applied to reduce the evaporation loss and photodegradation. Figure

5.14 showed the decrease of each HANs concentration during shaking period by the time. The result indicates that DCAN has the highest degradation rate at 0.69%/h following by DBAN, MCAN and MBAN at 0.26, 0.24 and 0.17%/h, respectively.

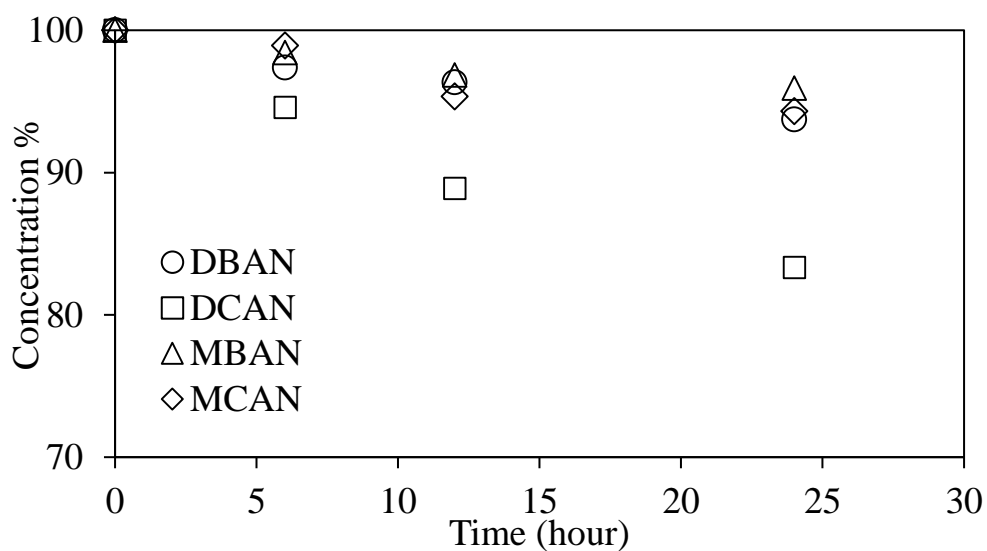


**Figure 5.20** The decrease of HANs concentration by the time.



## CHAPTER VII

### CONCLUSIONS

The main objective of this study is to investigate the removal of haloacetonitriles (HANs) in aqueous solution by adsorption on various carbonized metal-organic frameworks (MOFs). Five pristine MOFs were synthesized and modified by carbonization with N<sub>2</sub> flow at 900°C and pre-treatment by acid washing to investigate the effect of surface characteristics including; crystalline structure, functional group, and surface charge on adsorption performance and mechanism compared with commercial powder activated carbon (PAC S10). In addition, HANs characteristic also observed to investigate the effect of molecular weight, molecular size, water solubility and charges. All adsorbents were characterized their physicochemical properties. The adsorption kinetics, adsorption isotherms and mechanism, selective adsorption of HANs by comparing single- and mixed-solute solutions were also investigated under batch adsorption experiments.

According to the physicochemical property characterization results, the crystalline structure of material was exhibited based on XRD pattern along with reference with databased. FT-IR spectra demonstrated the presence of the surface functional groups and contaminant or by-product coverage form carbonization on the adsorbent surface. N<sub>2</sub> adsorption isotherms, which are represent the surface area, pore volume and pore distribution of materials. Morphology and component of adsorbents were investigated with SEM-EDS exhibit the morphology, average particle size and element component percentage at surface level, conclusion of characterization is the

material physicochemical property were change after surface carbonization and acid wash.

Pristine and carbonization MOFs which are ZIF-8(Zn), MIL-53(Al), MIL-88B(Fe), UiO-66(Zn), and HKUST-1(Cu) were successfully synthesized. After acid washing, the surface area and pore volume of carbonized ZIF-8 and MIL-88B were increased, whereas, carbonized HKUST-1 and UIO-66 were decreased. After HANs adsorption screening, WC-MIL-88B and WC-ZIF-8 were selected to study the adsorptive information of HANs compared with PAC S10.

For kinetic adsorption study, the pseudo-second-order model can be used to describe the adsorption kinetic of HANs onto the synthesized adsorbents. WC-MIL-88B performed fastest adsorption rate for all four HANs. The adsorption rates on WC-MOFs are in order of DBAN>DCAN>MBAN>MCAN. The kinetic results were implied that the adsorption process was dependent characteristic of the adsorbent and HANs. The HANs molecular size and the hydrophobicity influenced the adsorption rates of HANs and active sites of adsorbents.

For adsorption isotherm studies, the results indicated that the surface functional groups, metal complex of WC-MOFs significantly affected the adsorption capacity of four HANs. WC-MIL-88B (Fe) could efficiently adsorb HANs comparable with PAC S10, both of adsorption capacity and adsorption rate. WC-ZIF-8 performed a comparable adsorption capacity of four HANs with the PAC S10. Di-halogenic HANs (DBAN and DCAN) can be adsorbed by WC-MOFs much better than mono-halogenic HANs (MBAN and MCAN). Three isotherm models are used to describe adsorption isotherm including linear model, Freundlich's model, and



Langmuir's model. Most of the adsorption isotherms are fitted well with Langmuir's model. From XRD analysis, O-C=O and Fe-O functional groups of WC-MIL-88B might play the important role for adsorption of four HANs.

The results of selective adsorption study revealed that the molecular structure of HANs resulting hydrophobicity of the molecules, significantly affected the adsorption capacity and selectivity all adsorbents (WC-MOFs and PAC S10). Moreover, in low concentration application, adsorption sites of WC-MIL-88B are expected to be enough for mixed solute HANs adsorption, and the order of adsorption capacities do not change from the single-solute case.

The results of this study revealed that WC-MIL88B (Fe) and WC-ZIF-8 could be an alternative adsorbent to PAC S10 for HANs removal from tap water due to their excellent adsorption capacities. For recommendation, adsorption study from another type of DBPs should be conducted i.e. trihalomethanes (THMs) and haloacetic acids (HAAs). Moreover, the investigation related to the stability of the material should be conducted such as the metal release test and the release of dissolved organic compounds during adsorption process. In addition, cost-benefit analysis should be investigated for comparing with commercial adsorbents and the other treatment methods.

## REFERECES

- An, B., Cheng, K., Wang, C., Wang, Y., & Lin, W. (2016). Pyrolysis of Metal–Organic Frameworks to Fe<sub>3</sub>O<sub>4</sub>@Fe<sub>5</sub>C<sub>2</sub> Core–Shell Nanoparticles for Fischer–Tropsch Synthesis. *ACS Catalysis*, 6(6), 3610–3618. doi:10.1021/acscatal.6b00464
- Bakhtiari, N., Azizian, S., Alshehri, S. M., Torad, N. L., Malgras, V., & Yamauchi, Y. (2015). Study on adsorption of copper ion from aqueous solution by MOF-derived nanoporous carbon. *Microporous and Mesoporous Materials*, 217, 173–177.
- Bonilla-Petriciolet, A., Mendoza-Castillo, D. I., & Reynel-Ávila, H. E. (2017). *Adsorption processes for water treatment and purification*: Springer.
- Brunauer, S., Emmett, P. H., & Teller, E. (1938). Adsorption of gases in multimolecular layers. *Journal of the American Chemical Society*, 60(2), 309–319.
- Chiericatti, C., Basilico, J. C., Basilico, M. L. Z., & Zamaro, J. M. (2012). Novel application of HKUST-1 metal–organic framework as antifungal: Biological tests and physicochemical characterizations. *Microporous and Mesoporous Materials*, 162, 60–63.
- Do, X.-D., Hoang, V.-T., & Kaliaguine, S. (2011). MIL-53(Al) mesostructured metal–organic frameworks. *Microporous and Mesoporous Materials*, 141(1–3), 135–139. doi:10.1016/j.micromeso.2010.07.024
- Furukawa, H., Ko, N., Go, Y. B., Aratani, N., Choi, S. B., Choi, E., . . . Kim, J. (2010). Ultrahigh porosity in metal-organic frameworks. *Science*, 329(5990), 424–428.
- Gholizadeh Khasevani, S., & Gholami, M. R. (2018). Engineering a highly dispersed core@shell structure for efficient photocatalysis: A case study of ternary novel BiOI@MIL-88A(Fe)@g-C<sub>3</sub>N<sub>4</sub> nanocomposite. *Materials Research Bulletin*, 106, 93–102. doi:10.1016/j.materresbull.2018.05.024
- Gopal, K., Tripathy, S. S., Bersillon, J. L., & Dubey, S. P. (2007). Chlorination byproducts, their toxicodynamics and removal from drinking water. *Journal of hazardous materials*, 140(1–2), 1–6.
- Hou, S., Wu, Y. N., Feng, L., Chen, W., Wang, Y., Morlay, C., & Li, F. (2018). Green synthesis and evaluation of an iron-based metal-organic framework MIL-88B for efficient decontamination of arsenate from water. *Dalton Trans*, 47(7), 2222–2231. doi:10.1039/c7dt03775a
- Hrudey, S. E. (2009). Chlorination disinfection by-products, public health risk tradeoffs and me. *Water research*, 43(8), 2057–2092.
- Ilkiv, B., Petrovska, S., Sergiienko, R., Foya, O., Ilkiv, O., Shibata, E., . . . Zaulychnyy, Y. (2014). Electronic Structure of Hollow Graphitic Carbon Nanoparticles Fabricated from Acetylene Carbon Black. *Fullerenes, Nanotubes and Carbon Nanostructures*, 23(5), 449–454. doi:10.1080/1536383x.2014.885957
- Isaeva, V. I., Vedenyapina, M. D., Kulaishin, S. A., Lobova, A. A., Chernyshev, V. V., Kapustin, G. I., . . . Kustov, L. M. (2019). Adsorption of 2,4-dichlorophenoxyacetic acid in an aqueous medium on nanoscale MIL-53(Al) type materials. *Dalton Trans*, 48(40), 15091–15104. doi:10.1039/c9dt03037a

- Ivanchikova, I. D., Lee, J. S., Maksimchuk, N. V., Shmakov, A. N., Chesalov, Y. A., Ayupov, A. B., . . . Kholdeeva, O. A. (2014). Highly Selective H<sub>2</sub>O<sub>2</sub>-Based Oxidation of Alkylphenols to Benzoquinones Over MIL-125 Metal-Organic Frameworks. *European Journal of Inorganic Chemistry*, 2014(1), 132-139. doi:10.1002/ejic.201301098
- Jeong, C. H., Wagner, E. D., Siebert, V. R., Anduri, S., Richardson, S. D., Daiber, E. J., . . . Goslan, E. H. (2012). Occurrence and toxicity of disinfection byproducts in European drinking waters in relation with the HIWATE epidemiology study. *Environmental science & technology*, 46(21), 12120-12128.
- Jin, Z., & Yang, H. (2017). Exploration of Zr-Metal-Organic Framework as Efficient Photocatalyst for Hydrogen Production. *Nanoscale Res Lett*, 12(1), 539. doi:10.1186/s11671-017-2311-6
- Lee, Y., Kim, S., Kang, J. K., & Cohen, S. M. (2015). Photocatalytic CO<sub>2</sub> reduction by a mixed metal (Zr/Ti), mixed ligand metal-organic framework under visible light irradiation. *Chem Commun (Camb)*, 51(26), 5735-5738. doi:10.1039/c5cc00686d
- Li, B., Wen, H. M., Cui, Y., Zhou, W., Qian, G., & Chen, B. (2016). Emerging multifunctional metal-organic framework materials. *Advanced Materials*, 28(40), 8819-8860.
- Lin, K.-S., Adhikari, A. K., Ku, C.-N., Chiang, C.-L., & Kuo, H. (2012). Synthesis and characterization of porous HKUST-1 metal organic frameworks for hydrogen storage. *International Journal of Hydrogen Energy*, 37(18), 13865-13871. doi:10.1016/j.ijhydene.2012.04.105
- Luan, Y., Qi, Y., Gao, H., Andriamitantoa, R. S., Zheng, N., & Wang, G. (2015). A general post-synthetic modification approach of amino-tagged metal-organic frameworks to access efficient catalysts for the Knoevenagel condensation reaction. *Journal of Materials Chemistry A*, 3(33), 17320-17331. doi:10.1039/c5ta00816f
- Ma, M., Bétard, A., Weber, I., Al-Hokbany, N. S., Fischer, R. A., & Metzler-Nolte, N. (2013). Iron-Based Metal-Organic Frameworks MIL-88B and NH<sub>2</sub>-MIL-88B: High Quality Microwave Synthesis and Solvent-Induced Lattice "Breathing". *Crystal Growth & Design*, 13(6), 2286-2291. doi:10.1021/cg301738p
- Mahmoodi, N. M., Abdi, J., Taghizadeh, M., Taghizadeh, A., Hayati, B., Shekarchi, A. A., & Vossoughi, M. (2019). Activated carbon/metal-organic framework nanocomposite: Preparation and photocatalytic dye degradation mathematical modeling from wastewater by least squares support vector machine. *J Environ Manage*, 233, 660-672. doi:10.1016/j.jenvman.2018.12.026
- Maleki, A., Hayati, B., Naghizadeh, M., & Joo, S. W. (2015). Adsorption of hexavalent chromium by metal organic frameworks from aqueous solution. *Journal of Industrial and Engineering Chemistry*, 28, 211-216. doi:10.1016/j.jiec.2015.02.016
- Plewa, M. J., & Wagner, E. D. (2015). Charting a new path to resolve the adverse health effects of DBPs. *Occurrence, Formation, Health Effects, and Control of Disinfection By-Products*, 1190, 3-23.

- Prarat, P., Ngamcharussrivichai, C., Khaodhiar, S., & Punyapalakul, P. (2011). Adsorption characteristics of haloacetonitriles on functionalized silica-based porous materials in aqueous solution. *Journal of hazardous materials*, 192(3), 1210-1218.
- Safa, Y., & Bhatti, H. N. (2011). Adsorptive removal of direct textile dyes by low cost agricultural waste: Application of factorial design analysis. *Chemical Engineering Journal*, 167(1), 35-41.
- Sánchez-Sánchez, M., Getachew, N., Díaz, K., Díaz-García, M., Chebude, Y., & Díaz, I. (2015). Synthesis of metal–organic frameworks in water at room temperature: salts as linker sources. *Green Chemistry*, 17(3), 1500-1509. doi:10.1039/c4gc01861c
- Schwarzenbach, R. P., Egli, T., Hofstetter, T. B., Von Gunten, U., & Wehrli, B. (2010). Global water pollution and human health. *Annual Review of Environment and Resources*, 35, 109-136.
- Shen, K., Chen, X., Chen, J., & Li, Y. (2016). Development of MOF-derived carbon-based nanomaterials for efficient catalysis. *ACS Catalysis*, 6(9), 5887-5903.
- T, A., S, A., S, H., S, G., B, R., L, R. K., & N, R. (2018). Fabrication of corrosion resistant hydrophobic ceramic nanocomposite coatings on PEO treated AA7075. *Ceramics International*, 44(1), 874-884. doi:10.1016/j.ceramint.2017.10.014
- Tian, F., Cerro, A. M., Mosier, A. M., Wayment-Steele, H. K., Shine, R. S., Park, A., . . . Benz, L. (2014). Surface and stability characterization of a nanoporous ZIF-8 thin film. *The Journal of Physical Chemistry C*, 118(26), 14449-14456.
- Wang, Z., Ma, X., Yao, Z., Yu, Q., Wang, Z., & Lin, Y. (2018). Study of the pyrolysis of municipal sludge in N<sub>2</sub>/CO<sub>2</sub> atmosphere. *Applied Thermal Engineering*, 128, 662-671.
- Water, U. (2018). 2018 UN World Water Development Report, Nature-based Solutions for Water.
- Weiner, E. R. (2012). *Applications of environmental aquatic chemistry: a practical guide*: CRC press.
- Young, C., Salunkhe, R. R., Tang, J., Hu, C.-C., Shahabuddin, M., Yanmaz, E., . . . Yamauchi, Y. (2016). Zeolitic imidazolate framework (ZIF-8) derived nanoporous carbon: the effect of carbonization temperature on the supercapacitor performance in an aqueous electrolyte. *Physical Chemistry Chemical Physics*, 18(42), 29308-29315.
- Zhang, F., Zou, X., Sun, F., Ren, H., Jiang, Y., & Zhu, G. (2012). Growth of preferential orientation of MIL-53(Al) film as nano-assembler. *CrystEngComm*, 14(17). doi:10.1039/c2ce25318f
- Zhang, H., Chen, S., Zhang, H., Fan, X., Gao, C., Yu, H., & Quan, X. (2019). Carbon nanotubes-incorporated MIL-88B-Fe as highly efficient Fenton-like catalyst for degradation of organic pollutants. *Frontiers of Environmental Science & Engineering*, 13(2). doi:10.1007/s11783-019-1101-z
- Zhang, Y., Jia, Y., & Hou, L. a. (2018). Synthesis of zeolitic imidazolate framework-8 on polyester fiber for PM<sub>2.5</sub> removal. *RSC Advances*, 8(55), 31471-31477. doi:10.1039/c8ra06414h
- Zhao, L., Azhar, M. R., Li, X., Duan, X., Sun, H., Wang, S., & Fang, X. (2019). Adsorption of cerium (III) by HKUST-1 metal-organic framework from

- aqueous solution. *J Colloid Interface Sci*, 542, 421-428.  
doi:10.1016/j.jcis.2019.01.117
- Zhao, S., Yin, H., Du, L., He, L., Zhao, K., Chang, L., . . . Tang, Z. (2014). Carbonized nanoscale metal–organic frameworks as high performance electrocatalyst for oxygen reduction reaction. *ACS nano*, 8(12), 12660-12668.



## REFERENCES



จุฬาลงกรณ์มหาวิทยาลัย  
**CHULALONGKORN UNIVERSITY**



จุฬาลงกรณ์มหาวิทยาลัย  
**CHULALONGKORN UNIVERSITY**

## VITA

**NAME** Phattarawarin Rodbutr (Plam)  
**DATE OF BIRTH** 04 April 1995  
**PLACE OF BIRTH** Chonburi, Thailand  
**INSTITUTIONS ATTENDED** High school : Maryvit School  
Bachelor Degree : Faculty of environment and resource study, Mahidol university  
**HOME ADDRESS** 8 Moo 2 Najomtien Sattahip Chonburi

**PUBLICATION** -

**AWARD RECEIVED** -



จุฬาลงกรณ์มหาวิทยาลัย  
CHULALONGKORN UNIVERSITY